

## Translation and developmental robustness

### 1 DRMY1 promotes robust morphogenesis by sustaining the translation of cytokinin 2 signaling inhibitor proteins

3  
4 Shuyao Kong,<sup>1,2,†</sup> Mingyuan Zhu,<sup>1,2,3,†</sup> M. Regina Scarpin,<sup>4</sup> David Pan,<sup>1,2</sup> Longfei Jia,<sup>5</sup> Ryan E.  
5 Martinez,<sup>4</sup> Simon Alamos,<sup>6,7,8</sup> Batthula Vijaya Lakshmi Vadde,<sup>1,2</sup> Hernan G. Garcia,<sup>9,10,11,12,13</sup> Shu-  
6 Bing Qian,<sup>5</sup> Jacob O. Brunkard,<sup>4</sup> Adrienne H. K. Roeder<sup>1,2,14,\*</sup>

7  
8 <sup>1</sup> Weill Institute for Cell and Molecular Biology, Cornell University, Ithaca, NY 14853, USA

9 <sup>2</sup> Section of Plant Biology, School of Integrative Plant Science, Cornell University, Ithaca, NY 14853, USA

10 <sup>3</sup> Present address: Department of Biology, Duke University, Durham, NC 27708, USA

11 <sup>4</sup> Laboratory of Genetics, University of Wisconsin, Madison, WI 53706, USA

12 <sup>5</sup> Division of Nutritional Sciences, Cornell University, Ithaca, NY 14853, USA

13 <sup>6</sup> Environmental Genomics and Systems Biology Division, Lawrence Berkeley National Laboratory,  
14 Berkeley, CA 94720, USA

15 <sup>7</sup> Feedstocks Division, Joint BioEnergy Institute, Emeryville, CA 94608, USA

16 <sup>8</sup> Department of Plant and Microbial Biology, University of California at Berkeley, Berkeley, CA 94720, USA

17 <sup>9</sup> Biophysics Graduate Group, University of California at Berkeley, Berkeley, CA 94720, USA

18 <sup>10</sup> Department of Physics, University of California at Berkeley, Berkeley, CA 94720, USA

19 <sup>11</sup> Institute for Quantitative Biosciences-QB3, University of California at Berkeley, Berkeley, CA 94720, USA

20 <sup>12</sup> Department of Molecular and Cell Biology, University of California at Berkeley, Berkeley, CA 94720, USA

21 <sup>13</sup> Chan Zuckerberg Biohub-San Francisco, San Francisco, CA 94158, USA

22 <sup>14</sup> Lead Contact

23 <sup>†</sup> These authors contributed equally

24 <sup>\*</sup> Correspondence: ahr75@cornell.edu

### 27 SUMMARY

28 Robustness is the invariant development of phenotype despite environmental changes  
29 and genetic perturbations. In the *Arabidopsis* flower bud, four sepals robustly initiate and grow to  
30 constant size to enclose and protect the inner floral organs. We previously characterized the  
31 mutant *development related myb-like1* (*drmy1*), where 3-5 sepals initiate variably and grow to  
32 different sizes, compromising their protective function. The molecular mechanism underlying this  
33 loss of robustness was unclear. Here, we show that *drmy1* has reduced TARGET OF  
34 RAPAMYCIN (TOR) activity, ribosomal content, and translation. Translation reduction decreases  
35 the protein level of ARABIDOPSIS RESPONSE REGULATOR7 (ARR7) and ARABIDOPSIS  
36 HISTIDINE PHOSPHOTRANSFER PROTEIN 6 (AHP6), two cytokinin signaling inhibitors that  
37 are normally rapidly produced before sepal initiation. The resultant upregulation of cytokinin  
38 signaling disrupts robust auxin patterning and sepal initiation. Our work shows that the  
39 homeostasis of translation, a ubiquitous cellular process, is crucial for the robust spatiotemporal  
40 patterning of organogenesis.

41  
42  
43 Keywords: Robustness, TOR, translation, cytokinin, auxin, ribosomopathy, *Arabidopsis*, sepal,  
44 morphogenesis

## Translation and developmental robustness

### 45 INTRODUCTION

46

47 Robustness, or canalization, is the invariant, reproducible development of phenotype,  
48 unchanged by environmental fluctuations, genetic perturbations, or gene expression noise<sup>1–4</sup>.  
49 Commonly, within an individual, a given number of organs develop at well-defined positions to a  
50 robust final size and shape, which is crucial for fitness under stabilizing selection<sup>2</sup>. For example,  
51 transplanted eyes, limbs, and kidneys in mammals grow to a mature size similar to their donor,  
52 irrespective of the mature size of the same type of organ in the recipient<sup>5–7</sup>. The pairs of wings  
53 and halteres in *Drosophila* develop to robust, precisely coordinated final size and shape, which  
54 are required for flight<sup>8–11</sup>. The characteristic cruciform flower in *Brassicaceae* consists of four  
55 petals<sup>12</sup>, a trait that can contribute to pollinator attraction<sup>13</sup>. The robust positioning of leaves  
56 around the shoot apical meristem in plants, or phyllotaxis, ensures optimal light capture<sup>14–16</sup>. While  
57 these examples of developmental robustness have been documented for a long time, the  
58 underlying molecular mechanisms have just begun to be unveiled.

59

60 Earlier studies looking for genes involved in maintaining robustness have found *HEAT*  
61 *SHOCK PROTEIN 90 (HSP90)*. Mutations of *HSP90* cause a diverse array of phenotypic changes  
62 in plants, fruit fly, zebrafish, worm, and humans<sup>3,17,18</sup>. Notably, the display and severity of these  
63 changes vary between individuals and even between different parts of the same individual,  
64 indicating that developmental robustness is disrupted<sup>17,18</sup>. *HSP90* encodes a protein chaperone  
65 which has clients from nearly all developmental and signaling pathways<sup>3</sup>. *HSP90*, therefore, is a  
66 hub gene that affects numerous other genes within the gene network<sup>2</sup>. Disruption of such a hub  
67 gene would therefore trigger many defects in numerous developmental processes. Similarly,  
68 genes involved in central cellular processes such as chromatin remodelling<sup>19–21</sup>, transcription<sup>19,20</sup>,  
69 translation<sup>22,23</sup>, and protein degradation<sup>24,25</sup> are also hub genes, and they have been found to be  
70 important for developmental robustness in various systems including fungi, animals, and plants.  
71 How these broad-acting hub genes contribute to the robustness of tissue-specific developmental  
72 phenotypes is still largely unclear.

73

74 We have developed the *Arabidopsis* sepal as a system to elucidate the mechanisms  
75 maintaining robustness in organ size and shape<sup>26–28</sup>. Sepals are the outermost floral organs  
76 whose function is to enclose buds and protect the developing inner organs, i.e. petals, stamens,  
77 and carpels, before the flower blooms. To fulfill this protective function, each flower robustly  
78 develops four sepals of equal length, allowing them to close at the top (Figure 1A, top left); these  
79 four sepals are of equal width and positioned 90° from each other, leaving no gap on the sides  
80 (Figure 1A, middle left). This robustness in sepal size and shape stems from the robust initiation  
81 of the four sepal primordia from the floral meristem with precisely coordinated spatiotemporal  
82 patterns<sup>27</sup> (Figure 1A, bottom left). The initiated sepal primordia attain robust final size and shape  
83 by spatiotemporal averaging of cellular growth variability during sepal elongation, and  
84 synchronous progression of a whole-flower growth termination signal from tip to base<sup>26</sup>. In  
85 addition, noise in gene expression must be kept low to ensure sepal size robustness<sup>29</sup>. We  
86 previously characterized a mutant in *DEVELOPMENT RELATED MYB-LIKE 1 (DRMY1)* that

## Translation and developmental robustness

87 develops flowers where the inner organs are exposed due to gaps between sepals<sup>27</sup>. The gaps  
88 are caused by variability in sepal development. Specifically, some sepals are shorter than others,  
89 leaving gaps on the top (Figure 1A, top right); the arrangement of sepals around the flower deviate  
90 from the canonical form such that parts of the flower are not covered by a sepal, leaving gaps on  
91 the side (Figure 1A, middle right). This variability in the size, number, and position of the mature  
92 sepal originates from the earliest stages of floral development where the spatiotemporal pattern  
93 of sepal initiation becomes variable (Figure 1A, bottom right). Variability in sepal initiation, in turn,  
94 is driven by the loss of robust patterning of auxin and cytokinin<sup>27</sup>, two plant hormones critical for  
95 morphogenesis<sup>30-32</sup>, in the floral meristem before sepal initiation. However, the molecular  
96 mechanism through which DRMY1 maintains robust hormone patterning is still unknown.  
97

98 In this study, we elucidate a mechanism through which DRMY1 maintains robust hormone  
99 patterning and thus robust sepal initiation. Specifically, we find that DRMY1 maintains proper  
100 activity of TARGET OF RAPAMYCIN (TOR), a crucial regulator of ribosome level and mRNA  
101 translation<sup>33,34</sup>, and thereby sustains translation *in vivo*. When *DRMY1* is mutated, the levels of  
102 ARABIDOPSIS RESPONSE REGULATOR7 (ARR7) and ARABIDOPSIS HISTIDINE  
103 PHOSPHOTRANSFER PROTEIN 6 (AHP6), two cytokinin inhibitor proteins that are rapidly  
104 synthesized during hormone patterning prior to sepal initiation, are drastically reduced in the floral  
105 meristem. Consequently, cytokinin signaling uniformly increases in the meristem periphery,  
106 causing variability in auxin patterning and sepal initiation. We further propose that the increase in  
107 cytokinin signaling may be a survival mechanism to alleviate the translation rate reduction when  
108 ribosomal content is limited. In summary, our work shows that the hub processes of TOR signaling  
109 and translation, which occur in every cell, have very tissue-specific roles in maintaining robust  
110 organogenesis by sustaining the rapid synthesis of hormone signaling proteins.  
111  
112

## 113 RESULTS

### 114 The *drmy1* mutant has reduced TOR activity, ribosome content, and translation rate

115 *DRMY1* encodes a MYB/SANT domain protein which may exert transcriptional  
116 regulation<sup>27</sup>. To look for differentially expressed genes in *drmy1* which may be candidates  
117 underlying variable sepal initiation, we performed RNA-sequencing (RNA-seq) in *drmy1* and wild  
118 type (WT) of *apetala1* (*ap1*) *cauliflower* (*cal*) AP1-GR background<sup>35,36</sup>. The *ap1 cal* AP1-GR  
119 inflorescence produces numerous tightly packed ball-shaped meristems, which, upon induction,  
120 synchronously initiate sepal primordia, allowing us to collect large quantities of floral meristems  
121 with sepal primordia initiating (Stage 3)<sup>37</sup> (Figure S1A). We crossed *drmy1* into *ap1 cal* AP1-GR  
122 and performed RNA-seq on induced inflorescences of WT and *drmy1* in this background. We  
123 detected transcripts from a total of 21,496 genes, of which 1,042 (4.8%) were differentially  
124 expressed in *drmy1* (Figure S1B; Supplemental Dataset 1). We found that the 443 genes  
125 downregulated at the transcript level in *drmy1* were most enriched in the gene ontology (GO) term  
126 “Translation”, a fundamental and ubiquitous cellular process that converts genetic information  
127  
128

## Translation and developmental robustness

129 from transcript to protein. Within this term, genes encoding ribosomal components were most  
130 downregulated (Figure S1C). The 443 downregulated genes were also enriched in several other  
131 ribosome-related GO terms (Figure 1B). We therefore hypothesized that ribosomal abundance  
132 and translation are affected in *drmy1*, potentially altering the accumulation of proteins critical to  
133 developmental robustness.

134

135 To determine whether and how ribosomal abundance and translation are affected in  
136 *drmy1*, we performed polysome profiling in induced inflorescences of WT and *drmy1* in *ap1 cal*  
137 *AP1-GR* background. Compared to WT, all peaks corresponding to 40S, 60S, monosomes, and  
138 polysomes are drastically reduced in *drmy1* (Figure 1C; Supplemental Dataset 2). To see whether  
139 this reduction in ribosomal content affected *de novo* protein synthesis rate *in vivo*, we performed  
140 puromycin labeling. Samples were incubated with puromycin, an amino acid-tRNA analog that is  
141 incorporated into nascent polypeptide chains and can be detected using an anti-puromycin  
142 antibody to infer global translation rate<sup>38,39</sup>. In both young seedlings and induced *ap1 cal AP1-GR*  
143 inflorescences, we found that the puromycin level detected in *drmy1* mutant samples was much  
144 reduced compared to WT (Figure 1D), indicating a reduction in global translation rate. We  
145 hypothesized that reduced global translation rate should likely result in globally decreased protein  
146 levels. For this, we looked at a ubiquitously expressed membrane marker *UBQ10::mCherry-*  
147 *RCI2A*, and found that it had a small (~25%) but significant decrease in fluorescence intensity in  
148 the inflorescence meristem and young floral buds of *drmy1* compared with WT (Figure S1D, E).  
149 We also measured its fluorescence intensity in the ribosomal mutant *u14y* (*rpl4d*)<sup>40</sup> and we found  
150 that the decrease in fluorescence intensity in *drmy1* is even greater than in *u14y* (Figure S1F, G).  
151 Overall, these results show that ribosomal content and translation are indeed reduced in the  
152 *drmy1* mutant.

153

154 To test how the global repression of translation in *drmy1* impacts its proteome, we  
155 extracted total soluble protein from induced inflorescences of WT and *drmy1* in *ap1 cal AP-GR*  
156 background and performed mass spectrometry. We identified a total of 5,077 proteins, of which  
157 548 (10.8%) were differentially accumulated in *drmy1* (Figure S1B; Supplemental Dataset 1).  
158 These differentially accumulated proteins were enriched in GO terms related to translation and  
159 ribosomes (Figure 1E). Despite the overall reduction in ribosomes (Figure 1C), relative to other  
160 proteins, ribosomal components are more abundant in *drmy1* (Figure S1H; Supplemental Dataset  
161 1). This is not true for all proteins involved in translation; poly-A binding proteins and tRNA  
162 synthetases, for example, are relatively less abundant in *drmy1* than in WT. Moreover, the 26S  
163 proteasome responsible for targeted protein degradation is much more abundant in *drmy1* than  
164 in WT (Supplemental Dataset 1). In concert, these results demonstrate that the machinery  
165 responsible for maintaining protein homeostasis is substantially dysregulated in *drmy1*.

166

167 A key signaling pathway that regulates protein homeostasis is TARGET OF RAPAMYCIN  
168 (TOR)<sup>41,42</sup>. TOR is a hub that integrates information from light, sugars, nutrient availability, etc.,  
169 to promote growth-related processes, including ribosome biogenesis and translation, and to  
170 repress catabolic processes, including protein degradation by autophagy and the

## Translation and developmental robustness

171 proteasome<sup>33,34,43–45</sup>. TOR directly regulates the translation of specific mRNAs by promoting the  
172 phosphorylation of proteins, including LARP1, eIF3h, RISP, eS6, and 4EBPs, that impact  
173 translation initiation, reinitiation, or elongation of mRNAs with specific features, such as 5'TOP  
174 motifs or short upstream open reading frames (uORFs) in the 5' leaders of mRNAs<sup>34,42,46–52</sup>. TOR  
175 also indirectly increases overall protein synthesis rates by globally increasing ribosome levels.  
176 We therefore hypothesize that the overall decrease in ribosomal content and protein synthesis in  
177 *drmy1* may reflect altered TOR signaling. To test for signatures of transcriptomic changes that  
178 have been well defined in seedlings under TOR inhibition<sup>34,53,54</sup>, we performed RNA-seq on  
179 seedlings of WT, *drmy1*, WT treated with AZD-8055 (a potent TOR inhibitor), and mock-treated  
180 WT (Supplemental Dataset 3). We found that the *drmy1* mutation causes transcriptomic changes  
181 similar to TOR inhibition (Figure 1F). A significant portion of genes differentially expressed under  
182 TOR inhibition vs. mock were also differentially expressed in *drmy1* vs. WT (466/2044 = 22.8%;  
183 hypergeometric test,  $p = 4.7 \times 10^{-108}$ ). Not only were these 466 genes differentially expressed in  
184 both situations, but also most of them were coherently downregulated or upregulated (439/466 =  
185 94.2%, Chi-square test,  $p < 2.2 \times 10^{-16}$ ; Figure 1G, S1I). Genes coherently downregulated in both  
186 situations were enriched in GO terms related to translation and ribosomes, and, most strikingly,  
187 a quarter of them were under the GO term “translation” (Figure 1F, S1J). These similar  
188 transcriptomic changes support our hypothesis that TOR activity is reduced in *drmy1*. To further  
189 test this hypothesis, we measured TOR activity in WT and *drmy1* by assaying the phosphorylation  
190 of its direct substrate, RIBOSOMAL PROTEIN eS6 KINASE (S6K)<sup>55,56</sup>. While the total protein  
191 level of S6K did not change in *drmy1*, we found that S6K phosphorylation drastically decreased,  
192 demonstrating reduced TOR activity (Figure 1H, I). Overall, these results are consistent with the  
193 idea that *drmy1* has reduced TOR activity—a main pathway controlling ribosomal abundance and  
194 translation—which causes reduced ribosomal content and global translation rate.  
195

## 196 Defects in TOR activity, ribosome, and translation disrupt robust sepal initiation

197 We next asked whether defects in TOR activity, ribosome, or translation have any effects  
198 on robust sepal initiation like the *drmy1* mutation does (Figure 2A, 2B; also see Zhu et al.<sup>27</sup>). In a  
199 WT bud, initiation is robust in that four sepal primordia of similar size form evenly spaced around  
200 the periphery of the floral meristem (Figure 2A, 2H). Angles between them vary little, i.e., they are  
201 all at around 90° angles from each other (Figure 2I, 2J). By contrast, in *drmy1* buds, three to five  
202 sepal primordia initiate and grow to different sizes (Figure 2B, 2H; also see Zhu et al.<sup>27</sup>). Sepal  
203 primordia in *drmy1* buds are generally unevenly spaced, and angles between them have a high  
204 coefficient of variation (CV) (Figure 2I, 2J). To determine whether defects in ribosomes can cause  
205 the same sepal initiation defects, we imaged three ribosomal mutants, *ul4z* (*rpl4a*), *ul4y*, and *ul18z*  
206 (*rpl5a*)<sup>40</sup>, each mutated in a gene encoding a ribosomal component that is also downregulated in  
207 *drmy1* at the transcript level (Figure S1C). The *ul4z* mutant bud shows reduced size of the inner  
208 sepal primordia relative to the outer sepal primordia (Figure 2C), and slightly more variable spatial  
209 distribution of sepal primordia (Figure 2J), although it always develops four sepal primordia  
210 (Figure 2H). This is a weaker phenotype than *drmy1* but has similar characteristics. The *ul4y* and  
211 *ul18z* mutants show great variability in the number and position of sepal primordia (Figure 2D,

## Translation and developmental robustness

213 2E, 2H, 2J), more similar to *drmy1*. We also crossed these ribosomal mutants with *drmy1* to study  
214 sepal variability in the double mutants (Figure S2A-H). In *drmy1 ul4z*, *drmy1 ul4y*, and *drmy1*  
215 *ul18z/+*, on average, sepal initiation was as variable as in the *drmy1* single mutant (Figure S2I,  
216 S2J). However, there were buds with no outgrowth in the adaxial or lateral regions of the bud  
217 periphery (Figure S2B, S2E, S2G), buds with six sepal primordia (Figure S2C, S2F, S2H), and  
218 buds with two outer sepal primordia (Figure S2D, S2H), which were not seen in the *drmy1* single  
219 mutant. Note that we were unable to characterize the homozygous *drmy1 ul18z* double mutant  
220 because they were embryo-lethal (Figure S2K), further supporting the idea that ribosomal  
221 mutations enhance the phenotypic defects in *drmy1*.

222

223 We then imaged mutants with reduced TOR activity to determine whether sepal initiation  
224 is also less robust. *lst8-1-1* is a T-DNA insertional mutant of the TOR complex component LST8-  
225 1<sup>57</sup> and is weakly hypomorphic in TOR activity. We found that *lst8-1-1* shows variable sepal  
226 initiation in a small proportion of buds (4/41, 9.8%) (Figure 2F, 2H, 2J). The *spaghetti-1* mutant  
227 defective in TOR complex 1 (TORC1) assembly<sup>58</sup> showed a level of variability comparable to the  
228 *drmy1* mutant and the ribosomal mutants *ul4y* and *ul18z* (Figure 2G, 2H, 2J). Mutants with more  
229 severe disruption of TOR activity are embryo lethal and could not be analyzed<sup>58,59</sup>. These results  
230 show that reduction in TOR activity can cause variability in sepal initiation, similar to *drmy1*.

231

232 To corroborate these findings, we directly inhibited translation by *in vitro* culture of  
233 dissected WT inflorescences on 2  $\mu$ M cycloheximide (CHX, a chemical inhibitor of translation) for  
234 9-10 days. This is a low concentration that does not completely block translation, as  
235 inflorescences were still alive after 10 days in this condition. Compared with mock, CHX-treated  
236 inflorescences develop buds that have 2 to 6 sepal primordia of variable sizes that are unevenly  
237 spaced around the bud periphery (Figure 2K, 2M, 2N). These phenotypes are stronger than  
238 *drmy1*. Similarly, we directly inhibited TOR activity by application of 2 nmol Torin2 to the growing  
239 shoot apex twice a day for 15 days, and we observed variable sepal initiation (Figure 2L, 2M, 2N).  
240 Overall, these data show that inhibition of TOR activity and translation can disrupt the robustness  
241 of sepal initiation, in terms of sepal primordium number, position, and size.

242

243 We previously showed that *drmy1* buds develop sepals of different sizes because of  
244 increased differences in the initiation timing of sepals within the same bud. The late-initiating  
245 primordia remain smaller throughout development. They end up as smaller sepals relative to  
246 those that initiated earlier, leaving gaps that expose the developing inner floral organs<sup>27</sup>.  
247 Moreover, different buds have different temporal patterns of sepal initiation, contributing to  
248 between-bud variability of sepal phenotype<sup>27</sup>. We asked whether TOR or ribosomal defects  
249 similarly disrupt the relative timing of sepal initiation, within-bud and between-bud. We live imaged  
250 WT and *ul4y* every six hours during sepal initiation and quantified the amount of time the bud  
251 takes to initiate the inner and lateral sepals after it initiates the outer sepal. In WT, after the  
252 initiation of the outer sepal, most buds initiate the inner sepal within 6 hours and the lateral sepals  
253 within 12 hours (Figure 3A, 3C; also see Zhu et al.<sup>27</sup>). In *ul4y*, the time differences between outer  
254 and inner sepal initiation and between outer and lateral sepal initiation are longer (Figure 3B,

## Translation and developmental robustness

255 mean in Figure 3C). Moreover, these time differences are more variable across buds, indicating  
256 a loss of robustness in organ initiation timing (SD in Figure 3C). Similarly, we compared the sepal  
257 initiation timing in Torin2 vs mock-treated WT buds. While in most mock-treated buds, the inner  
258 and lateral sepals initiate within 12 hours after the outer sepal (Figure 3D, 3F), in Torin2-treated  
259 buds, sepals within the same bud initiates at vastly different times (Figure 3E, mean in Figure 3F),  
260 and the temporal pattern of sepal initiation is more variable across buds than mock (SD in Figure  
261 3F). These results show that TOR and ribosomal defects can disrupt the precisely orchestrated  
262 initiation timing of sepal primordia.

263

264 Does the variability in initiation timing cause variable sizes and gaps in mature sepals, as  
265 in *drmy1* (Figure S3A, B, G, H; also see Zhu et al. <sup>27</sup>)? We imaged the mature sepals of the  
266 ribosomal mutants *ul4z*, *ul4y*, *ul18z*, as well as the TOR component mutant *lst8-1-1*. Surprisingly,  
267 unlike *drmy1*, the sepals in *ul4z*, *ul4y*, *ul18z* enclose the inner floral organs perfectly, leaving no  
268 gaps, regardless of sepal number (Figure S3C-E). Small gaps still exist in buds of *lst8-1-1*,  
269 although sepal size differences appear greatly reduced (Figure S3F). Further dissection shows  
270 that in these mutants, sepals within the same flower are of similar sizes, although sepals from  
271 different flowers can be of vastly different sizes, most conspicuously for *lst8-1-1* (Figure S3I-N).  
272 This is unlike *drmy1*, where sepal size variability is equally high comparing sepals within the same  
273 flower or from different flowers (Figure S3H, S3M-N). Upon closer examination, while sepals  
274 initiating late in *drmy1* buds remain small, leaving a gap in the sepal whorl (Figure S3O-P), those  
275 in *ul4y* were able to catch up with the other sepals and close the gap (Figure S3Q). Our results  
276 suggest that there exists a size-coordinating mechanism independent of TOR or ribosomal  
277 functions that allows sepals within the same bud to reach the same mature length, and that this  
278 mechanism is disrupted in *drmy1*. Such a mechanism requires further investigation in the future.  
279

## 280 **Inhibition of TOR activity and translation increase cytokinin signaling and disrupts the** 281 **robust spatial pattern of auxin and cytokinin signaling**

282

283 Auxin and cytokinin are two important plant hormones critical to many aspects of plant  
284 development<sup>30-32</sup>, and there is accumulating evidence that they act synergistically in the shoot  
285 apical meristem to promote lateral organ initiation<sup>16,60,61</sup>. We previously showed that, in a WT floral  
286 meristem prior to sepal initiation, auxin and cytokinin signaling are concentrated at the four  
287 incipient primordia, which is required for robust sepal initiation from these regions (Figure 4A,  
288 S4A; Zhu et al.<sup>27</sup>). In the *drmy1* mutant, cytokinin signaling becomes stronger and diffuse around  
289 the bud periphery (Figure 4A-B). Auxin signaling also becomes more diffuse, forming irregular  
290 auxin maxima that are less focused than those in WT, except at the incipient outer sepal where it  
291 remains robust (Figure 4A, S4B; Zhu et al.<sup>27</sup>). These changes in hormone signaling correlate with  
292 variable sepal initiation (Figure S4B)<sup>27</sup>. We wondered whether ribosomal mutations have similar  
293 effects on auxin and cytokinin signaling. To this end, we imaged the auxin signaling reporter  
294 *DR5::3xVENUS-N7* and the cytokinin signaling reporter *TCS::GFP* in floral meristems of the  
295 ribosomal mutant *ul4y*. Both reporters lose their robust spatial pattern except in the incipient outer  
296 sepal (Figure 4A, S4C). The hormone signaling patterns were quantified by circular histogram

## Translation and developmental robustness

297 analysis (see Methods for details). For each of DR5 and TCS, WT buds showed four clear peaks  
298 ~90 degrees apart from each other, with very little signal in between, whereas in *drmy1* and *ul4y*,  
299 peaks were barely seen except at the incipient outer sepal (at 45 degrees), and there was greater  
300 noise and variation all around the bud (Figure 4C-D). Diffuse bands of auxin signaling that typically  
301 occurs in the adaxial or lateral periphery of *drmy1* and *ul4y* buds (Figure S4B and S4C, brackets)  
302 can later resolve into several distinct auxin maxima of various intensity and at various positions,  
303 correlated with the initiation of sepal primordia of various sizes at these same positions (Figure  
304 S4B and S4C, red arrowheads).

305

306 We also tested whether drug treatments that inhibit TOR activity or translation can disrupt  
307 the robust hormone patterning. Buds treated *in vitro* with the translation inhibitor CHX (2  $\mu$ M) for  
308 3 days showed a 50% increase in cytokinin signaling, and both auxin and cytokinin signaling  
309 became diffuse around the bud periphery (Figure 4E-H). By day 6, cytokinin signaling was still  
310 diffuse all around, and increased to more than two-fold relative to mock (Figure 4I, 4J, 4L). Auxin  
311 signaling formed maxima of variable number at variable positions (Figure 4I arrowheads, 4K),  
312 correlated with the variable initiation of sepal outgrowth at these positions (Figure S4D-E). Similar  
313 changes occurred in buds treated *in vitro* with the TOR inhibitor AZD-8055 (2  $\mu$ M) for 6 days  
314 (Figure 4I-L). For both CHX and AZD-8055, the disruptions of hormone signaling are similar to  
315 *drmy1*. *In vivo* treatment using another TOR inhibitor Torin2 for 15 days increased cytokinin  
316 signaling by 70%, although it did not make auxin and cytokinin signaling more diffuse (Figure  
317 S4F-I). Overall, these results show that defects in TOR activity and translation increase cytokinin  
318 signaling, and disrupt the precise spatial patterning of cytokinin and auxin signaling required for  
319 robust sepal initiation.

320

## 321 **An increase in cytokinin signaling is necessary and sufficient for variable auxin signaling 322 and sepal initiation under translation inhibition**

323

324 Auxin is a critical hormone in organogenesis<sup>62,63</sup>. As shown above, variable patterning of  
325 auxin signaling correlates with variable sepal initiation during inhibition of TOR activity and  
326 translation. We wondered what caused auxin to lose its robust patterning under such conditions.  
327 It was previously reported that the ribosomal mutants *ul4y*, *ul18z*, and *e124y* have reduced protein  
328 levels of AUXIN RESPONSE FACTOR (ARF) 3, 5, and 7<sup>64-66</sup>, key transcription factors that  
329 mediate the auxin signaling response<sup>67</sup>. The transcripts of these ARFs contain upstream open  
330 reading frames (uORFs), requiring translation reinitiation to translate their main open reading  
331 frames<sup>68,69</sup>, a process defective in the ribosomal mutants *ul4y*, *ul18z*, and *e124y*<sup>64-66</sup>. We therefore  
332 hypothesized that *drmy1* loses robust auxin signaling pattern because of reduced translation of  
333 uORF-containing transcripts, including those of certain ARFs. To begin, we utilized our  
334 transcriptomics and proteomics data, and considered that the protein-transcript ratio of a gene  
335 should reflect its level of translation, among other factors such as protein stability. Therefore,  
336 following our hypothesis, genes containing uORFs should, in general, have a lower protein-  
337 transcript ratio in *drmy1* than in WT. We calculated the difference of this ratio between *drmy1* and  
338 WT for all 5,086 gene-protein pairs in our inflorescence dataset, and compared the ratio against

## Translation and developmental robustness

339 the number of uORFs in each transcript (Figure S5A; uORF data from von Arnim et al.<sup>69</sup>). We  
340 found a small but significant decrease in the protein-transcript ratio in *drmy1* for the 724 genes  
341 containing at least 2 uORFs in their transcripts, supporting the hypothesis that *drmy1* has reduced  
342 translation reinitiation for uORF-containing transcripts, just like *ul4y*, *ul18z*, and *el24y*<sup>64–66</sup>. Then,  
343 we examined whether the translation reinitiation of uORF-containing ARFs are indeed reduced in  
344 the *drmy1* mutant. We selected *ARF3/ETTIN*, *ARF5/MONOPTEROS*, and *ARF6*, which have 2,  
345 6, and 6 uORFs respectively, and as controls, *ARF8* and *ARF10* which do not contain uORFs.  
346 None of these ARFs were differentially expressed in *drmy1* at the transcript level, except *ARF10*  
347 which was slightly upregulated (Figure S5B). We utilized promoter-fluorescent protein fusion  
348 reporters (Figure S5C) which have the same uORFs in the promoter region as the corresponding  
349 ARF genes if the genes have them. These reporters reflect transcriptional and uORF-mediated  
350 translational regulation. *pARF3::N3xGFP*, *pARF5::ER-EYFP-HDEL*, and *pARF6::N3xGFP*  
351 contain uORFs and thus, following our hypothesis, are expected to drastically decrease in  
352 fluorescence intensity in *drmy1* compared to WT. *pARF8::N3xGFP* and *pARF10::N3xGFP* do not  
353 have uORFs and are thus expected to have comparable or higher fluorescence intensity in *drmy1*.  
354 Surprisingly, we saw no correlation between the presence of uORFs and decrease in fluorescent  
355 intensity in *drmy1* (Figure S5C-D). While it might arise from additional layers of regulation on  
356 these ARFs, this result suggests that the decrease in translation reinitiation of uORF-containing  
357 ARFs is not the main factor explaining the loss of robust auxin signaling pattern in *drmy1*.  
358

359 It was previously reported that external application of cytokinin increases auxin  
360 biosynthesis in actively growing tissue including the shoot apex, young leaves, and roots<sup>70</sup>, and  
361 cytokinin application also changes the expression and polarity of PIN-FORMED (PIN) polar auxin  
362 transport carriers<sup>71,72</sup>. We previously noticed that external application of 6-benzylaminopurine  
363 (BAP), a synthetic cytokinin, induced additional convergence points of PIN1 and increased  
364 variability in auxin signaling, causing variability in sepal initiation (Zhu et al.<sup>27</sup>, in this reference  
365 see Fig. 4e, Extended Data Fig. 7e and 7f). Here, we confirmed this observation by circular  
366 histogram analysis (Figure 5A-D). While the mock-treated WT buds showed four clear peaks of  
367 DR5 signal with very little signal in between (Figure 5A-B), those treated with 5  $\mu$ M BAP showed  
368 a less robust spatial pattern, with less distinguishable peaks and larger variation all around the  
369 bud (Figure 5C-D). Thus, excessive cytokinin is sufficient for the variable spatial pattern of auxin  
370 signaling.  
371

372 We then wondered whether an increase in cytokinin signaling (Figure 4) is the cause of  
373 variable pattern of auxin signaling under translation-limited conditions such as *drmy1*. To test this  
374 hypothesis, we crossed *drmy1* containing the DR5 reporter with a triple mutant of *ARABIDOPSIS/*  
375 *RESPONSE REGULATOR (ARR) 1, 10, and 12*, the three most highly expressed B-type ARRs  
376 in our RNA-seq (Supplementary Dataset 1) which are crucial for the activation of cytokinin-  
377 responsive genes<sup>73</sup>. While buds of *arr1,10,12* did not show apparent phenotypic differences from  
378 WT, the quadruple mutant *drmy1 arr1,10,12* largely rescued the *drmy1* phenotype, with much  
379 less variability in sepal number and position (Figure 5E-G). While mature buds of *drmy1* have  
380 sepals of variable sizes, leaving gaps and exposing the inner floral organs (Figure S6D vs. S6A-

## Translation and developmental robustness

381 C), those of *drmy1 arr1,10,12* have sepals of robust sizes that are able to close (Figure S6E).  
382 Likewise, mutation in a cytokinin receptor *WOODEN LEG (WOL)/ARABIDOPSIS HISTIDINE*  
383 *KINASE 4 (AHK4)* showed a similar rescue of the *drmy1* sepal phenotype (Figure 5E-G, S6F).  
384 While the auxin signaling reporter DR5 was diffuse and variable in *drmy1* except in the incipient  
385 outer sepal (Figure 5H-I), in *drmy1 arr1,10,12*, it was focused in all the four incipient sepals that  
386 were robustly positioned, although the signal intensity in the incipient outer sepal was much higher  
387 than others (Figure 5J-K). These results indicate that cytokinin signaling is required for the  
388 increased variability in auxin signaling pattern and sepal initiation in *drmy1*.  
389

390 Furthermore, we wanted to test whether cytokinin signaling is required for variability in  
391 more general conditions where translation is inhibited. The translation inhibitor CHX disrupted  
392 robustness in auxin signaling and sepal initiation in WT (Figure 2K, 4E, 4I), and we tested whether  
393 these effects are still present in *arr1,10,12* and *wol* mutants. We found that, unlike WT, sepal  
394 initiation remained mostly robust in *arr1,10,12* and *wol* after ten days of 2  $\mu$ M CHX treatment  
395 (Figure 5L-N). While DR5 in WT became diffuse and occurred in variable positions after three  
396 days of CHX treatment (Figure 5O-P, arrow), DR5 in *arr1,10,12* remained robust and  
397 concentrated at the four incipient sepal primordia (Figure 5Q-R). These results suggest that  
398 elevated cytokinin signaling level is the primary cause for variability in auxin patterning under  
399 translation-inhibited conditions. Thus, in WT, maintaining a low level and focused cytokinin  
400 signaling is crucial for robust auxin patterning and sepal initiation.  
401

## 402 **Upregulation of cytokinin signaling is required to sustain translation and fitness in *drmy1***

403

404 Under translation-inhibited conditions, why does the plant upregulate cytokinin signaling  
405 at the cost of robust morphogenesis? Previous studies revealed that cytokinin signaling can  
406 stimulate translation<sup>74-78</sup>, by increasing transcription or protein abundance of ribosomal  
407 components or biogenesis factors<sup>79-81</sup> and modification of initiation and elongation factors<sup>82</sup>. We  
408 therefore hypothesized that an increase in cytokinin signaling under translation-inhibited  
409 conditions (such as *drmy1*) sustains a survivable rate of translation in a feedback loop. We first  
410 validated that, under our growth conditions, an increase in cytokinin signaling (*arr1 35S::ARR1*)  
411 is sufficient to increase global translation (Figure 6A; also see Karunadasa et al.<sup>74</sup>) in 14-day-old  
412 seedlings. We then tested whether cytokinin signaling is required to sustain global translation  
413 (Figure 6B-C). Compared to WT, the cytokinin receptor single mutant *wol* has a mild reduction in  
414 global translation rate at day 8 and a ~50% reduction at day 14. The *drmy1* single mutant shows  
415 drastically reduced global translation rate at day 8, but by day 14, global translation rate in *drmy1*  
416 increased and matched WT. In the *drmy1 wol* double mutant, however, translation rate was  
417 unable to recover at day 14 and remained lower than *drmy1*. Our data suggest that, in *drmy1*  
418 plants which has reduced TOR activity and ribosomal level (Figure 1), the upregulated cytokinin  
419 signaling is required to sustain global translation at nearly WT levels.  
420

421 We then hypothesized that an upregulation of cytokinin signaling in plants with reduced  
422 TOR activity and ribosomal content such as *drmy1* and the consequent restoration of global

## Translation and developmental robustness

423 translation would provide fitness benefits. Thus, we expect that removal of the cytokinin receptor  
424 WOL from *drmy1* and the consequent failure to sustain global translation should affect plant  
425 vitality and reproduction. We found that at day 14, the *drmy1* single mutant is slightly smaller than  
426 WT. In contrast, in the absence of WOL, growth of *drmy1 wol* plants were extremely retarded  
427 compared to *wol*, with tiny and chlorotic cotyledons and true leaves (Figure 6D). In older plants,  
428 the *drmy1* single mutant has similar rosette size and slightly shorter inflorescences compared to  
429 WT. In contrast, in the absence of WOL, *drmy1 wol* produced tiny rosettes and stunted  
430 inflorescences with a few chlorotic buds that develop into small, short siliques (Figure 6E, S6F).  
431 Similarly, when B-type ARR<sub>s</sub> are mutated, the growth of the *drmy1 arr1,10,12* quadruple mutant  
432 is much retarded compared to *arr1,10,12*. They produced slightly chlorotic and anthocyanin-rich  
433 rosettes, a tiny inflorescence composed of very few buds (Figure 6F, S6E) and, in the end, siliques  
434 in which all seeds had aborted (Figure 6G). Overall, these results show that *drmy1* requires the  
435 cytokinin signaling pathway for normal growth and reproduction. While it remains possible that  
436 unknown effects of the cytokinin signaling pathway other than promoting translation are critical  
437 for the proper growth of *drmy1*, our results are consistent with our hypothesis that the upregulation  
438 of global translation (Figure 6A) by increased cytokinin signaling (Figure 4) maintains a survivable  
439 level of protein synthesis in plants with reduced ribosomal content such as *drmy1* (Figure 1C).  
440

## 441 **TOR and translation inhibition decreases the protein level of cytokinin signaling inhibitors 442 ARR7 and AHP6**

443

444 What causes cytokinin signaling to increase in plants with reduced TOR activity and  
445 translation (Figure 4)? It was previously shown that *cis*-type cytokinins can be synthesized from  
446 tRNAs by the tRNA isopentenyltransferases (IPTs), IPT2 and IPT9<sup>83</sup>. We hypothesized that the  
447 decrease in global translation may increase the availability of tRNAs as substrates for cytokinin  
448 biosynthesis, increasing the level of cytokinins. To test this idea, we extracted cytokinins from  
449 induced inflorescences of WT and *drmy1* in *ap1 cal AP1-GR* background (Figure S1A). We  
450 measured the level of three cytokinin bases, *trans*-Zeatin (tZ), *cis*-Zeatin (cZ), and  
451 isopentenyladenine (iP), and their corresponding nucleosides (tZR, cZR, and iPR), using liquid  
452 chromatography-mass spectrometry. Surprisingly, we found no significant difference in their  
453 levels between WT and *drmy1*, and notably, the amount of *cis*-Zeatin was barely detectable in all  
454 samples (Figure S7A). This suggests that the increase in *cis*-type cytokinin synthesis is not the  
455 mechanism underlying the increase in cytokinin signaling under our translation-inhibited  
456 conditions.

457

458 We then considered the effects that a decrease in translation rate might have on the  
459 protein components of the cytokinin signaling pathway. In particular, A-type ARR<sub>s</sub>, which encode  
460 inhibitors of cytokinin signaling<sup>84-86</sup>, are rapidly induced upon cytokinin application and serve to  
461 dampen cytokinin response in the tissue<sup>87-89</sup>. Likewise, AHP6 is highly expressed in lateral organ  
462 primordia downstream of auxin signaling, which non-cell autonomously represses and restricts  
463 cytokinin signaling to robust spatial patterns<sup>16</sup>. The rapid synthesis of the A-type ARR and AHP6  
464 proteins may be crucial for maintaining the homeostasis of cytokinin signaling during

## Translation and developmental robustness

465 developmental processes. We therefore hypothesized that, during hormone patterning prior to  
466 sepal initiation, translation defects in *drmy1* cause reduced synthesis of these proteins,  
467 decreasing them to a level insufficient to repress cytokinin signaling (Figure 7A).

468

469 We started testing the level of protein reporters for a variety of cytokinin signaling  
470 components, in *drmy1* vs. WT and/or under translation or TOR inhibition. We reasoned that, given  
471 that the transcript level of most cytokinin signaling components do not significantly differ between  
472 *drmy1* and WT inflorescence tissue (Figure S7B), any changes in the level of these protein  
473 reporters should reflect post-transcriptional regulation, including mRNA translation. For A-type  
474 ARR, we were unable to detect fluorescence in the inflorescence of a published *pARR4::ARR4-GFP* line<sup>90</sup>. We reasoned that this was because A-type ARR have low protein levels (none was  
475 detected in our proteomics dataset) and short half-lives<sup>91</sup>. We therefore employed LlamaTagging,  
476 a recently developed method to visualize the abundance of nuclear-localized proteins with short  
477 half-lives<sup>92</sup>. Rapidly degraded proteins cannot be visualized through fusion with standard  
478 fluorescent proteins, because fluorescent proteins take time to mature before they fluoresce, and  
479 the protein of interest is degraded before the maturation of the fluorescent protein. On the other  
480 hand, the LlamaTag folds immediately. A LlamaTag with a high affinity for GFP can be encoded  
481 as a translational fusion with a nuclear-localized protein of interest. Soon after translation, the  
482 fusion immediately binds cytoplasm-localized GFP and translocates it to the nucleus. Thus,  
483 increased GFP fluorescence in the nucleus indicates higher abundance of the protein of interest  
484 (Figure 7B).

485

486 We focused on ARR7, the most highly expressed A-type ARR in our inflorescence RNA-  
487 seq (Figure S7B) which was also shown to be nuclear-localized<sup>93,94</sup>. We designed a construct with  
488 ARR7 fused with GFP-specific LlamaTag by a short linker, driven by the ARR7 native promoter  
489 (*pARR7::ARR7-linker-llama-ARR7ter*; *ARR7-llama* for short). This construct was co-transformed  
490 with cytoplasm-localized GFP containing a nuclear exclusion signal (*pUBQ10::sfGFP-nes-UBQ3ter*,  
491 *GFP-nes* for short; Figure 7C). As a proof of concept, we treated this reporter in WT  
492 background with 200 μM BAP. We found that GFP signal became more nuclear-localized within  
493 5 hours of the treatment (Figure S7C-D), agreeing with an increased expression and stability of  
494 A-type ARR proteins upon cytokinin application as previously reported<sup>91,95</sup>.

495

496 We then compared the localization of GFP signal in floral meristems of WT and *drmy1*  
497 before sepal initiation. According to the null hypothesis, increased cytokinin signaling in *drmy1*  
498 would cause an increase in ARR7 protein level and thus more nuclear-localized GFP signal in  
499 *drmy1* *ARR7-llama* *GFP-nes* than its WT counterpart. This is because cytokinin signaling  
500 increases the gene expression and protein stability of A-type ARR<sup>88,91,95,96</sup>. In contrast, according  
501 to our hypothesis, insufficient protein synthesis of A-type ARR contributes at least in part to  
502 increased in cytokinin signaling in *drmy1*, so we expect to see reduced ARR7 protein level and  
503 thus more cytoplasm-localized GFP signal in *drmy1* *ARR7-llama* *GFP-nes*. We found that WT  
504 buds had slightly more nuclear-localized GFP signal than cytoplasm-localized GFP signal, with  
505 brighter spots corresponding to the nucleus surrounded by darker grooves in between

## Translation and developmental robustness

507 corresponding to the cytoplasm (Figure 7D,E). In contrast, in the periphery of *drmy1* buds, GFP  
508 signal localizes more to the cytoplasm than to the nucleus, with darker spots surrounded by  
509 brighter grooves (Figure 7D,E). More nuclear GFP was present near the center of *drmy1* buds.  
510 This result indicates nuclear ARR7 protein concentration is reduced in the *drmy1* mutant,  
511 particularly in the zone where sepals initiate. To see whether this conclusion holds in other  
512 translation-inhibited conditions, we treated WT plants carrying the *ARR7-llama* and *GFP-nes*  
513 reporters with the translation inhibitor CHX and the TOR inhibitor AZD-8055. 2  $\mu$ M CHX treatment  
514 for 24 hours drastically reduced the nuclear localization of the GFP signal and increased its  
515 cytoplasmic localization (Figure 7F). 2  $\mu$ M AZD-8055 treatment for 72 hours had a milder but  
516 similar effect (Figure 7G). These treatments did not affect the localization of the GFP signal in  
517 plants without *ARR7-llama* (Figure S7E-H). These results show that conditions that decrease  
518 global protein synthesis greatly decrease the nuclear level of ARR7 protein.  
519

520 We also tested whether TOR or translation inhibition alter the protein level of AHP6. To  
521 this end, we imaged the *pAHP6::AHP6-VENUS*<sup>16</sup> protein reporter under mock, CHX, or AZD-8055  
522 treatment. While mock-treated buds highly accumulate the AHP6 protein in the four incipient sepal  
523 primordia, buds treated with CHX or AZD-8055 abolished AHP6 accumulation within 72 hours  
524 (Figure 7H). The *pAHP6::GFP-ER*<sup>97</sup> transcriptional reporter does not change under these  
525 treatments (Figure 7I), in agreement with our RNA-seq data of WT vs. *drmy1* (Figure S7B),  
526 suggesting that the change in AHP6 protein level is due to post-transcriptional regulation such as  
527 altered translation.  
528

529 It is possible that inhibition of TOR and translation results in a general, uniform reduction  
530 in the level of all proteins, not just for the cytokinin signaling inhibitors ARR7 and AHP6, but also  
531 for the positive regulators of cytokinin signaling. For this, we tested whether AHP3, a component  
532 of the cytokinin phosphorelay<sup>98,99</sup>, respond to TOR and translation inhibition. CHX treatment did  
533 not affect the level or spatial localization pattern of the *pAHP3::AHP3-GFP* reporter<sup>100</sup>, while AZD-  
534 8055 treatment only mildly decreased its level (Figure S7I). We also tested how the level of other,  
535 more generic proteins respond to TOR and translation inhibition. Unexpectedly, the level of  
536 *pUBQ10::mCherry-RCI2A* increased upon 72 hours of CHX or AZD-8055 treatments (Figure  
537 S7J). Overall, these results show that TOR and translation inhibition does not result in a uniform  
538 reduction in the level of all proteins, but specific proteins such as ARR7 and AHP6 are dramatically  
539 decreased. Further, these results are consistent with our hypothesis that depletion of cytokinin  
540 signaling inhibitor proteins, including ARR7 and AHP6, may underlie the upregulation of cytokinin  
541 signaling when the floral meristem is under TOR or translation inhibition (Figure 4).  
542

543 Having shown a reduction in the level of ARR7 and AHP6 greater than other proteins  
544 under TOR and translation inhibition, we next tested whether such a reduction contributes to the  
545 variability in sepal initiation also seen under such conditions (Figure 2). High-order mutant of A-  
546 type ARR<sub>s</sub> (*arr3,4,5,6,7,8,9,15*<sup>101</sup>) shows reduced size of the inner sepal primordium (Figure 7J,K)  
547 and a minor but significant increase in the positional variability of sepal primordia compared to  
548 WT (Figure 7Q), although sepal primordium number remains robust (Figure 7P). The *ahp6*

## Translation and developmental robustness

549 mutant<sup>16</sup> shows great variability of sepal primordium number, position, and size, although to a  
550 lower extent than *drmy1* (Figure 7J,L,P,Q). Similarly, if the reduction of ARR7 level in *drmy1*  
551 contributes to variability in sepal initiation, increasing ARR7 expression should restore sepal  
552 initiation robustness. While *ARR7-llama GFP-nes* plants phenocopy WT (Figure 7M), introducing  
553 the *ARR7-llama GFP-nes* constructs into *drmy1* plants partially restores robustness in sepal  
554 initiation, particularly in the position of sepal primordia (Figure 7N-Q). In older buds, while *drmy1*  
555 buds show great variability in sepal number and size resulting in gaps, some buds of *drmy1 ARR7-*  
556 *llama GFP-nes* have robustly sized sepals that are able to close properly (Figure S7K-N). Overall,  
557 these results show that reducing the level of cytokinin signaling inhibitor proteins ARR7 and AHP6  
558 create variability in sepal primordium initiation, and increasing their level in *drmy1* partially  
559 restores robustness. We propose that, during hormone patterning prior to sepal initiation, the rapid  
560 synthesis of these inhibitor proteins in response to auxin and cytokinin signaling is crucial for  
561 maintaining the homeostasis of cytokinin signaling and thus the robustness in sepal initiation.  
562

563 We also considered other hormone-related proteins that are dynamically regulated during  
564 organogenesis and thus may be depleted under translation defects. AUXIN/INDOLE-3-ACETIC  
565 ACID INDUCIBLE (Aux/IAA) proteins are auxin signaling inhibitors that are rapidly induced by  
566 auxin<sup>102,103</sup>. They bind auxin and are rapidly degraded by the ubiquitin E3 ligase SKP1, CUL1, F-  
567 BOX PROTEIN (SCF) complex involving TRANSPORT INHIBITOR RESPONSE1/AUXIN  
568 SIGNALING F-BOX (TIR1/AFB)<sup>104-107</sup>. Degradation is dependent on the Short Linear Motif (SLiM)  
569 degron contained within Domain II (DII)<sup>106-108</sup>. We hypothesized that the level of DII-containing  
570 proteins including Aux/IAAs would be drastically decreased in translation-inhibited conditions  
571 such as *drmy1* because they are unable to be rapidly synthesized to keep up with their  
572 degradation upon auxin signaling. To test this, we used the R2D2 reporter<sup>109</sup>, which contains a  
573 DII fused with 3xVENUS (*pUS7Y::DII-n3xVENUS*), and as a control, a mutated non-degraded DII  
574 fused with *tdTomato* (*pUS7Y::mDII-ntdTomato*). We compared this reporter in *drmy1* vs. WT. The  
575 ratio of *VENUS* to *tdTomato* was not reduced in *drmy1*, but instead slightly but significantly  
576 elevated (Figure S7O-P). In addition, *drmy1* has stochastic patches of DII-VENUS degradation,  
577 consistent with its often mislocalized auxin maxima (Figure 4A, S4B), unlike WT which had four  
578 patches of degradation corresponding to the four incipient sepal primordia where auxin maxima  
579 robustly form (Figure 4A, S4A). Overall, these results suggest that the level of DII-containing  
580 Aux/IAA proteins is not reduced in *drmy1*, despite the high requirement for synthesis due to their  
581 rapid turnover. They also indicate that not all proteins that are dynamically regulated in response  
582 to hormone signaling are equally affected by translation inhibition, which may result in different  
583 changes in hormone signaling output under such condition.  
584  
585

## 586 DISCUSSION

587 Robustness, the strikingly reproducible development of phenotype, has fascinated  
588 biologists for decades<sup>2</sup>. The *Arabidopsis* flower robustly develops four sepals of equal size. This  
589 stems from the robust initiation of four sepal primordia from the floral meristem, which is in turn

## Translation and developmental robustness

591 dictated by the robust patterning of auxin and cytokinin controlled by DRMY1<sup>27</sup>. Here we  
592 elucidated how DRMY1 controls robust hormone patterning and thus robust sepal initiation. We  
593 show that DRMY1 sustains TOR activity, ribosomal content, and translation. We further show that  
594 inhibition of TOR activity or translation is sufficient to cause variability in the timing, position, and  
595 number of sepal primordia, mimicking the *drmy1* phenotype. Our findings are in concert with  
596 previous studies that have shown robustness is often maintained by genes involved in central  
597 cellular processes<sup>2</sup>. In our case, the rate of translation in wild type maintains proper levels of  
598 ARR7 and AHP6, two cytokinin signaling inhibitor proteins, which need to be rapidly synthesized  
599 to dampen cytokinin signaling. Homeostasis of cytokinin signaling ensures robustness in auxin  
600 signaling patterns, and thus robustness in sepal initiation (Figure 7R, top). In the *drmy1* mutant,  
601 the reduced TOR activity, ribosomal content, and translation rate causes inability to rapidly  
602 synthesize these inhibitor proteins. Consequently, cytokinin signaling is elevated, disrupting the  
603 robust spatial pattern of auxin signaling, leading to variable sepal initiation (Figure 7R, bottom).  
604 Blocking cytokinin signaling in *drmy1* is sufficient to restore robust initiation of four sepal  
605 primordia, but has severe consequences on the overall fitness of the plant. Our results reveal how  
606 defects in hub cellular processes such as TOR signaling and translation can have tissue-specific  
607 phenotypic effects.

608

609 Although we propose that reduced TOR activity and mRNA translation affects  
610 developmental robustness through reduced synthesis of ARR7 and AHP6, we do not exclude  
611 other potential mechanisms that could contribute to the *drmy1* phenotype. For example, we  
612 observed that several subunits of the 26S proteasome are more abundant in *drmy1* than in WT  
613 (Supplemental Dataset 1), which could reflect or influence the accumulation of proteotoxic  
614 peptides and disrupt protein homeostasis<sup>110-114</sup>. This accumulation of 26S proteasomes could  
615 function upstream and/or downstream of the defect in TOR activity that impacts robust  
616 organogenesis<sup>34,115-120</sup>. Substantial future research will be needed to comprehensively define  
617 how DRMY1 participates in the complex interactions among TOR, mRNA translation, and  
618 proteolysis.

619

620 It was discovered long ago that extrinsic cytokinin application to plant tissue or cell-free  
621 extracts can promote mRNA translation<sup>75-78</sup>. Recent studies further confirmed that the up-  
622 regulation of translation by cytokinin is at least in part mediated by the cytokinin signaling  
623 pathway<sup>74,82</sup>. Here, we show that cytokinin signaling in floral buds is upregulated in translation-  
624 inhibited conditions, such as *drmy1*, AZD-8055 treatment, or CHX treatment (Figure 4), through  
625 reduced level of cytokinin inhibitor proteins (Figure 7; also potentially through other untested  
626 mechanisms). The enhanced cytokinin signaling maintains translation rate at a level necessary  
627 for the survival and reproduction of the plant (Figure 6). We propose that this represents a  
628 homeostasis mechanism where plants leverage increased cytokinin signaling to rescue the  
629 translation rate reduction caused by deficient TOR activity and ribosomal content (Figure 7R,  
630 bottom). It remains to be tested how widely this mechanism is applicable to other mutants with  
631 ribosomal defects, or whether parallel mechanisms operate in other species across kingdoms.

632

## Translation and developmental robustness

633 While translation-inhibited plants likely upregulate cytokinin signaling to maintain protein  
634 synthesis, this upregulation negatively affects developmental robustness. We have previously  
635 shown that exogenous cytokinin application to the WT floral meristem increases variability in PIN1  
636 convergence and auxin signaling patterns, and consequently, in sepal initiation. These effects are  
637 more pronounced in the *drmy1* mutant, which by itself has increased and diffuse cytokinin  
638 signaling<sup>27</sup>. Here, we provide additional evidence that increased and diffuse cytokinin signaling is  
639 necessary for such variability. While *drmy1* and CHX-treated WT floral meristems are variable in  
640 auxin signaling pattern and sepal initiation (Figure 2, 4), mutations in *wol* and *arr1,10,12*, which  
641 decreases cytokinin signaling, largely restore robustness (Figure 5). Robustness is also restored  
642 in the mature sepals of *drmy1 wol* and *drmy1 arr1,10,12*, enabling sepal closure (Figure S6).  
643 Similar effects in restoring robustness are seen when an extra functional transgene of *ARR7*  
644 (*pARR7::ARR7-llama*) is introduced to the *drmy1* mutant (Figure 7J-Q, S7K-N). Our results  
645 suggest that cytokinin upregulation is necessary and sufficient for variability in auxin patterning  
646 and sepal initiation, indicating that the cytokinin signaling changes are primary defects in *drmy1*,  
647 and the auxin signaling changes are secondary. Our results suggest a mechanism different from  
648 that previously reported in *ul4y*, *ul18z*, and *el24y*, where ribosomal mutations affect auxin  
649 signaling through reduced translation reinitiation of uORF-containing mRNAs, including those of  
650 AUXIN RESPONSE FACTOR (ARF) 3, 5, and 7<sup>64-66</sup>. While we found that uORF-containing  
651 mRNAs generally have reduced protein-transcript ratio in *drmy1* suggestive of reduced  
652 translation, we did not see a consensus reduction in the level of uORF-containing promoter  
653 reporters of ARFs (Figure S5). This suggests that the variable auxin signaling pattern in *drmy1* is  
654 unlikely to result from changes in uORF-mediated translational regulation of ARFs. Overall, our  
655 results suggest that homeostasis in cytokinin signaling is crucial for maintaining robust patterns  
656 of auxin signaling and robust morphogenesis in the floral meristem.  
657

658 Mutations affecting ribosome abundance or translation have long attracted interest due to  
659 the surprisingly tissue-specific phenotypes they cause<sup>121</sup>. In humans, these mutations have been  
660 associated with diseases collectively known as ribosomopathies, where patients show various  
661 abnormalities in blood, skeleton, hair, teeth, and pancreas, as well as intellectual disability and  
662 increased risk of cancer<sup>122-127</sup>. Ribosomal protein mutants have been characterized in numerous  
663 other species with similarly diverse impacts. They display a range of specific phenotypic changes,  
664 such as altered pigmentation and skeletal structure in mouse<sup>128-130</sup> and zebrafish<sup>131</sup>, shorter  
665 bristles and notched wing margins in fruit fly<sup>23,132</sup>, abnormal gonad development in worm<sup>133</sup>, and  
666 pointed leaves and abnormal vascular patterning in *Arabidopsis*<sup>64,66,134-136</sup>. Here, we show that  
667 the *Arabidopsis* mutant *drmy1* has reduced TOR activity, ribosomal content, and translation rate,  
668 causing variable sepal initiation which phenocopies the ribosomal mutants *ul4y* and *ul18z* and the  
669 TORC1 assembly mutant *spaghetti-1* (Figure 2, 3). We therefore propose that *drmy1* is an  
670 *Arabidopsis* ribosomopathy mutant like those previously characterized<sup>135</sup>.  
671

672 Several mechanisms have been proposed to explain why ribosomopathies do not usually  
673 cause a general reduction in growth, but rather affect development in tissue-specific ways. These  
674 include extra-ribosomal functions of certain ribosomal proteins<sup>137-141</sup>, altered translation behavior

## Translation and developmental robustness

675 of ribosomal variants on certain mRNAs<sup>142</sup>, different competitiveness of mRNAs for scarce  
676 ribosomes<sup>64–66,143–146</sup>, and high translation rate requirement for certain proteins<sup>147,148</sup>. For example,  
677 neurotransmitter release in animals relies on constant synthesis of the synaptic vesicle protein  
678 Syt1<sup>149</sup>. A *Drosophila* *Minute* mutant, *uS15*+/+, shows reduced synthesis of Syt1, which in turn  
679 reduces ecdysone secretion in 5-HT neurons, causing delayed larval-to-pupal transition<sup>147</sup>.  
680 Similarly, the human apoptosis inhibitor Mcl-1 has a half-life of ~30 min and thus requires a high  
681 translation rate to maintain its proper level. Under translation inhibition, the synthesis of Mcl-1 is  
682 unable to keep up with its degradation, causing apoptosis<sup>148</sup>. Here, we show that the levels of  
683 ARR7 and AHP6, which are rapidly induced by cytokinin and auxin signaling, respectively<sup>150,151</sup>,  
684 are drastically reduced under translation inhibition, which underlies the upregulation of cytokinin  
685 signaling and loss of robustness in auxin signaling and morphogenesis (Figure 7R). This  
686 mechanism parallels those previously found in animal systems<sup>147,148</sup>, highlighting how  
687 downregulation of proteins with high translational requirements can underlie the tissue-specificity  
688 of ribosomopathy. Outside the floral meristem, the *drmy1* mutant shows other phenotypic changes  
689 such as enlarged shoot apical meristem, reduced apical dominance, phyllotaxy defects, and  
690 reduced root system, all of which are related to altered cytokinin/auxin signaling activity<sup>27</sup>. Thus,  
691 our work highlights how defects in translation, which occurs in every cell, can have tissue-specific  
692 effects on how cells robustly arrange into organs.  
693

694 In addition, we note that not all proteins are equally reduced under broad translation  
695 inhibition. Our data suggest that the cytokinin signaling inhibitor proteins ARR7 and AHP6 are  
696 drastically reduced, compared to others such as AHP3, RCI2A, and GFP-nes. This suggests that  
697 the observed increase in cytokinin signaling under translation inhibition may be due to an  
698 imbalance in the relative levels of activators and inhibitors, which may further suggest that the  
699 inhibitor proteins are more temporally dynamic and thus have higher translational requirements  
700 during development. These hypotheses remain to be tested in future studies.  
701  
702

## 703 ACKNOWLEDGEMENTS

704 We thank Bella Burda, Frances Clark, Byron Rusnak, Erich Schwarz, Avilash Yadav, and Maura  
705 Zimmermann for comments and suggestions on the manuscript. We thank Frank Wellmer for the  
706 *ap1 cal 35S::AP1-GR* (Ler) seeds, Elliot Meyerowitz and Arnavaz Garda for the *DR5::3xVENUS-*  
707 *N7/PIN1::GFP* (Ler) seeds, Teva Vernoux and Géraldine Brunoud for the *TCS::GFP*, *TCS-DR5*  
708 (Col), *ahp6*, *pAHP6::AHP6-VENUS*, and *pAHP6::GFP-ER* seeds, Jan Smalle for the *arr1-1*  
709 *35S::ARR1* seeds, Joseph Kieber and Jamie Winshell for the *arr3,4,5,6,7,8,9,15* and  
710 *pARR4::ARR4-GFP* seeds, Thomas Greb and Min-Hao Chiang for the *pARF5::ER-ARF5-HDEL*  
711 seeds, and Jianru Zuo for the *pAHP3::AHP3-GFP* plasmid. We thank Georg Jander for advice  
712 and protocol for cytokinin extraction. We thank Brian Curtis and Frank Schroeder for help on mass  
713 spectrometry, and Sheng Zhang and Qin Fu for help on Xcalibur. We thank Richie Ragas, Yanã  
714 Rizzieri, and Ziqing Wei for assistance on experiments and data analysis. We thank Vicky  
715 Spencer and Minsung Kim for sharing the *in vivo* Torin2 treatment protocol. We thank Arabidopsis  
716 Biological Resource Center for providing seed stocks and plasmids used in this research.

## Translation and developmental robustness

717 Research reported in this publication was supported by the National Institute of General Medical  
718 Sciences of the National Institutes of Health (NIH) under award numbers R01GM134037,  
719 DP5OD023072, and R01GM145814; Cornell Graduate School new student fellowship (S.K.); and  
720 in part by a Schmittau-Novak Grant from the School of Integrative Plant Science, Cornell  
721 University (M.Z.). H.G.G. was supported by NIH Director's New Innovator Award (DP2  
722 OD024541-01) and NSF CAREER Award (1652236), NIH R01 Award (R01GM139913), and the  
723 Koret-UC Berkeley-Tel Aviv University Initiative in Computational Biology and Bioinformatics.  
724 H.G.G. is also a Chan Zuckerberg Biohub Investigator. We thank the Metabolomics Workbench<sup>152</sup>  
725 for providing the data repository for our cytokinin mass spectrometry data, which is funded by NIH  
726 under award numbers U2C-DK119886 and OT2-OD030544. We thank the Biotechnology  
727 Resource Center (BRC) Genomics Facility (RRID:SCR\_021727) of Cornell University for  
728 performing RNA-seq on *ap1 cal AP1-GR* inflorescence samples. We thank Novogene for  
729 performing seedling RNA-Seq library synthesis and sequencing. We thank the BRC Proteomics  
730 Facility (RRID:SCR\_021743) of Cornell University for performing mass spectrometry on *ap1 cal*  
731 *AP1-GR* inflorescence samples, and NIH SIG Grant 1S10 OD017992-01 for supporting the  
732 Orbitrap Fusion mass spectrometer. The content is solely the responsibility of the authors and  
733 does not necessarily represent the official views of the National Institutes of Health.

734

735

## 736 AUTHOR CONTRIBUTIONS

737 S.K.: Conceptualization, Investigation, Formal Analysis, Visualization, Writing - Original Draft,  
738 Writing - Review & Editing. M.Z.: Conceptualization, Investigation, Formal Analysis, Writing -  
739 Review & Editing. M.R.S: Investigation, Visualization. D.P.: Investigation, Formal Analysis,  
740 Visualization. L.J.: Investigation. R.E.M.: Investigation, Formal Analysis. S.A.: Methodology,  
741 Resources. B.V.L.V.: Methodology, Resources, Writing - Review & Editing. H.G.: Methodology,  
742 Resources, Writing - Review & Editing, Supervision. S.B.Q: Writing - Review & Editing,  
743 Supervision. J.O.B.: Resources, Writing - Review & Editing, Supervision. A.H.K.R:  
744 Conceptualization, Writing - Review & Editing, Supervision, Project administration, Funding  
745 acquisition.

746

747

## 748 DECLARATION OF INTERESTS

749 The authors declare no competing interests.

## Translation and developmental robustness

### 750 **FIGURE TITLES AND LEGENDS**

751

#### 752 **Figure 1. *drmy1* has reduced ribosome abundance, translation rate, and TOR activity.**

753 **(A)** Top row, stage 12 buds of WT (left) and *drmy1* (right) viewed from the side. Asterisk shows  
754 the gap between sepals with petals and carpels exposed. Middle row, stage 12 buds of WT (left)  
755 and *drmy1* (right) viewed from the top. Arrowheads point to sepals. Note that the *drmy1* bud has  
756 5 sepals of unequal size and unevenly spaced, exposing the stamens and carpels. Bottom row,  
757 stage 5 buds of WT (left) and *drmy1* (right) containing 35S::*mCitrine-RC12A* (plasma membrane  
758 marker). Arrowheads point to sepal primordia. Note that the *drmy1* bud has 5 sepal primordia of  
759 different sizes. Scale bars are 0.5 mm for stage 12 bud images and 25  $\mu$ m for stage 5 bud images.

760 **(B)** Gene ontology (GO) enrichment of downregulated genes in *drmy1* compared to WT, in the  
761 *ap1 cal AP1-GR* background. Shown are the top 8 GO terms and their enrichment p-values. A  
762 complete list can be found in Supplemental Dataset 1. Arrowheads highlight terms related to  
763 ribosome biogenesis or translation.

764 **(C)** Polysomal profiles of WT (blue) and *drmy1* (red) in the *ap1 cal AP1-GR* background,  
765 representative of 3 biological replicates each. Additional replicates are in Supplemental Dataset  
766 2. M, monosomes. P, polysomes.

767 **(D)** Puromycin labeling of WT vs *drmy1*. Left, WT and *drmy1* seedlings. From left to right: WT pre-  
768 treated with CHX, two biological replicates of WT pre-treated with mock, and two biological  
769 replicates of *drmy1* pre-treated with mock. All groups were then treated with puromycin. For  
770 seedlings to match in size, WT seedlings were 8 days old and *drmy1* seedlings were 10 days old.  
771 Right, WT and *drmy1* inflorescences of induced *ap1 cal AP1-GR* background. From left to right:  
772 WT co-treated with puromycin and CHX, three biological replicates of WT treated with puromycin,  
773 and three biological replicates of *drmy1* treated with puromycin. In both experiments, RuBisCO  
774 large subunit on Ponceau S-stained membrane is shown as a loading control (bottom). Ratio  
775 between puromycin and Ponceau S signals, normalized by the mean of WT, is shown on the  
776 bottom (p-values are from two-sided Student's t-test).

777 **(E)** Gene ontology (GO) enrichment of differentially accumulated proteins in *drmy1* compared to  
778 WT, in the *ap1 cal AP1-GR* background. Shown are the top 8 GO terms and their enrichment p-  
779 values. A complete list can be found in Supplemental Dataset 1. Arrowheads highlight terms  
780 related to ribosome biogenesis or translation.

781 **(F-G)** Coherent alteration of gene expression by *drmy1* and AZD-8055 TOR inhibitor treatment.  
782 **(F)** Scatterplot of RNA log2 fold change in *drmy1* vs WT (x-axis), and WT+AZD vs WT+Mock (y-  
783 axis), in 7-day-old seedlings. Genes are color-coded based on the following categories: genes in  
784 "Structural constituents of the ribosome" (GO:0003735) and its offspring terms (magenta); all  
785 other genes in "Translation" (GO:0006412) and its offspring terms (orange); all other genes (gray).  
786 Blue line shows a linear regression of all points ( $R^2 = 0.1446$ ,  $p < 2.2 \times 10^{-16}$ ). **(G)** Of the 466 genes  
787 that are differentially expressed under both conditions, 439 (94%) are coherently altered by AZD-  
788 8055 treatment and the *drmy1* mutation.

789 **(H-I)** Phosphorylation of the direct TOR substrate, S6K-pT449, in WT and *drmy1*. **(H)** A  
790 representative blot. Top, S6K-pT449. Middle, total S6K protein. Bottom, Ponceau S staining. Ratio  
791 between S6K-pT449 signal and Ponceau S signal is shown above the blots. **(I)** Ratio between

Translation and developmental robustness

792 S6K-pT449 and Ponceau S signals normalized by WT, quantified across in three experiments,  
793 shows that TOR activity decreased by half in *drmy1*. (mean  $\pm$  SD; \*, p<0.05).  
794

## Translation and developmental robustness

795 **Figure 2. Defects in TOR activity, ribosome, and translation disrupt robust sepal initiation.**  
796 **(A-G)** Representative images of stage 5 buds in WT (A), *drmy1* (B), *ul4z* (C), *ul4y* (D), *ul18z* (E),  
797 *lst8-1-1* (F), and *spaghetti-1* (G). Tissue morphology is visualized by either propidium iodide (a  
798 cell wall-staining dye) or a plasma membrane marker. Arrowheads indicate sepal primordia that  
799 are variable in number, position, and size. Note that *ul4z* flowers always develop four sepal  
800 primordia, although of different sizes; *lst8-1-1* occasionally (4/41, 9.8%) develops buds with more  
801 than four sepal primordia.  
802 **(H)** Quantification of sepal primordium number, comparing *drmy1* (n = 67 buds), *ul4z* (n = 52  
803 buds), *ul4y* (n = 53 buds), *ul18z* (n = 52 buds), *lst8-1-1* (n = 41 buds), and *spaghetti-1* (n = 84  
804 buds) with WT (n = 51 buds). Asterisks indicate statistically significant ( $p < 0.05$ ) differences from  
805 WT in Fisher's contingency table tests.  
806 **(I)** Illustration of robust versus variable positioning of sepal primordia. Primordia are considered  
807 robustly positioned if they are evenly distributed around the edge of the bud. Within each bud,  
808 angles between adjacent primordia with respect to the center of the bud are measured, and  
809 coefficient of variation (CV) is calculated. A bud with robustly positioned primordia would have  
810 similar angular values and a low CV value. A bud with variably positioned primordia would have  
811 very different angular values and a high CV value.  
812 **(J)** Quantification of variability in primordium positioning (CV) in the same buds as in (H), following  
813 illustration in (I). Asterisks indicate statistically significant ( $p < 0.05$ ) differences from WT in  
814 Wilcoxon's rank sum tests.  
815 **(K)** Representative images of buds from *in vitro*-cultured WT inflorescences treated with mock or  
816 2  $\mu$ M CHX for 9-10 days. Arrowheads indicate sepal primordia that are variable in number,  
817 position, and size.  
818 **(L)** Representative images of buds from WT plants treated with mock or 2 nmol Torin2 for 15  
819 days. Arrowheads indicate sepal primordia that are variable in number, position, and size.  
820 **(M-N)** Quantification of sepal primordium number (M) and positional variability (N) similar to (H,J),  
821 comparing CHX-treated (n = 31 buds), CHX-mock (n = 42 buds), Torin2-treated (n = 51 buds)  
822 and Torin2-mock buds (n = 56 buds). Scale bars in all micrographs, 25  $\mu$ m.

## Translation and developmental robustness

823 **Figure 3. TOR and ribosomal defects cause variability in the timing of sepal initiation.**  
824 **(A-C)** 6h-interval live imaging of the sepal initiation process in WT (A) and *ul4y* (B), which is  
825 quantified in (C). n = 48 buds for WT; n = 40 buds for *ul4y*.  
826 **(D-F)** 6h-interval live imaging of the sepal initiation process in buds from WT plants treated with  
827 mock or 2 nmol Torin2 twice a day for 15 days, which is quantified in (F). n = 31 buds for mock; n  
828 = 15 buds for Torin2.  
829 In **(A,B,D,E)**, top rows show the 35S::*mCitrine-RCI2A* membrane marker, and bottom rows show  
830 Gaussian curvature heatmaps of the same image stacks. Asterisks indicate sepal initiation  
831 events, defined as a dark red band (primordium with positive curvature) separated from the floral  
832 meristem by a dark blue band (boundary with negative curvature) in the heatmap. Scale bars, 25  
833  $\mu\text{m}$ .  
834 In **(C,F)**, the amount of time between outer and inner sepal initiation (left) and between outer and  
835 lateral sepal initiation (right) were calculated for each bud. Bar plot shows mean  $\pm$  SD which is  
836 also shown on top of each plot. Asterisks indicate statistically significant differences ( $p < 0.05$ ) in  
837 Wilcoxon's rank sum test (for mean) or Levene's test (for SD).

838

## Translation and developmental robustness

839 **Figure 4. Inhibition of TOR activity and translation cause variability in auxin and cytokinin  
840 signaling.**

841 **(A-D)** The ribosomal mutant *ul4y* loses robustness in auxin and cytokinin signaling. (A)  
842 Representative images of late stage 2 buds of WT, *drmy1*, and *ul4y*, showing the auxin signaling  
843 reporter *DR5::3xVENUS-N7* in yellow, the cytokinin signaling reporter *TCS::GFP* in cyan, and  
844 both merged with Chlorophyll (in WT) or *UBQ10::mCherry-RCI2A* (in *drmy1* and *ul4y*) in magenta.  
845 (B) Quantification of TCS intensity (integrated density divided by area) from maximum intensity  
846 projection images, normalized to mean of WT. Shown are mean  $\pm$  SD. Asterisks show statistically  
847 significant differences from WT in two-tailed Student's t-tests (*drmy1*,  $p = 2.1 \times 10^{-6}$ ; *ul4y*,  $p =$   
848  $3.4 \times 10^{-5}$ ). (C) Circular histogram of DR5 signal distribution. Each bud was divided into 360 sectors  
849 of 1° each. Within each sector, DR5 signal measured in pixel intensity units (0-255 range) was  
850 summed. This sum was plotted along the x-axis starting from the sector at 1:30 position (between  
851 the incipient outer sepal and incipient right sepal) going counterclockwise. I.e., in WT, the outer  
852 sepal is near 45°, the inner sepal near 225°, and the lateral sepals near 45° and 135° (vertical  
853 dotted lines). The mean was plotted as a solid line, and mean  $\pm$  SD was plotted as a shaded area.  
854 (D) Circular histogram of TCS signal distribution. Sample size for (A-D): WT,  $n = 12$  buds; *drmy1*,  
855  $n = 15$  buds; *ul4y*,  $n = 10$  buds.

856 **(E-H)** 3 days of translation inhibition causes increased and diffuse cytokinin signaling, and diffuse  
857 auxin signaling. (E) Representative images of late stage 2 WT buds treated *in vitro* with mock or  
858 2  $\mu$ M CHX for 3 days. Shown are *DR5::3xVENUS-N7* in yellow, *TCS::GFP* in cyan, and both  
859 merged with Chlorophyll in magenta. (F) Quantification of TCS intensity from maximum intensity  
860 projection images, normalized to mean of WT mock day 3. Shown are mean  $\pm$  SD. Asterisk shows  
861 statistically significant difference in a two-tailed Student's t-test ( $p = 2.0 \times 10^{-4}$ ). (G) Circular  
862 histogram of DR5 signal distribution. (H) Circular histogram of TCS signal distribution. Sample  
863 size for (E-H): WT mock day 3,  $n = 10$  buds; WT CHX day 3,  $n = 12$  buds.

864 **(I-L)** 6 days of TOR or translation inhibition causes increased and diffuse cytokinin signaling, and  
865 randomly positioned auxin signaling maxima. (I) Representative images of late stage 2 WT buds  
866 treated *in vitro* with mock, 2  $\mu$ M CHX, or 2  $\mu$ M AZD for 6 days. Shown are *DR5::3xVENUS-N7* in  
867 yellow, *TCS::GFP* in cyan, and both merged with Chlorophyll in magenta. Arrowheads point to  
868 randomly positioned auxin maxima. (J) Quantification of TCS intensity from maximum intensity  
869 projection images, normalized to mean of WT mock day 6. Shown are mean  $\pm$  SD. Asterisks show  
870 statistically significant differences from mock in two-tailed Student's t-tests (CHX,  $p = 1.0 \times 10^{-3}$ ;  
871 AZD,  $p = 1.2 \times 10^{-4}$ ). (K) Circular histogram of DR5 signal distribution. (L) Circular histogram of  
872 TCS signal distribution. Sample size for (I-L): WT mock day 6,  $n = 12$  buds; WT CHX day 6,  $n =$   
873 11 buds; WT AZD day 6,  $n = 10$  buds. Scale bars in all micrographs, 25  $\mu$ m.

## Translation and developmental robustness

874 **Figure 5. Cytokinin signaling is required for increased variability in auxin signaling and**  
875 **sepal initiation under translation inhibition.**

876 **(A-D)** Cytokinin treatment makes auxin signaling diffuse. Shown are late stage 2 WT buds under  
877 mock (A,B) or 5  $\mu$ M cytokinin (BAP) treatment (C,D) for 4 days. (A,C) Auxin signaling reporter  
878 *DR5* in yellow, and *DR5* merged with Chlorophyll in magenta. (B,D) Circular histograms of the  
879 *DR5* signal, showing mean (solid line) and mean  $\pm$  SD (shaded area). Arrows point to *DR5* signal  
880 in variable positions. Sample size: WT Mock n = 10, WT BAP n = 10. Also see Zhu et al. (2020),  
881 in this reference see Extended Data Figure 7e.

882 **(E-G)** Cytokinin signaling is required for variable sepal initiation in *drmy1*. (E) Stage 5 buds. Sepal  
883 primordia in *drmy1* are variable (arrowheads), which does not occur in *drmy1 arr1,10,12* and  
884 *drmy1 wol* mutants. (F,G) Quantification of sepal primordium number (F) and positional variability  
885 (G), comparing WT (n = 58) with *drmy1* (n = 31), *arr1,10,12* (n = 24) with *drmy1 arr1,10,12* (n =  
886 20), and *wol* (n = 36) with *drmy1 wol* (n = 39). Asterisks indicate statistically significant ( $p < 0.05$ )  
887 differences in Fisher's contingency table tests (F) and Wilcoxon's rank sum tests (G) respectively.

888 **(H-K)** Cytokinin signaling is required for variable patterning of auxin signaling in *drmy1*. Shown  
889 are late stage 2 buds of WT vs *drmy1* (H,I), and *arr1,10,12* vs *drmy1 arr1,10,12* (J,K). (H,J) Auxin  
890 signaling reporter *DR5* in yellow, and *DR5* merged with propidium iodide in magenta. Arrows point  
891 to diffuse *DR5* signal in variable positions of the *drmy1* bud. Arrowheads show four robust *DR5*  
892 maxima in the *drmy1 arr1,10,12* bud. (I,K) Circular histograms of the *DR5* signal, showing mean  
893 (solid line) and mean  $\pm$  SD (shaded area). For ease of visualization, circular histograms of *drmy1*  
894 and *drmy1 arr1,10,12* between 90 and 360 degrees are enlarged and shown as insets (y-axis  
895 range 0-0.4). Note the presence of *DR5* signal in inter-sepal regions in *drmy1* (black arrow) which  
896 is largely suppressed in *drmy1 arr1,10,12*. Sample size: WT n = 19, *drmy1* n = 16, *arr1,10,12* n =  
897 13, *drmy1 arr1,10,12* n = 9.

898 **(L-N)** Cytokinin signaling is required for variable sepal initiation under translation inhibition. (L)  
899 Stage 6 buds of WT, *arr1,10,12*, and *wol*, treated with Mock or 2  $\mu$ M CHX for 10 days. WT initiates  
900 sepal primordia at variable positions when treated with CHX (arrowheads), which does not occur  
901 in *arr1,10,12* and *wol*. (M,N) Quantification of sepal primordium number (M) and positional  
902 variability (N), comparing mock and CHX within each genotype. Sample size: WT Mock n = 29,  
903 WT CHX n = 19, *arr1,10,12* Mock n = 18, *arr1,10,12* CHX n = 19, *wol* Mock n = 15, *wol* CHX n =  
904 19. Asterisks indicate statistically significant ( $p < 0.05$ ) differences in Fisher's contingency table  
905 tests (M) and Wilcoxon's rank sum tests (N) respectively.

906 **(O-R)** Cytokinin signaling is required for diffuse auxin signaling under translation inhibition. Shown  
907 are late stage 2 buds of WT (O,P) and *arr1,10,12* (Q,R), treated with Mock or 2  $\mu$ M CHX for 3  
908 days. (O,Q) Auxin signaling reporter *DR5* in yellow, and *DR5* merged with Chlorophyll in magenta.  
909 Arrows point to diffuse *DR5* signal in variable positions in CHX-treated WT. Arrowheads show  
910 four robust *DR5* maxima in CHX-treated *arr1,10,12*. (P,R) Circular histograms of the *DR5* signal,  
911 showing mean (solid line) and mean  $\pm$  SD (shaded area). Sample size: WT Mock n = 17, WT CHX  
912 n = 18, *arr1,10,12* Mock n = 7, *arr1,10,12* CHX n = 7. Scale bars in all micrographs, 25  $\mu$ m.

913

## Translation and developmental robustness

914 **Figure 6. Upregulation of cytokinin signaling is required to maintain translation and fitness**  
915 **in *drmy1*.**  
916 **(A)** Puromycin labeling of WT seedlings with 4 h CHX pre-treatment (control), and three biological  
917 replicates each of WT and *arr1 35S::ARR1* seedlings with 4 h mock pre-treatment. All seedlings  
918 are 14 days old. RuBisCO large subunit in Ponceau S-stained membrane is shown as a loading  
919 control. Signal ratio between puromycin and Ponceau S, normalized to mean of WT, is show on  
920 the bottom. P-value is from a two-sided Student's t-test. Also see Karunadasa et al. (2020).  
921 **(B,C)** Puromycin labeling of WT seedlings with 4 h CHX pre-treatment (control), and two biological  
922 replicates of WT, *drmy1*, *wol*, and *drmy1 wol* seedlings with 4 h mock pre-treatment. Seedlings  
923 are 8 days old in (B) and 14 days old in (C). RuBisCO large subunit in Ponceau S-stained  
924 membrane is shown as a loading control. Letters show compact letter display of a Tukey's all-pair  
925 comparison in a one-way ANOVA model.  
926 **(D)** Representative 14 days old seedling images of WT, *drmy1*, *wol*, and *drmy1 wol* used in (C).  
927 Notice that *drmy1 wol* is very small and pale. Scale bars, 5 mm.  
928 **(E)** Representative aerial part images of 42 days old plants of WT, *drmy1*, *wol*, and *drmy1 wol*.  
929 Inset shows the zoomed-in *drmy1 wol* plant, which has a tiny rosette and a short inflorescence.  
930 Scale bars, 5 cm. See also Figure S6F.  
931 **(F)** Representative aerial part images of 74 days old plants of WT, *drmy1*, *arr1,10,12*, and *drmy1*  
932 *arr1,10,12*. Inset shows the zoomed-in *drmy1 arr1,10,12* plant, which has pale leaves  
933 accumulating anthocyanin and a short inflorescence. Scale bars, 5 cm. See also Figure S6E.  
934 **(G)** Dissected siliques of *arr1,10,12* (left) and *drmy1 arr1,10,12* (right) showing developing  
935 seeds. Notice that while *arr1,10,12* occasionally have aborted seeds, all seeds in the *drmy1*  
936 *arr1,10,12* siliques were aborted. Scale bars, 0.2 mm.

## Translation and developmental robustness

937 **Figure 7. ARR7 and AHP6 protein levels are reduced upon inhibition of TOR and**  
938 **translation.**

939 **(A)** The hypothesis. During hormone patterning prior to sepal initiation in the WT floral meristem,  
940 A-type ARR and AHP6 proteins are rapidly produced to dampen cytokinin signaling to a normal  
941 level. In *drmy1*, reduced protein synthesis causes reduced levels of these cytokinin signaling  
942 inhibitor proteins, resulting in an upregulation of cytokinin signaling.

943 **(B)** Illustration of Llama Tag. Plants were co-transformed with *ARR7-llama* (*pARR7::ARR7-linker-*  
944 *llama-ARR7ter*) and *GFP-nes* (*pUBQ10::sfGFP-nes-UBQ3ter*). Without *ARR7-llama*, GFP  
945 localizes to the cytosol due to the nuclear export sequence (nes). *ARR7-llama* is produced in the  
946 cytoplasm, C, and translocates into the nucleus, N. The Llama Tag on *ARR7-llama* binds to GFP  
947 and drags GFP into the nucleus (note that from our observation it is excluded from the nucleolus,  
948 NL). Thus, at low *ARR7-llama* levels, GFP signal is mainly in the cytoplasm. At intermediate  
949 *ARR7-llama* levels, GFP is at comparable levels between the cytoplasm and the nucleus, and no  
950 clear pattern can be seen. At high *ARR7-llama* levels, GFP is mainly seen in the nucleus.

951 **(C)** A *GFP-nes* bud showing localization of the GFP signal to the cytoplasm.

952 **(D,E)** GFP images of buds from two independent transgenic lines of *ARR7-llama GFP-nes*, 7-4  
953 (D) and 7-6 (E), of WT (top) vs *drmy1* (bottom) genotypes. Images are representative of n = 17  
954 (line 7-4, WT), n = 40 (line 7-4, *drmy1*), n = 9 (line 7-6, WT), and n = 6 (line 7-6, *drmy1*) buds.  
955 Note that GFP is more cytoplasm-localized in *drmy1* than WT, indicating reduced *ARR7-llama*  
956 protein level.

957 **(F)** GFP images of WT *ARR7-llama GFP-nes* buds treated with mock (top) or 2  $\mu$ M CHX (bottom)  
958 for 24 hours. The mock image is representative of n = 20 buds from three independent lines. The  
959 CHX image is representative of n = 19 buds from these same lines.

960 **(G)** GFP images of WT *ARR7-llama GFP-nes* buds treated with mock (top) or 2  $\mu$ M AZD-8055  
961 (bottom) for 72 hours. The mock image is representative of n = 13 buds from two independent  
962 lines. The AZD-8055 image is representative of n = 11 buds from these same lines. For (C-G),  
963 each image was brightened to reveal subcellular localization patterns of GFP. A square region  
964 taken from the image containing 5-10 cells is enlarged and shown on the top right. Within the  
965 square, GFP intensity was quantified along the dotted line and plotted on the bottom right. X-axis,  
966 pixels (range 0-238). Y-axis, GFP intensity (smoothed by taking the average intensity of 11-  
967 pixel neighborhoods; range 90-210 in gray value).

968 **(H-I)** Response of the AHP6 protein reporter (H) and transcriptional reporter (I) to mock, CHX,  
969 and AZD-8055 treatments for 72 hours. For (H), images are representative of n = 29 (mock), n =  
970 29 (CHX), and n = 34 (AZD-8055) buds in three experiments. For (I), images are representative  
971 of n = 11 (mock), n = 9 (CHX), and n = 12 (AZD-8055) buds in two experiments.

972 **(J-Q)** Reduction of A-type ARR and AHP6 protein levels contribute to the variability in sepal  
973 initiation. (J-O) Stage 5-6 buds of indicated genotype stained with propidium iodide. Arrowheads  
974 indicate sepal primordia that are variable in number, position, and/or size. Note that the  
975 *arr3,4,5,6,7,8,9,15* bud has an inner sepal that is slightly smaller than its outer sepal and  
976 positioned slightly right-skewed (K). The *ahp6* bud develops five sepal primordia of variable sizes  
977 and unevenly positioned (L). The *ARR7-llama GFP-nes* constructs partially rescue the *drmy1*  
978 phenotype in some buds (O, left) but not others (O, right). (P) Quantification of sepal primordium

## Translation and developmental robustness

979 number. Asterisk indicates statistically significance difference in a Fisher's exact test (WT vs  
980 *ahp6*,  $p = 3.026 \times 10^{-7}$ ; *drmy1* vs *drmy1 ARR7-llama GFP-nes*,  $p = 0.4389$ ). (Q) Quantification of  
981 variability in sepal primordium position. Asterisk indicates statistically significant difference in a  
982 Wilcoxon rank sum test (WT vs. *arr3,4,5,6,7,8,9,15*,  $p = 2.948 \times 10^{-4}$ ; WT vs *ahp6*,  $p = 2.137 \times 10^{-11}$ ;  
983 WT vs *ARR7-llama GFPnes*,  $p = 1$ ; *drmy1* vs *drmy1 ARR7-llama GFPnes*,  $p = 1.538 \times 10^{-7}$ ).  
984 Data for *drmy1* were reused from Figure 2H, 2J. Data for *ARR7-llama GFP-nes* and *drmy1 ARR7-llama GFP-nes*  
985 were pooled from two independent lines (7-4 and 7-6). Sample size: WT,  $n = 78$ ;  
986 *arr3,4,5,6,7,8,9,15*,  $n = 28$ ; *ahp6*,  $n = 106$ ; *ARR7-llama GFPnes*,  $n = 16$ ; *drmy1*,  $n = 67$ ; *drmy1 ARR7-llama GFP-nes*,  $n = 20$ .

987  
988 **(R)** Working model. In WT, DRMY1 maintains TOR activity and translation, which sustains the  
989 rapid production of cytokinin signaling inhibitors (ARR7 and AHP6) in response to cytokinin  
990 signaling. These inhibitors maintain cytokinin signaling at a normal level, allowing auxin and  
991 cytokinin signaling to interact and form robust spatial patterns. Robust patterning of auxin and  
992 cytokinin signaling gives rise to robustly initiated sepal primordia. In *drmy1*, due to decreased  
993 TOR signaling and translation rate, the meristem cannot rapidly produce cytokinin signaling  
994 inhibitor proteins in response to cytokinin signaling. As a result, cytokinin signaling is upregulated,  
995 which rescues the translation rate reduction in a homeostatic mechanism. This upregulation of  
996 cytokinin signaling disrupts the robust spatial pattern of both cytokinin and auxin signaling, which  
997 in turn causes variability in sepal initiation. Scale bars in all micrographs, 25  $\mu$ m.  
998

## Translation and developmental robustness

### 999 MATERIALS AND METHODS

1000

#### 1001 Plant material

1002 Most *Arabidopsis* plants were in Col-0 background (WT). *ap1 cal 35S::AP1-GR* was in Ler  
1003 background. *drmy1* (Col-0) was backcrossed to Ler twice and then crossed with *ap1 cal*  
1004 *35S::AP1-GR* to obtain *drmy1 ap1 cal 35S::AP1-GR*. R2D2 was originally in Col-Utrecht  
1005 background and was backcrossed twice into WT (Col-0) and *drmy1* (Col-0). The following mutants  
1006 and reporters were previously described: *drmy1-2*<sup>27</sup>, *wol-1*<sup>153</sup>, *spaghetti-1* (*tpr5-1*)<sup>154</sup>, *ahp6*<sup>16</sup>,  
1007 *arr3,4,5,6,7,8,9,15*<sup>101</sup>, *ap1 cal 35S::AP1-GR* (Ler)<sup>35,36</sup>, *arr1-1 35S::ARR1*<sup>74</sup>, *DR5::3xVENUS-*  
1008 *N7*<sup>155</sup>, *TCS::GFP*<sup>156</sup>, *pARF5::ER-EYFP-HDEL*<sup>157</sup>, *pUS7Y-mDII-NtdTomato-pUS7Y-DII-*  
1009 *N3xVENUS* (R2D2)<sup>109</sup>, *35S::mCirtine-RCI2A*<sup>27</sup>, *UBQ10::mCherry-RCI2A*<sup>27</sup>, *pAHP3::AHP3-*  
1010 *GFP*<sup>100</sup>, *pAHP6::AHP6-VENUS*<sup>16</sup>, and *pAHP6::GFP-ER*<sup>16,97</sup>. The following mutants and reporter  
1011 lines were obtained from *Arabidopsis* Biological Resource Center (ABRC): *ul4z* (SALK\_130595),  
1012 *ul4y* (SALK\_029203), *ul18z* (SALK\_089798), *arr1-3 arr10-5 arr12-1*<sup>158</sup> (CS39992), *Ist8-1-1*  
1013 (SALK\_002459), *pARF3::N3xGFP*<sup>159</sup> (CS67072), *pARF6::N3xGFP*<sup>159</sup> (CS67078),  
1014 *pARF8::N3xGFP*<sup>159</sup> (CS67082), *pARF10::N3xGFP*<sup>159</sup> (CS67086).

1015

#### 1016 Llama-tagged ARR7 construct

1017 For the LlamaTag system, we first generated plasmid *pVV13* containing linker-llama. We  
1018 amplified the LlamaTag (from a plasmid containing *vhhGFP4*<sup>160</sup>) and added a linker sequence of  
1019 *tccggagcagctcggtctccgctggcagcggccactagt* at its 5' end by two rounds of overlap PCRs.  
1020 Primers for the first round were oVV64 and oVV53, and primers for the second round were oVV35  
1021 and oVV53. After the second round, we A-tailed the PCR product according to the Promega  
1022 manufacturer's protocol. A-tailed product was ligated to the *pGEMTeasy* vector according to the  
1023 Promega ligation protocol, to create the plasmid *pVV13*.

1024 To make *pARR7::ARR7-llama*, a genomic fragment of *pARR7::ARR7* minus the stop  
1025 codon and terminator was amplified from the *Arabidopsis* (Col-0) genome using the primers  
1026 oSK197 and oSK198. The linker-llama fragment was PCR-amplified from *pVV13* using the  
1027 primers oSK199 and oSK200. The *ARR7* stop codon, 3' UTR, and terminator was amplified from  
1028 the *Arabidopsis* (Col-0) genome using the primers oSK201 and oSK202. *pMLBART* backbone  
1029 was digested with *NotI*, and all fragments were assembled into *pMLBART* using NEBuilder  
1030 according to the manufacturer's protocol.

1031 To make *pUBQ10::sfGFP-NES:UBQ3ter*, sfGFP sequence was amplified from the *35S-*  
1032 *sfGFP-nosT* plasmid<sup>161</sup> (Addgene # 80129) using primers UsfGM-F1 and UsfGnes-R1. The  
1033 *UBQ10* promoter was amplified from the *UPG* plasmid<sup>162</sup> (Addgene # 161003) using primers  
1034 OutALFd and UsfGM-R1. The *UBQ3* terminator was amplified from the *UPG* plasmid<sup>162</sup> (Addgene  
1035 # 161003) using primers UsfGnes-F1 and OutALRb. Primer overhangs spanning the junction  
1036 between sfGFP and the *UBQ3* terminator contain the sequence of the mouse PKI $\alpha$  NES.  
1037 *pCambia1300* backbone was digested with *BamHI* and *KpnI*, and all fragments were Gibson-  
1038 assembled into the backbone. Sequences of primers, *pARR7::ARR7-llama*, and *pUBQ10::sfGFP-*  
1039 *NES:UBQ3ter* can be found in Supplemental Dataset 5.

## Translation and developmental robustness

1040 Col-0 plants were co-transformed with *pARR7::ARR7-llama* and *pUBQ10::sfGFP-NES:UBQ3ter*, and selected with Basta (for *pARR7::ARR7-llama*) + Hygromycin (for *pUBQ10::sfGFP-NES:UBQ3ter*). Surviving T1 plants were screened for clear nuclear signal in the inflorescence, and 5 independent T1 plants were selected and crossed into *drmy1*. F2 plants from each line were again selected with Basta + Hygromycin and genotyped. One line showed co-segregation with the *DRMY1* locus. Two lines showed severe silencing in the F2 and could not be used. Two lines (7-4 and 7-6), though with minor silencing in F2, were used for imaging and image analysis. F3 plants of 7-4 and 7-6 had severe silencing, and therefore only F2 were imaged.

### 1049 Plant growth conditions

1050 For most experiments, seeds were sown in wetted Lamber Mix LM-111 soil and stratified  
1051 at 4°C for 3-5 days. For experiments including *drmy1 wol* and *drmy1 arr1,10,12*, all seeds were  
1052 sown onto ½ MS plates with 0.05% (w/v) MES, 1% (w/v) sucrose, 1.2% (w/v) agar, pH 5.7, and  
1053 stratified at 4°C for a week. They were grown for 7-10 days before being transplanted to soil (for  
1054 imaging of inflorescence or aerial part of the plant) or left on the plates until desired time of the  
1055 experiment (for seedling imaging or puromycin labeling).

1056 Most plants were grown under 16 h – 8 h light-dark cycles (fluorescent light, ~100 µmol  
1057 m<sup>-1</sup> s<sup>-1</sup>) at 22°C in a Percival walk-in growth chamber. We found that the *drmy1* phenotype is more  
1058 pronounced in this condition than under continuous light. The *ap1 cal 35S::AP1-GR* and *drmy1*  
1059 *ap1 cal 35S::AP1-GR* plants were grown in soil under continuous light at 16°C to prevent  
1060 premature floral induction.

1061

### 1062 Flower staging

1063 Flower buds were staged as previously described<sup>37</sup>. Briefly, stage 1 is when the floral  
1064 meristem emerges, but not yet separated, from the inflorescence meristem. Stage 2 is when the  
1065 floral meristem separates from the inflorescence meristem but with no floral organs initiated.  
1066 Stage 3 is when sepal primordia initiate. Stage 4 is when sepal primordia bend to cover part of  
1067 the floral meristem. Stage 5 is when stamen primordia initiate. Stage 6 is when sepal primordia  
1068 completely cover the floral meristem.

1069

### 1070 RNA-seq data collection and analysis

1071 For RNA-seq in the inflorescence, bolting *ap1 cal 35S::AP1-GR* and *drmy1 ap1 cal*  
1072 35S::AP1-GR plants were induced daily with an aqueous solution containing 10 µM  
1073 dexamethasone (Sigma-Aldrich), 0.01% (v/v) ethanol, and 0.015% (v/v) Silwet L-77  
1074 (Rosecare.com). When sepals initiated from the floral meristems, usually on the fourth day after  
1075 three daily inductions, three inflorescence samples per genotype (including inflorescence  
1076 meristems and buds under stage 6) were collected and immediately put into liquid nitrogen. RNA  
1077 extraction, library preparation, RNA-seq, and data analysis for inflorescence samples were done  
1078 as previously described<sup>27</sup> with a few changes. After read mapping, genes with at least two raw  
1079 reads in at least two biological replicates in either WT or *drmy1* were kept for downstream  
1080 analysis. For differentially expressed genes, we set a log2 fold change threshold of ±1 and a BH-  
1081 adjusted p-value threshold of 0.05. For GO term enrichment, gene-GO mapping data was

## Translation and developmental robustness

1082 obtained from TAIR (<https://www.arabidopsis.org>  
1083 /download\_files/GO\_and\_PO\_Annotations/Gene\_Ontology\_Annotations/ATH\_GO\_GOSLIM.txt)  
1084 . The R package “topGO”<sup>163</sup> (version 2.38.1) was used for the enrichment, with statistic “fisher”,  
1085 algorithm “weight01”, annotation function “annFUN.gene2GO”, and minimum node size 10. The  
1086 results were ranked by their p-value, and the first 8 terms were plotted.

1087 For RNA-seq in seedlings, WT and *drmy1* seedlings were grown to quiescence (7 days)  
1088 in ½ MS liquid media as previously described<sup>34</sup>. After 7 days, the media was replaced with ½ MS  
1089 liquid media containing 15 mM glucose and incubated for 24 hours to activate TOR. Seedlings  
1090 were then incubated with or without AZD-8055 in addition to 15 mM glucose in ½ MS liquid media  
1091 for 2 hours before collecting tissue. RNA was extracted from 100 mg pooled seedlings using the  
1092 Spectrum Plant Total RNA Kit (Sigma). This RNA was used as a template for RNA-Seq library  
1093 synthesis and sequencing, which was performed by Novogene. RNA-seq data for AZD-8055  
1094 treated WT and *drmy1* seedlings were preprocessed with fastp (v. 0.22.0) using default  
1095 parameters. Preprocessed reads were then mapped to the TAIR10 reference genome using  
1096 STAR (v. 2.7.10z\_alpha\_220314). Following alignment, BAM output files from STAR were used  
1097 to generate feature counts for transcripts using subread-featureCounts (v. 2.0.3) and the  
1098 Araport11 transcriptome. TPMs were generated using TPMCalculator (v. 0.0.3). Differential  
1099 expression analysis was performed using feature count data and DESeq2 (v. 1.36.0).

1100 A list of genes with uORFs based on gene models of the TAIR10 Arabidopsis genome  
1101 assembly were downloaded from von Arnim et al.<sup>69</sup>. For each gene, within each genotype, protein-  
1102 transcript ratio was calculated as the ratio between mean protein abundance and mean transcript  
1103 TPM across all bio-reps in our proteomics and RNA-seq datasets, respectively. This was log2-  
1104 transformed, and the difference between *drmy1* and WT was calculated. This was used as an  
1105 indicator of translation rate difference between *drmy1* and WT, although we acknowledge that  
1106 other factors such as protein stability may affect this number. This was plotted against the number  
1107 of uORFs in each gene model (0, 1, or  $\geq 2$ ).  
1108

## 1109 Proteomics

1110 Five induced inflorescence samples of WT and *drmy1* in *ap1 cal AP1-GR* background  
1111 were collected as described above. Samples were ground in liquid nitrogen. Total soluble proteins  
1112 were extracted in ice-cold extraction buffer (50 mM PBS-HCl (pH 8.0) buffer with 150 mM NaCl,  
1113 2% NP-40, 1 mM PMSF, 1x Roche cOmplete protease inhibitor cocktail (Sigma 11697498001),  
1114 and 1x Halt TM Phosphatase inhibitor cocktail (ThermoFisher 78420)) and filtered through  
1115 Pierce™ Micro-Spin Columns (30  $\mu$ m pore size; Thermo Scientific 89879). Extracts were  
1116 RuBisCO-depleted using Seppro Bubisco Kit (Sigma SEP070-1KT), concentrated, denatured,  
1117 reduced, cysteine blocked, trypsin-digested, and TMT 10-plex labeled. Then, mass spectrometry  
1118 was done using an UltiMate 3000 RSLCnano / Orbitrap Fusion system (Thermo Scientific). Raw  
1119 data was searched against the NCBI protein database using PD 2.3 (Thermo Scientific) with  
1120 Sequest HT searching engine. Precursor-based protein identification and relative quantification  
1121 was done using the standard processing workflow in PD 2.3, with an additional node of Minora  
1122 Feature Detector. Proteins with at least 2 supporting peptides were kept for downstream analysis.  
1123 For each protein, data was fit with an ANOVA model and a p-value was calculated. Proteins with

## Translation and developmental robustness

1124 a p-value < 0.05 were considered differentially accumulated in *drmy1*. GO term enrichment was  
1125 done as above, using genes corresponding to the differentially accumulated proteins.  
1126

### 1127 Polysome extraction and profiling

1128 Three induced inflorescence samples of WT and *drmy1* in *ap1 cal AP1-GR* background  
1129 were collected as described above, and polysomes were extracted as previously described<sup>164</sup>.  
1130 Briefly, samples were ground in liquid nitrogen, mixed with an extraction buffer twice the volume  
1131 of pulverized tissue (0.2 M Tris pH 9.0, 0.2 M KCl, 0.025 M EGTA, 0.035 M MgCl<sub>2</sub>, 1% (w/v) Brij-  
1132 35, 1% (v/v) Triton X-100, 1% (v/v) Igepal CA-630, 1% (v/v) Tween-20, 1% (w/v) Sodium  
1133 deoxycholate, 1% (v/v) Polyoxyethylene 10 tridecyl ether, 5 mM Dithiothreitol, 1 mM  
1134 Phenylmethylsulfonyl fluoride, 100 µg/ml cycloheximide, 100 µg/ml chloramphenicol, 40 U/ml  
1135 RNasin, 10 U/ml DNase I), and let sit on ice for 10 min. Samples were centrifuged at 4°C 4,000 g  
1136 for 5 min, supernatant was transferred to a new tube, centrifuged at 4°C 16,000 g for 15 min, and  
1137 supernatant was filtered through Miracloth.

1138 Polysome extracts were profiled as previously described<sup>165</sup>. Briefly, 600 µl of each sample  
1139 were loaded onto a 15%-45% sucrose density gradient and centrifuged at 4°C 32,000 rpm in a  
1140 SW41 rotor. Separated samples were fractionated at a rate of 0.375 mL/min in an Isco  
1141 fractionation system, and absorbance at 254 nm was recorded.  
1142

### 1143 Puromycin labeling

1144 Puromycin labeling was done as previously described<sup>39</sup>, with slight modifications.

1145 In seedlings, when comparing WT and *drmy1*, in order to control for plant size, WT  
1146 seedlings were grown for 8 days and *drmy1* seedlings were grown for 10 days (Figure 1E). When  
1147 comparing WT, *drmy1*, *wol*, and *drmy1 wol*, we were unable to control for plant size because  
1148 *drmy1 wol* seedlings were too small. We therefore controlled for plant age, and seedlings were  
1149 grown to specified age (8 days for Figure 6B and 14 days for Figure 6C). Seedlings were  
1150 harvested from plates and incubated with an incubation buffer (½ MS, 0.05% (w/v) MES, 1% (w/v)  
1151 sucrose, 0.1% (v/v) Tween-20, 0.1% (v/v) DMSO, 1x Gamborg vitamin mix, pH 5.7), with or  
1152 without 50 µM CHX, for 4 hours in an illuminated growth chamber. Then, the buffer was replaced  
1153 with a fresh incubation buffer (which is same as above, but contains 50 µM puromycin (GoldBio  
1154 P-600-100)), and incubation continued for another 45 min.

1155 In inflorescences of WT and *drmy1* in *ap1 cal AP1-GR* background, inflorescences were  
1156 DEX-induced as described above. Inflorescence samples were collected and put in an incubation  
1157 buffer (½ MS, 1% (w/v) sucrose, 0.02% (v/v) Silwet L-77, 0.1% (v/v) DMSO, 50 µM puromycin,  
1158 1x Gamborg vitamin mix, pH 5.7), with or without 100 µM CHX. Samples were vacuum infiltrated  
1159 for 15 minutes and then put on a rocking shaker in an illuminated growth chamber for 45 minutes.

1160 In both cases, at the end of the incubation, samples were washed three times with water,  
1161 blot dry, weighed, and frozen in liquid nitrogen. Soluble proteins were extracted as described  
1162 above. Puromycin incorporated into the proteins were detected in a Western blot using a mouse-  
1163 origin anti-puromycin monoclonal antibody (12D10, Sigma MABE343, lot # 3484967) and a goat-  
1164 anti-mouse HRP-conjugated secondary antibody (Abcam ab6789, lot # 3436981). RuBisCO large  
1165 subunit in Ponceau S-stained membrane was used as a loading control. Quantification was done

## Translation and developmental robustness

1166 in ImageJ. A background signal was determined using blank regions, and subtracted from all  
1167 quantified signals (separately for puromycin and Ponceau S).

1168

### 1169 **TOR activity assay**

1170 WT and *drmy1* seedlings were grown in a six-well plate containing ½ MS liquid media.  
1171 After seven days, the media were replaced with half-strength MS liquid media plus 15 mM glucose  
1172 and incubated for 24 hours. At least 120 quiescent seedlings per sample were collected and  
1173 frozen in liquid nitrogen. Protein was then extracted from the plant tissue in 100 mM MOPS (pH  
1174 7.6), 100 mM NaCl, 5% SDS, 0.5% b-mercaptoethanol, 10% glycerin, 2 mM PMSF, and 1x  
1175 PhosSTOP phosphatase inhibitor (Sigma). S6K-pT449 was detected by Western blot using a  
1176 phosphospecific antibody (Abcam ab207399) and an HRP-conjugated goat anti-rabbit IgG  
1177 secondary antibody (Jackson Immuno Research 111-035-003). Total S6K was detected using a  
1178 custom monoclonal antibody described by Busche et al.<sup>166</sup>. Total protein visualized in Ponceau  
1179 S-stained membrane was used as a loading control.

1180

### 1181 **Confocal microscopy**

1182 Confocal imaging of reporter lines in the inflorescence were done as previously  
1183 described<sup>27</sup>. Briefly, main inflorescences (not side branches) were cut and dissected with a  
1184 Dumont tweezer (Electron Microscopy Sciences, style 5, no. 72701-D) to remove buds older than  
1185 stage 9 or 10. The inflorescences were then inserted upright into a small petri dish (VWR, 60 x  
1186 15 mm) containing inflorescence culture medium (1/2 MS, 1% (w/v) sucrose, 1x Gamborg vitamin  
1187 mixture, 0.1% (v/v) plant preservative mixture (Plant Cell Technology) 1% (w/v) agarose, pH 5.8),  
1188 leaving most of the stem inside the medium and the buds outside. They were then further  
1189 dissected to reveal stage 6 and younger buds, immersed with water, and imaged under a  
1190 Zeiss710 upright confocal microscope with a 20x Plan-Apochromat water-dipping lens (1.0 NA).  
1191 For live imaging experiments, inflorescence samples were put in a continuous-light growth  
1192 chamber between time points. To prevent bacterial growth, samples were transferred onto fresh  
1193 media every 2 to 3 days, and for live imaging experiments lasting longer than 6 days, once in the  
1194 middle, plants were incubated with an aqueous solution of 100 µg/ml Carbenicillin (GoldBio, C-  
1195 103-5, lot # 0129.091814A) for 30 minutes.

1196 To visualize tissue morphology of inflorescence samples without a reporter, samples were  
1197 stained for 5 minutes with an aqueous solution of 0.1 mg/ml propidium iodide (PI) and 0.1% (v/v)  
1198 Tween-20, washed three times with water, and imaged.

1199 The following laser and wavelength were used in confocal imaging. Chlorophyll, excitation  
1200 488 nm, emission 647-721 nm. PI, excitation 514 nm, emission 566-659 nm. mCherry, excitation  
1201 594 nm, emission 600-659 nm. tdTomato, excitation 561 nm, emission 566-595 nm. For  
1202 EYFP/VENUS/mCitrine, in 35S::*mCitrine-RC12A*, excitation 514 nm, emission 519-580 nm; in  
1203 *DR5::3xVENUS-N7*, excitation 514 nm, emission 519-569 nm; in *pARF5::ER-EYFP-HDEL*,  
1204 excitation 514 nm, emission 519-550 nm; in *R2D2*, excitation 488 nm, emission 493-551 nm. For  
1205 GFP/sfGFP, in *pARR7::ARR7-llama UBQ10::sfGFP-NES*, excitation 488 nm, emission 493-569  
1206 nm; in *pARF3::N3xGFP*, *pARF6::N3xGFP*, *pARF8::N3xGFP*, and *pARF10::N3xGFP*, excitation  
1207 488 nm, emission 493-564 nm; in *TCS::GFP*, excitation 488 nm, emission 493-513 nm.

## Translation and developmental robustness

1208

### 1209 **Visualization of tissue morphology**

1210 For single-channel image stacks intended for the visualization of tissue morphology  
1211 (35S::*mCitrine-RCI2A* or PI), stacks were 3D-rendered using the ZEN confocal software  
1212 (Processing -> 3D). Parameters were set to best visualize tissue morphology, typically, minimum  
1213 5-10, ramp 60-80, maximum 100. Buds were rotated to desired orientation, and screenshots were  
1214 taken using the “Create Image” button. For fluorophores that are dimmer, less sharp, or have a  
1215 noisy background (*UBQ10::mCherry-RCI2A* or Chlorophyll), stacks were converted from LSM to  
1216 TIF using ImageJ<sup>167,168</sup>, loaded into MorphoGraphX<sup>169</sup>, and screenshots were taken using the  
1217 built-in screenshot function in MorphoGraphX.

1218 To aid visualizing tissue morphology and determine the timing of sepal initiation, each  
1219 stack was fitted with a surface, and a Gaussian curvature heatmap was calculated from the  
1220 surface (see below). We consider a sepal primordium as initiated when we see a dark red band  
1221 of positive Gaussian curvature (primordium) separated from the center of the floral meristem by  
1222 a dark blue band of negative Gaussian curvature (boundary)<sup>27</sup>.

1223 Gaussian curvature heatmaps were calculated as previously described<sup>27</sup>, with slight  
1224 modifications. Briefly, stacks underwent the following processes in MorphoGraphX: Gaussian blur  
1225 (3 times; X/Y/Z sigma = 1  $\mu\text{m}$  for the first 2 times, and 2  $\mu\text{m}$  for the third time), edge detection  
1226 (threshold = 2000-8000 depending on the brightness of the stack, multiplier = 2.0, adapt factor =  
1227 0.3, fill value = 30000), marching cube surface (cube size = 8  $\mu\text{m}$ , threshold = 20000), subdivide  
1228 mesh, smooth mesh (passes = 5), subdivide mesh, smooth mesh (passes = 5), project mesh  
1229 curvature (type = Gaussian, neighborhood = 10  $\mu\text{m}$ , autoscale = no, min curv = -0.0015, max curv  
1230 = 0.0015). For ease of visualization, the lookup table “jet” was applied to the mesh.

1231

### 1232 **Quantification of sepal initiation robustness**

1233 For sepal primordium number, screenshots were taken of stage 3-6 buds of indicated  
1234 genotypes, in either ZEN or MorphoGraphX. The number of sepal primordia initiated were  
1235 counted from these screenshots.

1236 For variability in sepal primordium positioning, within each bud, an angular distance was  
1237 measured between each pair of adjacent sepal primordia (with vertex at the center of the bud),  
1238 using ImageJ. Note that the last pair was not measured – the angular distance was calculated as  
1239 the sum of all other angular distances subtracted from 360°. A CV value (standard deviation  
1240 divided by mean) was calculated from all the measured or calculated angular distances. Buds  
1241 with sepal primordia evenly distributed around the bud periphery should have a small CV value,  
1242 i.e. all angles are around 90° for four-sepal buds (or 72° for five-sepal buds, etc.). Buds whose  
1243 sepal primordia distributed variably or randomly around the bud periphery will have widely varying  
1244 angular distances between adjacent sepal primordia, and thus large CV values.

1245 Relative sepal initiation timing was quantified as previously described<sup>27</sup>. Briefly, dissected  
1246 inflorescence samples were live-imaged every 6 hours. A Gaussian curvature heatmap was  
1247 generated for each sample at each time point and was used to determine the time point at which  
1248 a sepal primordium initiates. A sepal primordium is considered initiated at time point T<sub>n</sub> if it is  
1249 absent at time point T<sub>(n-1)</sub> but becomes present at time point T<sub>n</sub>. Within the same bud, we

## Translation and developmental robustness

1250 counted the number of time points between outer and inner sepal initiation, and between outer  
1251 and lateral sepal initiation, and multiplied them by 6 hours to get the relative initiation timing of  
1252 these sepals.

1253

### 1254 Quantification of fluorescent reporters

1255 For *TCS::GFP*, *pARF3::N3xGFP*, *pARF5::ER-YFP-HDEL*, *pARF6::N3xGFP*,  
1256 *pARF8::N3xGFP*, *pARF10::N3xGFP*, *pUS7Y::mDII-NtdTomato*, *pUS7Y::DII-N3xVENUS*, and  
1257 *UBQ10::mCherry-RCI2A*, total signal (integrated density) was quantified from maximum intensity  
1258 projection images using ImageJ<sup>167,168</sup>. Fluorescence intensity was measured in pixel intensity  
1259 units (0-255 range). Signal intensity was calculated as total signal divided by area.

1260 For both *TCS::GFP* and *DR5:3xVENUS-N7*, circular histogram analysis was done as  
1261 previously described<sup>27</sup>. Briefly, individual buds were cropped out of image stacks, channels were  
1262 split using FIJI and saved in TIF format, and TIF stacks were imported into MorphoGraphX. Signal  
1263 from outside the buds (e.g. inflorescence meristem, parts of other buds within the same image)  
1264 was manually removed using the Voxel Edit function. Buds were positioned so that the incipient  
1265 sepal primordia are in the XY plane: the incipient outer sepal is at 45°, the incipient inner sepal  
1266 and the inflorescence meristem are at 225°, and the incipient lateral sepals are at 135° and 315°,  
1267 respectively. Fluorescence intensity was measured in pixel intensity units (0-255 range). A circular  
1268 histogram of bin width 1° centered around the Z axis was exported for each replicate expressing  
1269 *DR5* and/or *TCS*. Multiple circular histograms of the same reporter and genotype were pooled  
1270 and mean ± SD were plotted.

1271 For GFP signal in plants carrying *pUBQ10::sfGFP-nes-UBQ3ter* and *pARR7::ARR7-linker-llama-ARR7ter* reporters, screenshots were taken in MorphoGraphX as described above.  
1272 Screenshots were subtracted of a background determined using blank regions with no tissue, and  
1273 brightened to the same level to reveal differences in GFP distribution patterns. A square region  
1274 containing 5-10 cells were taken from each screenshot, and GFP intensity (in gray value ranging  
1275 from 0 to 255) along a straight line of 239 pixels in length was quantified using ImageJ<sup>167,168</sup>  
1276 (Analyze -> Plot profile). For ease of visualization, the curves were smoothed by taking the  
1277 average of the gray value of 11 neighboring pixels (including itself) as the value of each pixel.

1278 For VENUS or GFP signal in *pAHP6::AHP6-VENUS*, *pAHP6::GFP-ER*, *pAHP3::AHP3-GFP*, and *pUBQ10::mCherry-RCI2A* under mock, CHX, or AZD-8055 treatment, total signal at 24  
1279 hours (for CHX) or 72 hours (AZD-8055) was normalized by bud area in the 2D projection to get  
1280 the signal intensity. To account for bud-to-bud differences in signal intensity prior to treatment,  
1281 the signal intensity was normalized to the 0-hour time point (pre-treatment). Relative level  
1282 between treatment and mock was calculated by normalizing this value to the mean of mock.

1283

### 1284 In vitro drug treatments on inflorescence samples

1285 For cycloheximide (CHX) treatment, a stock solution of 10 mM CHX was made from  
1286 powder (Sigma C1988) in pH 4.0 water. The stock was filter-sterilized and stored in -20°C, and  
1287 added to autoclaved inflorescence culture medium to a final concentration of 2 µM just before  
1288 use. For AZD-8055 treatment, a stock solution of 16 mM AZD-8055 was prepared from powder  
1289 (Cayman Chemical 16978) in DMSO within days of use, and stored in -80°C. The stock was  
1290

## Translation and developmental robustness

1292 added to autoclaved inflorescence culture medium to a final concentration of 2  $\mu$ M. 0.0125% (v/v)  
1293 DMSO was added to the mock medium. For 6-benzylaminopurine (BAP) treatment, a stock  
1294 solution of 50 mM BAP was prepared from powder (Alfa Aesar A14678) in DMSO, and stored in  
1295 -80°C. The stock was added to autoclaved inflorescence culture medium to a final concentration  
1296 of 5  $\mu$ M. 0.01% (v/v) DMSO was added to the mock medium.

1297 Inflorescences were dissected and inserted into regular inflorescence culture medium  
1298 without drugs, and pre-treatment image stacks were captured. Then, they were transferred into  
1299 specified treatment or mock media, and imaged at the specified time points. For live imaging,  
1300 inflorescence samples were transferred onto new medium after each imaging session.

1301

### 1302 *In vivo* Torin2 treatment

1303 Starting at 14 days after germination, twice each day for 15 days, 2 nmol of Torin2  
1304 (Cayman Chemical 14185) in 20  $\mu$ l of aqueous solution containing 0.5% DMSO and 0.5% Tween-  
1305 20 was applied to the center of the rosette using a pipette. For mock, 20  $\mu$ l aqueous solution  
1306 containing 0.5% DMSO and 0.5% Tween-20 was applied. At the end of the 15-day treatment  
1307 period, inflorescences were dissected and put in the inflorescence culture medium for imaging.

1308 To prevent Torin2 degradation, throughout the duration of this experiment, the Torin2  
1309 stock solution in DMSO was kept in -80°C and replaced each week, and the treatment and mock  
1310 solutions were kept in 4°C and replaced each day.

1311

### 1312 Imaging of whole plant, whole inflorescence, siliques, and mature sepals

1313 For whole-plant imaging, aerial parts of the plants were removed from the pots, flattened,  
1314 put on a dark cloth, and imaged with a cell phone (iPhone 12, iOS 16.2).

1315 For whole-inflorescence imaging, inflorescences consisting of open flowers and unopened  
1316 buds were removed from the plant and held with forceps. Images were taken under a Zeiss Stemi  
1317 2000-C Stereo Microscope with a cell phone (iPhone 12, iOS 16.2).

1318 For siliques imaging, siliques on inflorescences sufficiently distant from the shoot apex that  
1319 were developed and started to ripen were picked with forceps, opened with a razor blade, and  
1320 imaged under a Zeiss Stemi 2000-C Stereo Microscope with a cell phone (iPhone 12, iOS 16.2).

1321 Mature sepal imaging was done as previously described<sup>26,27</sup>. Briefly, mature sepals from  
1322 stage 15 flowers (10<sup>th</sup> to 25<sup>th</sup> flower on the inflorescence) were dissected and sandwiched  
1323 between two slides to flatten. Images were taken using a Canon Powershot A640 camera  
1324 attached to a Zeiss Stemi 2000-C Stereo Microscope. Minor damages were manually fixed, and  
1325 undesired objects such as pollen grains were manually removed from these images. Sepals with  
1326 major damages were discarded. Then, a contour was extracted from each sepal using custom  
1327 python scripts<sup>26</sup>. This gave us measurements such as length, width, area, etc. of each sepal. To  
1328 measure between-flower variability of length, within each genotype and for each of outer, inner,  
1329 and lateral positions, a CV (standard deviation divided by mean) of all sepals was calculated (for  
1330 example, a CV of length of all outer sepals in WT). To determine statistical significance, genotypes  
1331 were compared pairwise using permutation tests. To measure within-flower variability of length,  
1332 a CV was calculated for all sepals within each flower (for example, a CV of length of outer, inner,  
1333 and two lateral sepals in WT bud #10). For accurate calculation of CV, flowers with length data of

## Translation and developmental robustness

1334 at least four sepals were included in the analysis. To determine statistical significance, genotypes  
1335 were compared pairwise using Wilcoxon rank sum tests.

1336

### 1337 Cytokinin extraction and measurement

1338 Cytokinin extraction was based on a previously published protocol<sup>170</sup> with modifications.  
1339 Briefly, five inflorescence samples of induced *ap1 cal 35S::AP1-GR*, and six inflorescence  
1340 samples of induced *drmy1 ap1 cal 35S::AP1-GR* were collected as described above. Samples  
1341 were ground in liquid nitrogen and twice extracted in methanol : water : formic acid (15:4:1). 200  
1342 pg of BAP per sample was added as an internal control. Extracts were centrifuged at 14,650 rpm  
1343 in -4°C for 30 min, and supernatant was evaporated of methanol and reconstituted in 1% (v/v)  
1344 acetic acid. Samples were passed through an Oasis MCX SPE column (Waters 186000252),  
1345 washed with 1% acetic acid, washed with methanol, and eluted with 0.35 M ammonia in 70%  
1346 methanol. Eluents were evaporated to complete dryness, reconstituted in 5% acetonitrile, and  
1347 sent for LC-MS.

1348 LC-MS was done as previously described<sup>171</sup>, with modifications. Briefly, 1 µl of each  
1349 sample was injected into a Thermo Fisher Scientific Vanquish Horizon UHPLC System coupled  
1350 with a Thermo Q Exactive HF hybrid quadropole-orbitrap high-resolution mass spectrometer  
1351 equipped with a HESI ion source. Samples were separated on a C18 ODS column (AQUITY  
1352 UPLC BEH C18, 1.7 µm, 2.1 × 100 mm, Waters), at a flow rate of 0.3 ml/min, with linear gradients  
1353 of solvent A (0.1% formic acid) and solvent B (0.1% formic acid in methanol) according to the  
1354 following profile: 0 min, 99.0% A + 1.0% B; 4.0 min, 55.0% A + 45.0% B; 7 min, 30.0% A + 70.0%  
1355 B; and then with isocratic conditions: 8 min, 1.0% A + 99.0% B; 12 min, 99.0% A + 1.0% B.  
1356 Cytokinins were detected using the positive ion mode.

1357 For tZ, tZR, iP, iPR, and the internal control BAP, peaks were identified from an external  
1358 standard mix composed of 0.1 µg/ml each of BAP (Alfa Aesar A14678), tZ (Sigma Z0876), tZR  
1359 (Sigma Z3541), iP (Cayman Chemical 17906), and iPR (Cayman chemical 20522) in 5%  
1360 acetonitrile. For cZ and cZR, peaks were identified based on previously reported precursor m/z  
1361 and retention time<sup>172</sup>. Using Xcalibur (Thermo Scientific), peak area was quantified for each  
1362 cytokinin in each sample, normalized against the peak area of BAP (internal control) and sample  
1363 fresh weight, and then normalized against the average abundance of tZ in WT samples.

1364

### 1365 Software

1366 Image processing was done in ImageJ (version 2.9.0/1.53t, build a33148d777)<sup>167,168</sup> and  
1367 MorphoGraphX (version 2.0, revision 1-294, CUDA version 11.40)<sup>169</sup>.

1368 Data processing was done in RStudio (R version 4.0.5 “Shake and Throw” (2021-03-  
1369 31))<sup>173</sup>. Graphs were made using the package ggplot2 (version 3.3.3)<sup>174</sup>. Fisher’s contingency  
1370 table tests were done using the function fisher.test in R. Wilcoxon rank sum tests were done using  
1371 the function wilcox.test in R. Hypergeometric tests were done using the function phyper in R. Data  
1372 fitting with ANOVA was done using the function aov in R.

1373 Figures were assembled in Adobe Illustrator (version 25.4.1). An RGB color profile “Image  
1374 P3” was used for all the figures.

1375

## Translation and developmental robustness

### 1376 **Accession numbers**

1377 RNA-seq data for *ap1 cal AP1-GR* and *drmy1 ap1 cal AP1-GR* inflorescence tissue were  
1378 deposited in Gene Expression Omnibus (GEO) under accession number GSE230100. RNA-seq  
1379 data for WT and *drmy1* seedlings treated with mock or AZD-8055 were deposited in NIH  
1380 BioProject under accession number PRJNA961813. Mass spectrometry data for proteomics were  
1381 deposited in the ProteomeXchange Consortium via the PRIDE<sup>175</sup> partner repository under  
1382 accession number PXD041723 (reviewer username: reviewer\_pxd041723@ebi.ac.uk, and  
1383 password: 8pl3ZD1l). Mass spectrometry data for cytokinins were deposited in NIH's National  
1384 Metabolomics Data Repository (NMDR) website, the Metabolomics Workbench<sup>152</sup>, under  
1385 accession number ST002571.

1386

## Translation and developmental robustness

### 1387 **SUPPLEMENTAL INFORMATION TITLES AND LEGENDS**

1388

#### 1389 **Supplemental Figure 1. Evidence that the *drmy1* mutant has ribosomal and translation** 1390 **defects, associated with Figure 1.**

1391 (A) The *drmy1* phenotype is reproduced in the *ap1 cal AP1-GR* system (Ler background). Shown  
1392 are representative buds of *ap1 cal AP1-GR* (top row) and *drmy1 ap1 cal AP1-GR* (bottom row) at  
1393 day 0 (before DEX induction), day 3 (after 3 DEX inductions, when tissue is collected for RNA,  
1394 protein, or cytokinin extraction), and day 5 (after 5 DEX inductions). Arrowheads show sepal  
1395 primordia that are of variable number, position, and sizes. Asterisks indicate periphery of the floral  
1396 meristem that has limited or no sepal outgrowth. Scale bars, 25  $\mu$ m.

1397 (B) Summary of the inflorescence RNA-seq and proteomics datasets. Shown are numbers of  
1398 genes in each category. Down, downregulated in *drmy1*; NS, not significantly changed between  
1399 *drmy1* and WT; Up, upregulated in *drmy1*; NA, not available. Note that in the combined dataset  
1400 (gene-protein pairs), different genes encoding for the same protein were separately counted, so  
1401 were different proteins encoded by the same gene. See also Supplemental Dataset 1.

1402 (C) Violin and box plots of log2 fold change in RNA between *drmy1* and WT in induced *ap1 cal*  
1403 *AP1-GR* inflorescence, for genes encoding ribosomal components (“Structural constituents of the  
1404 ribosome” GO:0003735, and its offspring terms) and all other genes involved in translation  
1405 (“Translation” GO:0006412, and its offspring terms). The following genes are labeled on the  
1406 graph: *UL4Z* (AT3G09630), log2FC = -0.492; *UL4Y* (AT5G02870), log2FC = -0.509; *UL18Z*  
1407 (AT3G25520), log2FC = -0.459.

1408 (D-G) Fluorescence of a constitutively expressed marker supports the hypothesis that *drmy1* has  
1409 reduced translation rate. (D-F) Representative confocal images of *UBQ10::mCherry-RCI2A* in  
1410 dissected inflorescences of WT (D), *drmy1* (E), and *ul4y* (F). Numbers show how the signal is  
1411 divided based on the stage of floral meristem when quantified (IM+1, inflorescence meristem plus  
1412 stage 1; 2, stage 2; 3, stage 3). Scale bars, 25  $\mu$ m. (G) Signal intensity (i.e. integrated density  
1413 divided by area) in all images divided as in (D-F). Mean  $\pm$  SD are shown. Data was fit using a  
1414 two-way ANOVA model with genotype and stage as two additive factors. Asterisks show  
1415 statistically significant pairwise contrasts between WT and *drmy1* ( $p < 2 \times 10^{-16}$ ) and between WT  
1416 and *ul4y* ( $p = 2.1 \times 10^{-15}$ ). Sample sizes: WT IM+1, n = 30; *drmy1* IM+1, n = 22; *ul4y* IM+1, n = 18;  
1417 WT stage 2, n = 99; *drmy1* stage 2, n = 100; *ul4y* stage 2, n = 52; WT stage 3, n = 39; *drmy1*  
1418 stage 3, n = 27; *ul4y* stage 3, n = 26.

1419 (H) Violin and box plots of log2 fold change in protein level between *drmy1* and WT in induced  
1420 *ap1 cal AP1-GR* inflorescence, for genes in the same categories as in (C). The following genes  
1421 are labeled on the graph: *UL4Z* (AT3G09630), log2FC = 0.352; *UL4Y* (AT5G02870), log2FC =  
1422 0.811; *UL18Z* (AT3G25520), log2FC = 0.742.

1423 (I) Coherent regulation of gene expression by *drmy1* and AZD-8055. Shown is a contingency  
1424 table of genes downregulated (Down), not significantly changed (NS), and upregulated (Up) in  
1425 *drmy1* vs WT (columns), and in AZD-8055-treated WT vs mock-treated WT (rows). Bold font  
1426 shows the number of genes in each category, and gray font shows the expected number of genes  
1427 if there were no correlation between two conditions (calculated as row margin  $\times$  column margin /  
1428 total number of genes). Categories where the number of genes is above expectation are

## Translation and developmental robustness

1429 highlighted blue, and categories where the number of genes is below expectation are highlighted  
1430 red. Chi-square test  $p < 2.2 \times 10^{-16}$ .

1431 **(J)** Gene ontology enrichment of genes coherently downregulated by both *drmy1* and AZD-8055.  
1432 Shown are the top 8 terms and their enrichment p-values. Note that the first 7 terms are all related  
1433 to ribosome and translation. A complete list can be found in Supplementary Dataset 3.

1434

## Translation and developmental robustness

### 1435 **Supplemental Figure 2. Ribosomal mutations enhance the *drmy1* phenotype, associated 1436 with Figure 2.**

1437 **(A-H)** Examples of stage 5 buds from *drmy1* (A), *drmy1 ul4z* (B-D), *drmy1 ul4y* (E-F), and *drmy1*  
1438 *ul18z/+* (G-H). In (B,E,G) sepal primordia within each bud have bigger size differences than typical  
1439 *drmy1* single mutant buds; asterisks show giant outer sepal primordia and brackets show bud  
1440 peripheral regions with little or no primordium outgrowth. In (C,F,H), arrowheads show 6 sepal  
1441 primordia within each bud, which does not occur in *drmy1*. In (D,H), asterisks show the presence  
1442 of two outer sepal primordia within a bud, instead of one in *drmy1*. Scale bars, 25 $\mu$ m.

1443 **(I-J)** Quantification of sepal primordium number (I) and positional variability (J), comparing each  
1444 of *drmy1 ul4z* (n = 60), *drmy1 ul4y* (n = 61), and *drmy1 ul18z/+* (n = 69) with *drmy1* (n = 67). “ns”  
1445 indicates no significant difference in Fisher’s contingency table tests (I) and Wilcoxon’s rank sum  
1446 tests (J) respectively. Data for *drmy1* is reused from Figure 2H, 2J.

1447 **(K)** Dissected young siliques of a *drmy1 ul18z/+* plant. Arrowheads point to aborted ovules. Scale  
1448 bar, 200  $\mu$ m.

1449

## Translation and developmental robustness

1450 **Supplemental Figure 3. Sepal primordia in ribosome and TOR mutants catch up in growth**  
1451 **to form uniformly sized mature sepals within the bud, associated with Figure 3.**

1452 **(A-F)** Inflorescences (left) of WT (A), *drmy1* (B), *ul4z* (C), *ul4y* (D), *ul18z* (E), and *lst8-1-1* (F), with  
1453 boxed regions enlarged (right). Blue arrowheads show sepals of regular length, and red  
1454 arrowheads show sepals shorter than others. Note that sepals in *drmy1* were unable to close due  
1455 to unequal lengths, while sepals in *ul4z*, *ul4y*, and *ul18z*, and close like in WT. Sepals in *lst8-1-1*  
1456 were unable to close although there is no apparent variation in length. Scale bars, 0.5 mm.

1457 **(G-L)** Dissected sepals from a bud of WT (G), *drmy1* (H), *ul4z* (I), *ul4y* (J), *ul18z* (K), and two  
1458 buds of *lst8-1-1* (L). Note that sepals in the *drmy1* bud are of different sizes. Sepals within each  
1459 bud of *ul4z*, *ul4y*, *ul18z*, and *lst8-1-1* are of similar sizes, although there can be variation between  
1460 different buds of the same genotype. O, outer sepal. I, inner sepal. L, lateral sepal. Scale bars,  
1461 200  $\mu$ m.

1462 **(M)** Quantification of between-flower variability of sepal length. Length was measured from all  
1463 imaged sepals of each genotype and each position (outer, inner, lateral), and coefficient of  
1464 variation (CV) was calculated. A two-sided permutation test (100,000 permutations) for CV  
1465 difference not equating to zero was done for each pair of genotypes, and results were represented  
1466 by letters. Sample size: Outer sepal, WT n = 35, *drmy1* n = 43, *ul4z* n = 37, *ul4y* n = 42, *ul18z* n  
1467 = 39, *lst8-1-1* n = 43. Inner sepal, WT n = 34, *drmy1* n = 46, *ul4z* n = 38, *ul4y* n = 44, *ul18z* n =  
1468 37, *lst8-1-1* n = 44. Lateral sepal, WT n = 65, *drmy1* n = 84, *ul4z* n = 81, *ul4y* n = 89, *ul18z* n =  
1469 76, *lst8-1-1* n = 82.

1470 **(N)** Quantification of within-flower variability of length. Flowers with length data from at least four  
1471 sepals were analyzed. A CV of length from all sepals within each flower was calculated, and mean  
1472  $\pm$  SD was plotted, grouped by genotype. A Wilcoxon rank sum test was done for each pair of  
1473 genotypes, and results were represented by letters. Sample size: WT n = 31 buds, *drmy1* n = 38  
1474 buds, *ul4z* n = 33 buds, *ul4y* n = 36 buds, *ul18z* n = 32 buds, *lst8-1-1* n = 39 buds.

1475 **(O-Q)** Live imaging of sepal development from stage 3 to 6 in WT (O), *drmy1* (P), and *ul4y* (Q),  
1476 showing chlorophyll or propidium iodide channel, and Gaussian curvature of the surface. Note  
1477 that both *drmy1* and *ul4y* have inner sepals that initiate late (day 2, asterisk). The *drmy1* inner  
1478 sepal develops slowly, and leaves the bud open at day 3 (red arrowhead). The *ul4y* inner sepal  
1479 catches up with the rest of the sepals and closes the bud (blue arrowhead). Scale bars, 25  $\mu$ m.

1480

## Translation and developmental robustness

### 1481 **Supplemental Figure 4. Inhibition of TOR activity and translation causes auxin maxima** 1482 **formation at variable positions, correlated with variable positions of sepal primordia,** 1483 **associated with Figure 4.**

1484 **(A-E)** Variable patterning of auxin signaling in *drmy1*, *ul4y*, and CHX-treated WT buds  
1485 corresponds to variable sepal initiation. During the time course, top rows show *DR5::3xVENUS-*  
1486 *N7* (yellow), middle rows show composites of *DR5* (yellow) and Chlorophyll (magenta), and  
1487 bottom rows show Gaussian curvature of the Chlorophyll channel. In the last time point, buds  
1488 were stained with propidium iodide (top), and Gaussian curvature of the propidium iodide channel  
1489 is shown on the bottom.

1490 (A) In WT, four robustly positioned auxin maxima at day 1 correlates with four robustly positioned  
1491 sepal primordia at day 4 (blue arrowheads). (B) In *drmy1*, at day 1 there are three robustly  
1492 positioned auxin maxima (blue arrowheads). At day 2, a diffuse band of auxin signaling occurs in  
1493 the adaxial periphery of the bud, joining with one of the lateral auxin maxima (red bracket). At day  
1494 3, this diffuse band splits into three auxin maxima (red arrowheads), making a total of 5. The  
1495 maxima correlate with the five sepal primordia at day 4, three at robust positions (blue  
1496 arrowheads) and two at irregular positions (red arrowheads). (C) In *ul4y*, at day 1 there are two  
1497 auxin maxima at robust positions (blue arrowheads), one at robust lateral position but much  
1498 weaker (red arrowhead), and a band of weak auxin signaling in the adaxial periphery of the bud  
1499 (red bracket). At day 2, the weak auxin maxima at the lateral position got stronger, and the weak  
1500 band at the adaxial position split into two auxin maxima (red arrowheads). These five auxin  
1501 maxima correspond to the five sepal primordia at day 3, three in robust positions (blue  
1502 arrowheads) and two in irregular positions (red arrowheads). (D) In a mock-treated WT bud, four  
1503 robust auxin maxima at day 6 of the treatment grow into four robust sepal primordia at day 9 (blue  
1504 arrowheads). (E) In a CHX-treated WT bud, at day 6 there are three stronger auxin maxima (blue  
1505 arrowheads) and two weaker ones (red arrowheads), corresponding to three bigger regions of  
1506 outgrowth (blue arrowheads) and two smaller ones (red arrowheads) at day 9. For ease of display,  
1507 the DR5 channel in CHX-treated WT was brightened three times relative to mock.

1508 **(F-I)** TOR inhibition using Torin2 causes increased cytokinin signaling, and occasional spatial  
1509 variability in auxin and cytokinin signaling. (F) Late stage 2 buds of WT treated *in vivo* with mock  
1510 or 2 nmol Torin2 twice a day for 15 days. Shown are *DR5::3xVENUS-N7* in yellow, *TCS::GFP* in  
1511 cyan, and both merged with propidium iodide in magenta. Note that 3/16 (19%) buds had variable  
1512 number and position of DR5 and TCS maxima, and 13/16 (81%) had robust DR5 and TCS  
1513 maxima, although TCS intensity is higher than mock in both cases. (G) Quantification of TCS  
1514 intensity from maximum intensity projection images, normalized to the mean of WT mock. Shown  
1515 are mean  $\pm$  SD. Asterisk shows statistical significance in a two-tailed Student's t-test ( $p = 1.2 \times 10^{-4}$ ). (H) Circular histograms of DR5 signal distribution (mean  $\pm$  SD). (I) Circular histograms of TCS  
1516 signal distribution (mean  $\pm$  SD). For calculation of circular histograms, please see Figure 4  
1517 legends and Materials and Methods. Sample size: WT mock,  $n = 11$  buds; WT Torin2,  $n = 16$   
1518 buds. Scale bars in all micrographs, 25  $\mu$ m.  
1519

## Translation and developmental robustness

### 1520 **Supplemental Figure 5. Translation of uORF-containing ARFs is not universally 1521 downregulated in *drmy1*, associated with Figure 5.**

1522 **(A)** *drmy1* has a lower protein-transcript ratio than WT for genes with at least 2 uORFs. 5,086  
1523 transcript-protein pairs in our inflorescence dataset were grouped according to the maximum  
1524 number of uORFs in all transcript isoforms (0, n = 3,485; 1, n = 874;  $\geq 2$ , n = 724) (von Arnim et  
1525 al., 2014). For each pair, protein-transcript ratio was calculated, log-transformed, and the  
1526 difference between *drmy1* and WT was plotted. A negative value means this gene has less protein  
1527 per transcript in *drmy1* than WT, and could indicate reduced translation or protein stability.  
1528 Medians for each group: 0 uORF, -0.00367; 1 uORF, -0.00808;  $\geq 2$  uORFs, -0.0243. Asterisk  
1529 show statistically significant difference from Group 0 in a Wilcoxon rank sum test ( $p = 3.167 \times 10^{-4}$ ), while ns means no significant difference from Group 0 ( $p = 0.167$ ).

1530 **(B-D)** There is no universal decrease in the expression of uORF-containing ARF reporters. (B)  
1531 Transcript level of three activator ARFs (ARF5, ARF6, ARF8) and two repressor ARFs (ARF3,  
1532 ARF10) in inflorescence RNA-seq (n = 3 per genotype). ARF3, ARF5, and ARF6 contain  
1533 uORFs before the main ORF, and ARF8 and ARF10 do not. Asterisk indicates statistically  
1534 significant differences between WT and *drmy1* from DESeq2 output. p values: ARF3, p = 0.583;  
1535 ARF5, p = 0.497; ARF6, p = 0.603; ARF8, p = 0.058; ARF10 p = 0.019. (C) Transcriptional  
1536 reporters for these ARFs in stage 2 buds of WT and *drmy1* (cyan, GFP or YFP; magenta,  
1537 propidium iodide). Note that the *pARF3*, *pARF5*, and *pARF6* reporters contain the same uORFs  
1538 as the genes, reflecting a combination of transcriptional and uORF regulations. Scale bars, 20  
1539  $\mu\text{m}$ . (D) Quantification of GFP intensity. Sample size: *pARF3* WT, n = 22; *pARF3* *drmy1*, n = 25;  
1540 *pARF5* WT, n = 22; *pARF5* *drmy1*, n = 22; *pARF6* WT, n = 19; *pARF6* *drmy1*, n = 28; *pARF8*  
1541 WT, n = 25; *pARF8* *drmy1*, n = 31; *pARF10* WT, n = 20; *pARF10* *drmy1*, n = 29. Asterisks show  
1542 statistically significant differences between WT and *drmy1* in Wilcoxon rank sum tests. p values:  
1543 *pARF3*, p = 0.3797; *pARF5*, p =  $6.22 \times 10^{-5}$ ; *pARF6*, p =  $2.868 \times 10^{-13}$ ; *pARF8*, p = 0.5127;  
1544 *pARF10* p =  $7.073 \times 10^{-14}$ .

Translation and developmental robustness

1546 **Supplemental Figure 6. Cytokinin signaling causes variability in mature sepal number and**  
1547 **size in *drmy1*, associated with Figure 5.**

1548 Shown are top-view inflorescence images of WT (A), *arr1,10,12* (B), *wol* (C), *drmy1* (D), *drmy1*  
1549 *arr1,10,12* (E), and *drmy1 wol* (F), with boxed areas of individual buds enlarged and shown on  
1550 the right. In the enlarged views, blue arrowheads point to sepals of regular size, and red  
1551 arrowheads point to sepals that are much smaller. Scale bars, 0.5 mm.

1552

## Translation and developmental robustness

1553 **Supplemental Figure 7. Investigating other mechanisms that may explain the observed**  
1554 **changes in hormone signaling.**

1555 **(A)** Cytokinin abundance does not significantly change in *drmy1*. Shown is mean  $\pm$  SD of levels  
1556 of trans-zeatin (tZ), cis-Zeatin (cZ), N<sup>6</sup>-( $\Delta^2$ -Isopentenyl)adenine (iP), trans-Zeatin riboside (tZR),  
1557 cis-Zeatin riboside (cZR), and N<sup>6</sup>-( $\Delta^2$ -Isopentenyl)adenosine (iPR) quantified by LC-MS in  
1558 induced WT and *drmy1* inflorescences of *ap1 cal AP1-GR* background. Levels are normalized to  
1559 the mean tZ level in WT. Sample size: n = 5 for WT; n = 6 for *drmy1*. ns, no significant difference  
1560 between WT and *drmy1* in two-sided Wilcoxon rank sum tests. P-values: tZ, p = 0.2468; cZ, p =  
1561 0.7922; iP, p = 0.2468; tZR, p = 0.1775; cZR, p = 0.6623; iPR, p = 0.6623.

1562 **(B)** Expression of cytokinin signaling components in WT vs *drmy1* inflorescences of *ap1 cal AP1-*  
1563 *GR* background (from Supplemental Dataset 1).

1564 **(C-D)** The *ARR7-llama GFP-nes* reporter responds to externally applied cytokinin. Shown are  
1565 GFP images of the same bud before (C) or after (D) 5 hours of 200  $\mu$ M BAP treatment. Images  
1566 are representative of n = 9 buds from two independent lines.

1567 **(E-H)** CHX (E-F) or AZD-8055 (G-H) treatments do not change the subcellular localization of GFP-  
1568 nes. Images are representative of n = 10 buds (E), n = 9 buds (F), n = 10 buds (G), and n = 11  
1569 buds (H). For (C-H), each image was brightened to reveal patterns of GFP distribution. A square  
1570 region taken from the image containing 5-10 cells is enlarged and shown on the top right. Within  
1571 the square, GFP intensity was quantified along the dotted line and plotted on the bottom right. X-  
1572 axis, pixels (range 0-238). Y-axis, GFP intensity (smoothed by taking the average intensity of  
1573 11-pixel neighborhoods; range 90-175 in gray value). Scale bars, 25  $\mu$ m.

1574 **(I-J)** Response of *pAHP3::AHP3-GFP* (I) and *pUBQ10::mCherry-RCI2A* (J) to mock, CHX, and  
1575 AZD-8055 treatments for 72 hours. Scale bars, 25  $\mu$ m. For (I), images are representative of n =  
1576 13 (mock), n = 15 (CHX), and n = 16 (AZD-8055) buds in two experiments. For (J), images are  
1577 representative of n = 12 (mock), n = 9 (CHX), and n = 10 (AZD-8055) buds in two experiments.

1578 **(K-N)** The *ARR7-llama GFP-nes* construct partially rescues the mature sepal variability in *drmy1*.  
1579 Shown are inflorescence images of WT (K), *ARR7-llama GFP-nes* (L), *drmy1* (M), and *drmy1*  
1580 *ARR7-llama GFP-nes* (N). The boxed regions were enlarged and shown on the right of each  
1581 panel. Note that while *drmy1* buds have normal-sized (blue arrowheads) and smaller (red  
1582 arrowheads) sepals, some buds in *drmy1* *ARR7-llama GFP-nes* have robustly sized sepals (N,  
1583 middle) while others still show variability (N, right). Scale bars, 0.5 mm.

1584 **(O-P)** *drmy1* has decreased and disrupted pattern of DII degradation. **(O)** Representative images  
1585 of WT and *drmy1* showing *DII-n3xVENUS* (cyan), *mDII-ntdTomato* (magenta), and merge. For  
1586 ease of display, the *VENUS* channel was brightened 3 times relative to the *tdTomato* channel.  
1587 Scale bars, 25  $\mu$ m. **(P)** Quantification of *VENUS/tdTomato* ratio. A background of 6 gray value  
1588 per pixel (determined in blank regions) were subtracted before calculation of ratios. Sample size:  
1589 WT, n = 8 buds; *drmy1*, n = 19 buds. Asterisk shows statistically significant difference in a  
1590 Wilcoxon rank sum test (p = 0.01335).

1591

Translation and developmental robustness

1592 **Supplemental Dataset 1. Inflorescence RNA-seq and proteomics.**

1593

1594 **Supplemental Dataset 2. Unprocessed ribosome profiles.**

1595

1596 **Supplemental Dataset 3. Seedling RNA-seq.**

1597

1598 **Supplemental Dataset 4. Data used in graphs.**

1599

1600 **Supplemental Dataset 5. DNA sequences.**

1601

## Translation and developmental robustness

1602 **REFERENCES**

1603 1. Kaneko, K. (2007). Evolution of robustness to noise and mutation in gene expression  
1604 dynamics. *PLoS One* 2, e434. 10.1371/journal.pone.0000434.

1605 2. Lachowiec, J., Queitsch, C., and Kliebenstein, D.J. (2016). Molecular mechanisms  
1606 governing differential robustness of development and environmental responses in plants.  
1607 *Ann. Bot.* 117, 795–809. 10.1093/aob/mcv151.

1608 3. Zabinsky, R.A., Mason, G.A., Queitsch, C., and Jarosz, D.F. (2019). It's not magic –  
1609 Hsp90 and its effects on genetic and epigenetic variation. *Semin. Cell Dev. Biol.* 88, 21–  
1610 35. 10.1016/j.semcdb.2018.05.015.

1611 4. Waddington, C.H. (1942). Canalization of Development and the Inheritance of Acquired  
1612 Characters. *Nature* 150, 563–566.

1613 5. Twitty, V.C., and Schwind, J.L. (1931). The growth of eyes and limbs transplanted  
1614 heteroplastically between two species of *Ambystoma*. *J. Exp. Zool.* 59, 61–86.  
1615 10.1002/jez.1400590105.

1616 6. Silber, S.J. (1976). Growth of Baby Kidneys Transplanted Into Adults. *Arch. Surg.* 111,  
1617 75–77. 10.1001/archsurg.1976.01360190077014.

1618 7. Summerbell, D., and Lewis, J.H. (1975). Time, place and positional value in the chick  
1619 limb bud. *J. Embryol. Exp. Morphol.* 33, 621–643. 10.1242/dev.33.3.621.

1620 8. Parker, J., and Struhl, G. (2020). Control of *Drosophila* wing size by morphogen range  
1621 and hormonal gating. *Proc. Natl. Acad. Sci. U. S. A.* 117, 31935–31944.  
1622 10.1073/pnas.2018196117.

1623 9. Garelli, A., Gontijo, A.M., Miguela, V., Caparros, E., and Dominguez, M. (2012). Imaginal  
1624 discs secrete insulin-like peptide 8 to mediate plasticity of growth and maturation.  
1625 *Science* 336, 579–582. 10.1126/science.1216735.

1626 10. Crickmore, M.A., and Mann, R.S. (2006). Hox control of organ size by regulation of  
1627 morphogen production and mobility. *Science* 313, 63–68. 10.1126/science.1128650.

1628 11. Recasens-Alvarez, C., Ferreira, A., and Milán, M. (2017). JAK/STAT controls organ size  
1629 and fate specification by regulating morphogen production and signalling. *Nat. Commun.*  
1630 8, 10–12. 10.1038/ncomms13815.

1631 12. Irish, V.F. (2008). The *Arabidopsis* petal: a model for plant organogenesis. *Trends Plant*  
1632 *Sci.* 13, 430–436. 10.1016/j.tplants.2008.05.006.

1633 13. Fenster, C.B., Armbruster, W.S., Wilson, P., Dudash, M.R., and Thomson, J.D. (2004).  
1634 Pollination syndromes and floral specialization. *Annu. Rev. Ecol. Evol. Syst.* 35, 375–403.  
1635 10.1146/annurev.ecolsys.34.011802.132347.

1636 14. King, S., Beck, F., and Lüttge, U. (2004). On the mystery of the golden angle in  
1637 phyllotaxis. *Plant, Cell Environ.* 27, 685–695. 10.1111/j.1365-3040.2004.01185.x.

1638 15. Smith, R.S., Guyomarc'h, S., Mandel, T., Reinhardt, D., Kuhlemeier, C., and  
1639 Prusinkiewicz, P. (2006). A plausible model of phyllotaxis. *Proc. Natl. Acad. Sci. U. S. A.*  
1640 103, 1301–1306. 10.1073/pnas.0510457103.

1641 16. Besnard, F., Refahi, Y., Morin, V., Marteaux, B., Brunoud, G., Chambrier, P., Rozier, F.,  
1642 Mirabet, V., Legrand, J., Lainé, S., et al. (2014). Cytokinin signalling inhibitory fields  
1643 provide robustness to phyllotaxis. *Nature* 505, 417–421. 10.1038/nature12791.

1644 17. Queitsch, C., Sangster, T.A., and Lindquist, S. (2002). Hsp90 as a capacitor of  
1645 phenotypic variation. *Nature* 417, 618–624. 10.1038/nature749.

1646 18. Rutherford, S.L., and Lindquist, S. (1998). Hsp90 as a capacitor for morphological  
1647 evolution. *Nature* 396, 336–342. 10.1038/24550.

1648 19. Lehner, B., Crombie, C., Tischler, J., Fortunato, A., and Fraser, A.G. (2006). Systematic  
1649 mapping of genetic interactions in *Caenorhabditis elegans* identifies common modifiers of  
1650 diverse signaling pathways. *Nat. Genet.* 38, 896–903. 10.1038/ng1844.

1651 20. Levy, S.F., and Siegal, M.L. (2008). Network hubs buffer environmental variation in

## Translation and developmental robustness

1652 21. *Saccharomyces cerevisiae*. PLoS Biol. 6, 2588–2604. 10.1371/journal.pbio.0060264.

1653 22. Folta, A., Severing, E.I., Krauskopf, J., van de Geest, H., Verver, J., Nap, J.P., and Mlynarova, L. (2014). Over-expression of Arabidopsis AtCHR23 chromatin remodeling ATPase results in increased variability of growth and gene expression. BMC Plant Biol. 14, 76. 10.1186/1471-2229-14-76.

1654 23. Hintze, M., Katsanos, D., Shahrezaei, V., and Barkoulas, M. (2021). Phenotypic Robustness of Epidermal Stem Cell Number in *C. elegans* Is Modulated by the Activity of the Conserved N-acetyltransferase nath-10/NAT10. Front. Cell Dev. Biol. 9, 640856. 10.3389/fcell.2021.640856.

1655 24. Marygold, S.J., Roote, J., Reuter, G., Lambertsson, A., Ashburner, M., Millburn, G.H., Harrison, P.M., Yu, Z., Kenmochi, N., Kaufman, T.C., et al. (2007). The ribosomal protein genes and Minute loci of *Drosophila melanogaster*. Genome Biol. 8, R216. 10.1186/gb-2007-8-10-r216.

1656 25. Wang, S., Kurepa, J., and Smalle, J.A. (2009). The *Arabidopsis* 26S proteasome subunit RPN1a is required for optimal plant growth and stress responses. Plant Cell Physiol. 50, 1721–1725. 10.1093/pcp/pcp105.

1657 26. Gallois, J.L., Guyon-Debast, A., Lecureuil, A., Vezon, D., Carpentier, V., Bonhomme, S., and Guerche, P. (2009). The *Arabidopsis* proteasome RPT5 subunits are essential for gametophyte development and show accession-dependent redundancy. Plant Cell 21, 442–459. 10.1105/tpc.108.062372.

1658 27. Hong, L., Dumond, M., Tsugawa, S., Sapala, A., Routier-Kierzkowska, A.L., Zhou, Y., Chen, C., Kiss, A., Zhu, M., Hamant, O., et al. (2016). Variable Cell Growth Yields Reproducible Organ Development through Spatiotemporal Averaging. Dev. Cell 38, 15–32. 10.1016/j.devcel.2016.06.016.

1659 28. Zhu, M., Chen, W., Mirabet, V., Hong, L., Bovio, S., Strauss, S., Schwarz, E.M., Tsugawa, S., Wang, Z., Smith, R.S., et al. (2020). Robust organ size requires robust timing of initiation orchestrated by focused auxin and cytokinin signalling. Nat. Plants 6, 686–698. 10.1038/s41477-020-0666-7.

1660 29. Roeder, A.H.K. (2021). *Arabidopsis* sepals: A model system for the emergent process of morphogenesis. Quant. Plant Biol. 2, e14. 10.1017/qpb.2021.12.

1661 30. Trinh, D.-C., Martin, M., Bald, L., Maizel, A., Trehin, C., and Hamant, O. (2023). Increased gene expression variability hinders the formation of regional mechanical conflicts leading to reduced organ shape robustness. Proc. Natl. Acad. Sci. 120, e2302441120. 10.1073/pnas.2302441120.

1662 31. Jing, H., and Strader, L.C. (2019). Interplay of auxin and cytokinin in lateral root development. Int. J. Mol. Sci. 20, 486. 10.3390/ijms20030486.

1663 32. Hussain, S., Nanda, S., Zhang, J., Rehmani, M.I.A., Suleman, M., Li, G., and Hou, H. (2021). Auxin and Cytokinin Interplay during Leaf Morphogenesis and Phyllotaxy. Plants 10, 1732. 10.3390/plants10081732.

1664 33. Schaller, G.E., Bishopp, A., and Kieber, J.J. (2015). The yin-yang of hormones: Cytokinin and auxin interactions in plant development. Plant Cell 27, 44–63. 10.1105/tpc.114.133595.

1665 34. Ingargiola, C., Duarte, G.T., Robaglia, C., Leprince, A.S., and Meyer, C. (2020). The plant target of rapamycin: A conduit TOR of nutrition and metabolism in photosynthetic organisms. Genes (Basel). 11, 1285. 10.3390/genes1111285.

1666 35. Scarpin, M.R., Leiboff, S., and Brunkard, J.O. (2020). Parallel global profiling of plant tor dynamics reveals a conserved role for LARP1 in translation. eLife 9, e58795. 10.7554/eLife.58795.

1667 36. Yu, H., Ito, T., Wellmer, F., and Meyerowitz, E.M. (2004). Repression of AGAMOUS-LIKE 24 is a crucial step in promoting flower development. Nat. Genet. 36, 157–161. 10.1038/ng1286.

## Translation and developmental robustness

1703 36. Wellmer, F., Alves-Ferreira, M., Dubois, A., Riechmann, J.L., and Meyerowitz, E.M.  
1704 (2006). Genome-wide analysis of gene expression during early *Arabidopsis* flower  
1705 development. *PLoS Genet.* 2, 1012–1024. 10.1371/journal.pgen.0020117.

1706 37. Smyth, D.R., Bowman, J.L., and Meyerowitz, E.M. (1990). Early flower development in  
1707 *Arabidopsis*. *Plant Cell* 2, 755–767. 10.1105/tpc.2.8.755.

1708 38. Goodman, C.A., and Hornberger, T.A. (2013). Measuring protein synthesis with SUnSET:  
1709 A valid alternative to traditional techniques? *Exerc. Sport Sci. Rev.* 41, 107–115.  
1710 10.1097/JES.0b013e3182798a95.

1711 39. Van Hoewyk, D. (2016). Use of the non-radioactive SUnSET method to detect decreased  
1712 protein synthesis in proteasome inhibited *Arabidopsis* roots. *Plant Methods* 12, 20.  
1713 10.1186/S13007-016-0120-Z.

1714 40. Scarpin, M.R., Busche, M., Martinez, R.E., Harper, L.C., Reiser, L., Szakonyi, D.,  
1715 Merchante, C., Lan, T., Xiong, W., Mo, B., et al. (2023). An updated nomenclature for  
1716 plant ribosomal protein genes. *Plant Cell* 35, 640–643. 10.1093/plcell/koac333.

1717 41. Schepetilnikov, M., and Ryabova, L.A. (2018). Recent discoveries on the role of tor  
1718 (Target of rapamycin) signaling in translation in plants. *Plant Physiol.* 176, 1095–1105.  
1719 10.1104/pp.17.01243.

1720 42. Scarpin, M.R., Simmons, C.H., and Brunkard, J.O. (2022). Translating across kingdoms:  
1721 target of rapamycin promotes protein synthesis through conserved and divergent  
1722 pathways in plants. *J. Exp. Bot.* 73, 7016–7025. 10.1093/jxb/erac267.

1723 43. Brunkard, J.O. (2020). Exaptive Evolution of Target of Rapamycin Signaling in  
1724 Multicellular Eukaryotes. *Dev. Cell* 54, 142–155. 10.1016/j.devcel.2020.06.022.

1725 44. Battaglioni, S., Benjamin, D., Wälchli, M., Maier, T., and Hall, M.N. (2022). mTOR  
1726 substrate phosphorylation in growth control. *Cell* 185, 1814–1836.  
1727 10.1016/j.cell.2022.04.013.

1728 45. Valvezan, A.J., and Manning, B.D. (2019). Molecular logic of mTORC1 signalling as a  
1729 metabolic rheostat. *Nat. Metab.* 1, 321–333. 10.1038/s42255-019-0038-7.

1730 46. Schepetilnikov, M., Kobayashi, K., Geldreich, A., Caranta, C., Robaglia, C., Keller, M.,  
1731 and Ryabova, L.A. (2011). Viral factor TAV recruits TOR/S6K1 signalling to activate  
1732 reinitiation after long ORF translation. *EMBO J.* 30, 1343–1356. 10.1038/emboj.2011.39.

1733 47. Schepetilnikov, M., Dimitrova, M., Mancera-Martínez, E., Geldreich, A., Keller, M., and  
1734 Ryabova, L.A. (2013). TOR and S6K1 promote translation reinitiation of uORF-containing  
1735 mRNAs via phosphorylation of eIF3h. *EMBO J.* 32, 1087–1102. 10.1038/emboj.2013.61.

1736 48. Schepetilnikov, M., Makarian, J., Srour, O., Geldreich, A., Yang, Z., Chicher, J.,  
1737 Hammann, P., and Ryabova, L.A. (2017). GTPase ROP2 binds and promotes activation  
1738 of target of rapamycin, TOR, in response to auxin. *EMBO J.* 36, 886–903.  
1739 10.15252/embj.201694816.

1740 49. Chen, G.H., Liu, M.J., Xiong, Y., Sheen, J., and Wu, S.H. (2018). TOR and RPS6  
1741 transmit light signals to enhance protein translation in deetiolating *Arabidopsis* seedlings.  
1742 *Proc. Natl. Acad. Sci. U. S. A.* 115, 12823–12828. 10.1073/pnas.1809526115.

1743 50. Mancera-Martínez, E., Dong, Y., Makarian, J., Srour, O., Thiébeaud, O., Jamsheer, M.,  
1744 Chicher, J., Hammann, P., Schepetilnikov, M., and Ryabova, L.A. (2021).  
1745 Phosphorylation of a reinitiation supporting protein, RISP, determines its function in  
1746 translation reinitiation. *Nucleic Acids Res.* 49, 6908–6924. 10.1093/nar/gkab501.

1747 51. Dong, Y., Srour, O., Lukhovitskaya, N., Makarian, J., Baumberger, N., Galzitskaya, O.,  
1748 Elser, D., Schepetilnikov, M., and Ryabova, L.A. (2023). Functional analogs of  
1749 mammalian 4E-BPs reveal a role for TOR in global plant translation. *Cell Rep.* 42,  
1750 112892. 10.1016/j.celrep.2023.112892.

1751 52. Dasgupta, A., Camacho, R.A.U., Enganti, R., Cho, S.K., Tucker, L.L., Torreverde, J.S.,  
1752 Abraham, P.E., and Arnim, A.G. von (2024). A phosphorylation-deficient ribosomal  
1753 protein eS6 is largely functional in *Arabidopsis thaliana*, rescuing mutant defects from

## Translation and developmental robustness

1754 global translation and gene expression to photosynthesis and growth. *Plant Direct* 8,  
1755 e566. 10.1002/pld3.566.

1756 53. Xiong, Y., McCormack, M., Li, L., Hall, Q., Xiang, C., and Sheen, J. (2013). Glucose-TOR  
1757 signalling reprograms the transcriptome and activates meristems. *Nature* 496, 181–186.  
1758 10.1038/nature12030.

1759 54. Riegler, S., Servi, L., Scarpin, M.R., Godoy Herz, M.A., Kubaczka, M.G., Venhuizen, P.,  
1760 Meyer, C., Brunkard, J.O., Kalyna, M., Barta, A., et al. (2021). Light regulates alternative  
1761 splicing outcomes via the TOR kinase pathway. *Cell Rep.* 36, 109676.  
1762 10.1016/j.celrep.2021.109676.

1763 55. Obomighie, I., Lapenas, K., Murphy, B.E., Bowles, A.M.C., Bechtold, U., and Prischi, F.  
1764 (2021). The Role of Ribosomal Protein S6 Kinases in Plant Homeostasis. *Front. Mol.*  
1765 *Biosci.* 8, 636560. 10.3389/fmolb.2021.636560.

1766 56. Xiong, Y., and Sheen, J. (2012). Rapamycin and glucose-target of rapamycin (TOR)  
1767 protein signaling in plants. *J. Biol. Chem.* 287, 2836–2842. 10.1074/jbc.M111.300749.

1768 57. Moreau, M., Azzopardi, M., Clément, G., Dobrenel, T., Marchive, C., Renne, C., Martin-  
1769 Magniette, M.L., Taconnat, L., Renou, J.P., Robaglia, C., et al. (2012). Mutations in the  
1770 *Arabidopsis* homolog of LST8/GβL, a partner of the target of Rapamycin kinase, impair  
1771 plant growth, flowering, and metabolic adaptation to long days. *Plant Cell* 24, 463–481.  
1772 10.1105/tpc.111.091306.

1773 58. Brunkard, J.O., Xu, M., Regina Scarpin, M., Chatterjee, S., Shemyakina, E.A., Goodman,  
1774 H.M., and Zambryski, P. (2020). TOR dynamically regulates plant cell-cell transport. *Proc.*  
1775 *Natl. Acad. Sci. U. S. A.* 117, 5049–5058. 10.1073/pnas.1919196117.

1776 59. Menand, B., Desnos, T., Nussaume, L., Bergert, F., Bouchez, D., Meyer, C., and  
1777 Robaglia, C. (2002). Expression and disruption of the *Arabidopsis* TOR (target of  
1778 rapamycin) gene. *Proc. Natl. Acad. Sci. U. S. A.* 99, 6422–6427.  
1779 10.1073/pnas.092141899.

1780 60. Zhao, Z., Andersen, S.U., Ljung, K., Dolezal, K., Miotk, A., Schultheiss, S.J., and  
1781 Lohmann, J.U. (2010). Hormonal control of the shoot stem-cell niche. *Nature* 465, 1089–  
1782 1092. 10.1038/nature09126.

1783 61. Yoshida, S., Mandel, T., and Kuhlemeier, C. (2011). Stem cell activation by light guides  
1784 plant organogenesis. *Genes Dev.* 25, 1439–1450. 10.1101/gad.631211.

1785 62. Du, F., Guan, C., and Jiao, Y. (2018). Molecular Mechanisms of Leaf Morphogenesis.  
1786 *Mol. Plant* 11, 1117–1134. 10.1016/j.molp.2018.06.006.

1787 63. Taylor-Teeples, M., Lanctot, A., and Nemhauser, J.L. (2016). As above, so below:  
1788 Auxin's role in lateral organ development. *Dev. Biol.* 419, 156–164.  
1789 10.1016/j.ydbio.2016.03.020.

1790 64. Nishimura, T., Wada, T., Yamamoto, K.T., and Okada, K. (2005). The *Arabidopsis* STV1  
1791 protein, responsible for translation reinitiation, is required for auxin-mediated gynoecium  
1792 patterning. *Plant Cell* 17, 2940–2953. 10.1105/tpc.105.036533.

1793 65. Zhou, F., Roy, B., and von Arnim, A.G. (2010). Translation reinitiation and development  
1794 are compromised in similar ways by mutations in translation initiation factor eIF3h and the  
1795 ribosomal protein RPL24. *BMC Plant Biol.* 10, 193. 10.1186/1471-2229-10-193.

1796 66. Rosado, A., Li, R., Van De Ven, W., Hsu, E., and Raikhel, N. V. (2012). *Arabidopsis*  
1797 ribosomal proteins control developmental programs through translational regulation of  
1798 auxin response factors. *Proc. Natl. Acad. Sci. U. S. A.* 109, 19537–19544.  
1799 10.1073/pnas.1214774109.

1800 67. Cancé, C., Martin-Arevalillo, R., Boubekeur, K., and Dumas, R. (2022). Auxin response  
1801 factors are keys to the many auxin doors. *New Phytol.* 235, 402–419.  
1802 10.1111/nph.18159.

1803 68. Kim, B.H., Cai, X., Vaughn, J.N., and Von Arnim, A.G. (2007). On the functions of the h  
1804 subunit of eukaryotic initiation factor 3 in late stages of translation initiation. *Genome Biol.*

## Translation and developmental robustness

1805 8, R60. 10.1186/gb-2007-8-4-r60.

1806 69. Von Arnim, A.G., Jia, Q., and Vaughn, J.N. (2014). Regulation of plant translation by  
1807 upstream open reading frames. *Plant Sci.* 214, 1–12. 10.1016/j.plantsci.2013.09.006.

1808 70. Jones, B., Ljung, K., Gunnerås, S.A., Petersson, S. V., Tarkowski, P., Graham, N., May,  
1809 S., Dolezal, K., and Sandberg, G. (2010). Cytokinin regulation of auxin synthesis in  
1810 *Arabidopsis* involves a homeostatic feedback loop regulated via auxin and cytokinin  
1811 signal transduction. *Plant Cell* 22, 2956–2969. 10.1105/tpc.110.074856.

1812 71. Marhavý, P., Duclercq, J., Weller, B., Feraru, E., Bielach, A., Offringa, R., Friml, J.,  
1813 Schwechheimer, C., Murphy, A., and Benková, E. (2014). Cytokinin controls polarity of  
1814 PIN1-dependent Auxin transport during lateral root organogenesis. *Curr. Biol.* 24, 1031–  
1815 1037. 10.1016/j.cub.2014.04.002.

1816 72. Růžčka, K., Šimášková, M., Duclercq, J., Petrášek, J., Zažímalová, E., Simon, S., Friml,  
1817 J., Van Montagu, M.C.E., and Benková, E. (2009). Cytokinin regulates root meristem  
1818 activity via modulation of the polar auxin transport. *Proc. Natl. Acad. Sci. U. S. A.* 106,  
1819 4284–4289. 10.1073/pnas.0900060106.

1820 73. Müller, B., and Sheen, J. (2007). Advances in cytokinin signaling. *Science* 318, 68–69.  
1821 10.1126/science.1145461.

1822 74. Karunadasa, S.S., Kurepa, J., Shull, T.E., and Smalle, J.A. (2020). Cytokinin-induced  
1823 protein synthesis suppresses growth and osmotic stress tolerance. *New Phytol.* 227, 50–  
1824 64. 10.1111/nph.16519.

1825 75. Szwejkowska, A., Gwoidi, E., and Spychal, M. (1980). The Cytokinin Control of Protein  
1826 Synthesis in Plants. In *Metabolism and Molecular Activities of Cytokinins*, J. Guern and C.  
1827 Peaud-Lenoel, eds. (Springer-Verlag Berlin Heidelberg), pp. 212–217. 10.1007/978-3-  
1828 642-68035-9.

1829 76. Woźny, A., and Gwóźdż, E.A. (1980). The effect of cytokinin on the polyribosome  
1830 formation in cucumber cotyledons. *Biochem. und Physiol. der Pflanz.* 175, 476–480.  
1831 10.1016/s0015-3796(80)80032-1.

1832 77. Klyachko, N.L., Yakovleva, L.A., Shakirova, F.M., and Kulaeva, O.N. (1982). Cell-free  
1833 translation of polyribosomes from detached pumpkin cotyledons: Effects of starvation and  
1834 cytokinin. *Biol. Plant.* 24, 374–380. 10.1007/BF02909106.

1835 78. Short, K.C., Tepfer, D.A., and Fosket, D.E. (1974). Regulation of polyribosome formation  
1836 and cell division in cultured soybean cells by cytokinin. *J. Cell Sci.* 15, 75–87.

1837 79. Brenner, W.G., and Schmülling, T. (2012). Transcript profiling of cytokinin action in  
1838 *Arabidopsis* roots and shoots discovers largely similar but also organ-specific responses.  
1839 *BMC Plant Biol.* 12, 112. 10.1186/1471-2229-12-112.

1840 80. Kiba, T., Naitou, T., Koizumi, N., Yamashino, T., Sakakibara, H., and Mizuno, T. (2005).  
1841 Combinatorial microarray analysis revealing *Arabidopsis* genes implicated in cytokinin  
1842 responses through the His→Asp phosphorelay circuitry. *Plant Cell Physiol.* 46, 339–355.  
1843 10.1093/pcp/pcp033.

1844 81. Černý, M., Kuklová, A., Hoehenwarter, W., Fragner, L., Novák, O., Rotková, G., Jedelský,  
1845 P.L., Žáková, K., Šmehilová, M., Strnad, M., et al. (2013). Proteome and metabolome  
1846 profiling of cytokinin action in *Arabidopsis* identifying both distinct and similar responses  
1847 to cytokinin down- and up-regulation. *J. Exp. Bot.* 64, 4193–4206. 10.1093/jxb/ert227.

1848 82. Černý, M., Dycka, F., Bobál'ová, J., and Brzobohatý, B. (2011). Early cytokinin response  
1849 proteins and phosphoproteins of *Arabidopsis thaliana* identified by proteome and  
1850 phosphoproteome profiling. *J. Exp. Bot.* 62, 921–937. 10.1093/jxb/erq322.

1851 83. Miyawaki, K., Tarkowski, P., Matsumoto-Kitano, M., Kato, T., Sato, S., Tarkowska, D.,  
1852 Tabata, S., Sandberg, G., and Kakimoto, T. (2006). Roles of *Arabidopsis* ATP/ADP  
1853 isopentenyltransferases and tRNA isopentenyltransferases in cytokinin biosynthesis.  
1854 *Proc. Natl. Acad. Sci. U. S. A.* 103, 16598–16603. 10.1073/pnas.0603522103.

1855 84. Ren, B., Liang, Y., Deng, Y., Chen, Q., Zhang, J., Yang, X., and Zuo, J. (2009). Genome-

## Translation and developmental robustness

1856 wide comparative analysis of type-A *Arabidopsis* response regulator genes by  
1857 overexpression studies reveals their diverse roles and regulatory mechanisms in  
1858 cytokinin signaling. *Cell Res.* 19, 1178–1190. 10.1038/cr.2009.88.

1859 85. Ferreira, F.J., and Kieber, J.J. (2005). Cytokinin signaling. *Curr. Opin. Plant Biol.* 8, 518–  
1860 525. 10.1016/j.pbi.2005.07.013.

1861 86. Kakimoto, T. (2003). Perception and Signal Transduction of Cytokinins. *Annu. Rev. Plant  
1862 Biol.* 54, 605–627. 10.1146/annurev.arplant.54.031902.134802.

1863 87. Jain, M., Tyagi, A.K., and Khurana, J.P. (2006). Molecular characterization and  
1864 differential expression of cytokinin-responsive type-A response regulators in rice (*Oryza  
1865 sativa*). *BMC Plant Biol.* 6, 1. 10.1186/1471-2229-6-1.

1866 88. To, J.P.C., Haberer, G., Ferreira, F.J., Deruère, J., Mason, M.G., Schaller, G.E., Alonso,  
1867 J.M., Ecker, J.R., and Kieber, J.J. (2004). Type-A *Arabidopsis* response regulators are  
1868 partially redundant negative regulators of cytokinin signaling. *Plant Cell* 16, 658–671.  
1869 10.1105/tpc.018978.

1870 89. Kiba, T., Yamada, H., Sato, S., Kato, T., Tabata, S., Yamashino, T., and Mizuno, T.  
1871 (2003). The type-A response regulator, ARR15, acts as a negative regulator in the  
1872 cytokinin-mediated signal transduction in *Arabidopsis thaliana*. *Plant Cell Physiol.* 44,  
1873 868–874. 10.1093/pcp/pcg108.

1874 90. Acheampong, A.K., Shanks, C., Cheng, C.Y., Eric Schaller, G., Dagdas, Y., and Kieber,  
1875 J.J. (2020). EXO70D isoforms mediate selective autophagic degradation of type-A ARR  
1876 proteins to regulate cytokinin sensitivity. *Proc. Natl. Acad. Sci. U. S. A.* 117, 27034–  
1877 27043. 10.1073/pnas.2013161117.

1878 91. To, J.P.C., Deruère, J., Maxwell, B.B., Morris, V.F., Hutchison, C.E., Ferreira, F.J.,  
1879 Schaller, G.E., and Kieber, J.J. (2007). Cytokinin regulates type-A *Arabidopsis* response  
1880 regulator activity and protein stability via two-component phosphorelay. *Plant Cell* 19,  
1881 3901–3914. 10.1105/tpc.107.052662.

1882 92. Bothma, J.P., Norstad, M.R., Alamos, S., and Garcia, H.G. (2018). LlamaTags: A  
1883 Versatile Tool to Image Transcription Factor Dynamics in Live Embryos. *Cell* 173, 1810–  
1884 1822.e16. 10.1016/j.cell.2018.03.069.

1885 93. Imamura, A., Yoshino, Y., and Mizuno, T. (2001). Cellular Localization of the Signaling  
1886 Components of *Arabidopsis* His-to-Asp Phosphorelay. *Biosci. Biotechnol. Biochem.* 65,  
1887 2113–2117. 10.1271/bbb.65.2113.

1888 94. Lee, D.J., Kim, S., Ha, Y.M., and Kim, J. (2008). Phosphorylation of *Arabidopsis*  
1889 response regulator 7 (ARR7) at the putative phospho-accepting site is required for ARR7  
1890 to act as a negative regulator of cytokinin signaling. *Planta* 227, 577–587.  
1891 10.1007/s00425-007-0640-x.

1892 95. Buechel, S., Leibfried, A., To, J.P.C., Zhao, Z., Andersen, S.U., Kieber, J.J., and  
1893 Lohmann, J.U. (2010). Role of A-type *Arabidopsis* Response Regulators in meristem  
1894 maintenance and regeneration. *Eur. J. Cell Biol.* 89, 279–284.  
1895 10.1016/j.ejcb.2009.11.016.

1896 96. Xie, M., Chen, H., Huang, L., O’Neil, R.C., Shokhirev, M.N., and Ecker, J.R. (2018). A B-  
1897 ARR-mediated cytokinin transcriptional network directs hormone cross-regulation and  
1898 shoot development. *Nat. Commun.* 9, 1604. 10.1038/s41467-018-03921-6.

1899 97. Mähönen, A.P., Bishopp, A., Higuchi, M., Nieminen, K.M., Kinoshita, K., Törmäkangas,  
1900 K., Ikeda, Y., Oka, A., Kakimoto, T., and Helariutta, Y. (2006). Cytokinin signaling and its  
1901 inhibitor AHP6 regulate cell fate during vascular development. *Science* 311, 94–98.  
1902 10.1126/science.1118875.

1903 98. Kieber, J.J., and Schaller, G.E. (2018). Cytokinin signaling in plant development.  
1904 *Development* 145, dev149344. 10.1242/dev.149344.

1905 99. Hwang, I., Chen, H.C., and Sheen, J. (2002). Two-component signal transduction  
1906 pathways in *Arabidopsis*. *Plant Physiol.* 129, 500–515. 10.1104/pp.005504.

## Translation and developmental robustness

1907 100. Feng, J., Wang, C., Chen, Q., Chen, H., Ren, B., Li, X., and Zuo, J. (2013). S-  
1908 nitrosylation of phosphotransfer proteins represses cytokinin signaling. *Nat. Commun.* 4,  
1909 1529. 10.1038/ncomms2541.

1910 101. Zhang, W., To, J.P.C., Cheng, C.Y., Eric Schaller, G., and Kieber, J.J. (2011). Type-A  
1911 response regulators are required for proper root apical meristem function through post-  
1912 transcriptional regulation of PIN auxin efflux carriers. *Plant J.* 68, 1–10. 10.1111/j.1365-  
1913 313X.2011.04668.x.

1914 102. Abel, S., Nguyen, M.D., and Theologis, A. (1995). The *PS-IAA4/5-like* Family of Early  
1915 Auxin-inducible mRNAs in *Arabidopsis thaliana*. *J. Mol. Biol.* 251, 533–549.  
1916 10.1006/jmbi.1995.0454.

1917 103. Park, J.Y., Kim, H.J., and Kim, J. (2002). Mutation in domain II of IAA1 confers diverse  
1918 auxin-related phenotypes and represses auxin-activated expression of Aux/IAA genes in  
1919 steroid regulator-inducible system. *Plant J.* 32, 669–683. 10.1046/j.1365-  
1920 313X.2002.01459.x.

1921 104. Abel, S., Oeller, P.W., and Theologis, A. (1994). Early auxin-induced genes encode  
1922 short-lived nuclear proteins. *Proc. Natl. Acad. Sci. U. S. A.* 91, 326–330.  
1923 10.1073/pnas.91.1.326.

1924 105. Zenser, N., Ellsmore, A., Leasure, C., and Callis, J. (2001). Auxin modulates the  
1925 degradation rate of Aux/IAA proteins. *Proc. Natl. Acad. Sci. U. S. A.* 98, 11795–11800.  
1926 10.1073/pnas.211312798.

1927 106. Worley, C.K., Zenser, N., Ramos, J., Rouse, D., Leyser, O., Theologis, A., and Callis, J.  
1928 (2000). Degradation of Aux/IAA proteins is essential for normal auxin signalling. *Plant J.*  
1929 21, 553–562. 10.1046/j.1365-313X.2000.00703.x.

1930 107. Ramos, J.A., Zenser, N., Leyser, O., and Callis, J. (2001). Rapid degradation of  
1931 auxin/indoleacetic acid proteins requires conserved amino acids of domain II and is  
1932 proteasome dependent. *Plant Cell* 13, 2349–2360. 10.1105/tpc.13.10.2349.

1933 108. Figueiredo, M.R.A. de, and Strader, L.C. (2022). Intrinsic and extrinsic regulators of  
1934 Aux/IAA protein degradation dynamics. *Trends Biochem. Sci.* 47, 865–874.  
1935 10.1016/j.tibs.2022.06.004.

1936 109. Liao, C.Y., Smet, W., Brunoud, G., Yoshida, S., Vernoux, T., and Weijers, D. (2015).  
1937 Reporters for sensitive and quantitative measurement of auxin response. *Nat. Methods*  
1938 12, 207–210. 10.1038/nmeth.3279.

1939 110. Radhakrishnan, S.K., Lee, C.S., Young, P., Beskow, A., Chan, J.Y., and Deshaies, R.J.  
1940 (2010). Transcription Factor Nrf1 Mediates the Proteasome Recovery Pathway after  
1941 Proteasome Inhibition in Mammalian Cells. *Mol. Cell* 38, 17–28.  
1942 10.1016/j.molcel.2010.02.029.

1943 111. Gladman, N.P., Marshall, R.S., Lee, K.H., and Vierstra, R.D. (2016). The proteasome  
1944 stress regulon is controlled by a pair of NAC transcription factors in *arabidopsis*. *Plant*  
1945 *Cell* 28, 1279–1296. 10.1105/tpc.15.01022.

1946 112. Njomen, E., and Tepe, J.J. (2019). Proteasome Activation as a New Therapeutic  
1947 Approach to Target Proteotoxic Disorders. *J. Med. Chem.* 62, 6469–6481.  
1948 10.1021/acs.jmedchem.9b00101.

1949 113. Anderson, R.T., Bradley, T.A., and Smith, D.M. (2022). Hyperactivation of the  
1950 proteasome in *Caenorhabditis elegans* protects against proteotoxic stress and extends  
1951 lifespan. *J. Biol. Chem.* 298, 102415. 10.1016/j.jbc.2022.102415.

1952 114. Kandel, R., Jung, J., and Neal, S. (2024). Proteotoxic stress and the ubiquitin proteasome  
1953 system. *Semin. Cell Dev. Biol.* 156, 107–120. 10.1016/j.semcdb.2023.08.002.

1954 115. Quy, P.N., Kuma, A., Pierres, P., and Mizushima, N. (2013). Proteasome-dependent  
1955 activation of mammalian target of rapamycin complex 1 (mTORC1) is essential for  
1956 autophagy suppression and muscle remodeling following denervation. *J. Biol. Chem.* 288,  
1957 1125–1134. 10.1074/jbc.M112.399949.

## Translation and developmental robustness

1958 116. Zhao, J., Zhai, B., Gygi, S.P., and Goldberg, A.L. (2015). MTOR inhibition activates  
1959 overall protein degradation by the ubiquitin proteasome system as well as by autophagy.  
1960 Proc. Natl. Acad. Sci. U. S. A. 112, 15790–15797. 10.1073/pnas.1521919112.

1961 117. Zhang, Y., Nicholatos, J., Dreier, J.R., Ricoult, S.J.H., Widenmaier, S.B., Hotamisligil,  
1962 G.S., Kwiatkowski, D.J., and Manning, B.D. (2014). Coordinated regulation of protein  
1963 synthesis and degradation by mTORC1. Nature 513, 440–443. 10.1038/nature13492.

1964 118. Zhao, J., Garcia, G.A., and Goldberg, A.L. (2016). Control of proteasomal proteolysis by  
1965 mTOR. Nature 529, E1–E2. 10.1038/nature16472.

1966 119. Zhang, Y., and Manning, B.D. (2016). Zhang & Manning reply. Nature 529, E2–E3.  
1967 10.1038/nature16473.

1968 120. Rousseau, A., and Bertolotti, A. (2016). An evolutionarily conserved pathway controls  
1969 proteasome homeostasis. Nature 536, 184–189. 10.1038/nature18943.

1970 121. Mills, E.W., and Green, R. (2017). Ribosomopathies: There's strength in numbers.  
1971 Science 358, eaan2755. 10.1126/science.aan2755.

1972 122. Warren, A.J. (2018). Molecular basis of the human ribosomopathy Shwachman-Diamond  
1973 syndrome. Adv. Biol. Regul. 67, 109–127. 10.1016/j.jbior.2017.09.002.

1974 123. Hawer, H., Mendelsohn, B.A., Mayer, K., Kung, A., Malhotra, A., Tuupanen, S., Schleit,  
1975 J., Brinkmann, U., and Schaffrath, R. (2020). Diphthamide-deficiency syndrome: a novel  
1976 human developmental disorder and ribosomopathy. Eur. J. Hum. Genet. 28, 1497–1508.  
1977 10.1038/s41431-020-0668-y.

1978 124. Armistead, J., Patel, N., Wu, X., Hemming, R., Chowdhury, B., Basra, G.S., Del Bigio,  
1979 M.R., Ding, H., and Triggs-Raine, B. (2015). Growth arrest in the ribosomopathy, bowen-  
1980 conradi syndrome, is due to dramatically reduced cell proliferation and a defect in mitotic  
1981 progression. Biochim. Biophys. Acta - Mol. Basis Dis. 1852, 1029–1037.  
1982 10.1016/j.bbadi.2015.02.007.

1983 125. Zhou, C., Zang, D., Jin, Y., Wu, H., Liu, Z., Du, J., and Zhang, J. (2011). Mutation in  
1984 ribosomal protein L21 underlies hereditary hypotrichosis simplex. Hum. Mutat. 32, 710–  
1985 714. 10.1002/humu.21503.

1986 126. Dixon, M.J. (1995). Treacher Collins syndrome. J. Med. Genet. 32, 806–808.  
1987 10.1136/jmg.32.10.806.

1988 127. Gazda, H.T., Sheen, M.R., Vlachos, A., Choesmel, V., O'Donohue, M.F., Schneider, H.,  
1989 Darras, N., Hasman, C., Sieff, C.A., Newburger, P.E., et al. (2008). Ribosomal Protein L5  
1990 and L11 Mutations Are Associated with Cleft Palate and Abnormal Thumbs in Diamond-  
1991 Blackfan Anemia Patients. Am. J. Hum. Genet. 83, 769–780. 10.1016/j.ajhg.2008.11.004.

1992 128. Oliver, E.R., Saunders, T.L., Tarlé, S.A., and Glaser, T. (2004). Ribosomal protein L24  
1993 defect in belly spot and tail (*Bst*), a mouse *Minute*. Development 131, 3907–3920.  
1994 10.1242/dev.01268.

1995 129. McGowan, K.A., Li, J.Z., Park, C.Y., Beaudry, V., Tabor, H.K., Sabnis, A.J., Zhang, W.,  
1996 Fuchs, H., De Angelis, M.H., Myers, R.M., et al. (2008). Ribosomal mutations cause p53-  
1997 mediated dark skin and pleiotropic effects. Nat. Genet. 40, 963–970. 10.1038/ng.188.

1998 130. Oristian, D.S., Slooíman, L.G., Zhou, X., Wang, L., Farach-Carson, M.C., and Kirn-  
1999 Safran, C.B. (2009). Ribosomal protein L29/HIP deficiency delays osteogenesis and  
2000 increases fragility of adult bone in mice. J. Orthop. Res. 27, 28–35. 10.1002/jor.20706.

2001 131. Uechi, T., Nakajima, Y., Nakao, A., Torihara, H., Chakraborty, A., Inoue, K., and  
2002 Kenmochi, N. (2006). Ribosomal protein gene knockdown causes developmental defects  
2003 in zebrafish. PLoS One 1, e37. 10.1371/journal.pone.0000037.

2004 132. Marygold, S.J., Coelho, C.M.A., and Leevers, S.J. (2005). Genetic analysis of RpL38 and  
2005 RpL5, two minute genes located in the centric heterochromatin of chromosome 2 of  
2006 *Drosophila melanogaster*. Genetics 169, 683–695. 10.1534/genetics.104.034124.

2007 133. Lee, C.C., Tsai, Y.T., Kao, C.W., Lee, L.W., Lai, H.J., Ma, T.H., Chang, Y.S., Yeh, N.H.,  
2008 and Lo, S.J. (2014). Mutation of a Nopp140 gene *dao-5* alters rDNA transcription and

## Translation and developmental robustness

2009        increases germ cell apoptosis in *C. elegans*. *Cell Death Dis.* 5, e1158.  
2010        10.1038/cddis.2014.114.

2011        134. Ito, T., Kim, G.T., and Shinozaki, K. (2000). Disruption of an *Arabidopsis* cytoplasmic  
2012        ribosomal protein S13-homologous gene by transposon-mediated mutagenesis causes  
2013        aberrant growth and development. *Plant J.* 22, 257–264. 10.1046/j.1365-  
2014        313X.2000.00728.x.

2015        135. Horiguchi, G., Mollá-Morales, A., Pérez-Pérez, J.M., Kojima, K., Robles, P., Ponce, M.R.,  
2016        Micol, J.L., and Tsukaya, H. (2011). Differential contributions of ribosomal protein genes  
2017        to *Arabidopsis thaliana* leaf development. *Plant J.* 65, 724–736. 10.1111/j.1365-  
2018        313X.2010.04457.x.

2019        136. Zhao, H., Lü, S., Li, R., Chen, T., Zhang, H., Cui, P., Ding, F., Liu, P., Wang, G., Xia, Y.,  
2020        et al. (2015). The *Arabidopsis* gene *D/G6* encodes a large 60S subunit nuclear export  
2021        GTPase 1 that is involved in ribosome biogenesis and affects multiple auxin-regulated  
2022        development processes. *J. Exp. Bot.* 66, 6863–6875. 10.1093/jxb/erv391.

2023        137. Takagi, M., Absalon, M.J., McLure, K.G., and Kastan, M.B. (2005). Regulation of p53  
2024        translation and induction after DNA damage by ribosomal protein L26 and nucleolin. *Cell*  
2025        123, 49–63. 10.1016/j.cell.2005.07.034.

2026        138. Deisenroth, C., and Zhang, Y. (2010). Ribosome biogenesis surveillance: Probing the  
2027        ribosomal protein-Mdm2-p53 pathway. *Oncogene* 29, 4253–4260.  
2028        10.1038/onc.2010.189.

2029        139. Warner, J.R., and McIntosh, K.B. (2009). How Common Are Extraribosomal Functions of  
2030        Ribosomal Proteins? *Mol. Cell* 34, 3–11. 10.1016/j.molcel.2009.03.006.

2031        140. Dutt, S., Narla, A., Lin, K., Mullally, A., Abayasekara, N., Megerdichian, C., Wilson, F.H.,  
2032        Currie, T., Khanna-Gupta, A., Berliner, N., et al. (2011). Haploinsufficiency for ribosomal  
2033        protein genes causes selective activation of p53 in human erythroid progenitor cells.  
2034        *Blood* 117, 2567–2576. 10.1182/blood-2010-07-295238.

2035        141. Danilova, N., Sakamoto, K.M., and Lin, S. (2008). Ribosomal protein S19 deficiency in  
2036        zebrafish leads to developmental abnormalities and defective erythropoiesis through  
2037        activation of p53 protein family. *Blood* 112, 5228–5237. 10.1182/blood-2008-01-132290.

2038        142. Girardi, T., Vereecke, S., Sulima, S.O., Khan, Y., Fancello, L., Briggs, J.W., Schwab, C.,  
2039        De Beeck, J.O., Verbeeck, J., Royaert, J., et al. (2018). The T-cell leukemia-associated  
2040        ribosomal RPL10 R98S mutation enhances JAK-STAT signaling. *Leukemia* 32, 809–819.  
2041        10.1038/leu.2017.225.

2042        143. Ludwig, L.S., Gazda, H.T., Eng, J.C., Eichhorn, S.W., Thiru, P., Ghazvinian, R., George,  
2043        T.I., Gotlib, J.R., Beggs, A.H., Sieff, C.A., et al. (2014). Altered translation of GATA1 in  
2044        Diamond-Blackfan anemia. *Nat. Med.* 20, 748–753. 10.1038/nm.3557.

2045        144. Khajuria, R.K., Munschauer, M., Ulirsch, J.C., Fiorini, C., Ludwig, L.S., McFarland, S.K.,  
2046        Abdulhay, N.J., Specht, H., Keshishian, H., Mani, D.R., et al. (2018). Ribosome Levels  
2047        Selectively Regulate Translation and Lineage Commitment in Human Hematopoiesis.  
2048        *Cell* 173, 90-103.e19. 10.1016/j.cell.2018.02.036.

2049        145. In, K., Zaini, M.A., Müller, C., Warren, A.J., Von Lindern, M., and Calkhoven, C.F. (2016).  
2050        Shwachman-Bodian-Diamond syndrome (SBDS) protein deficiency impairs translation re-  
2051        initiation from C/EBP $\alpha$  and C/EBP $\beta$  mRNAs. *Nucleic Acids Res.* 44, 4134–4146.  
2052        10.1093/nar/gkw005.

2053        146. Kondrashov, N., Pusic, A., Stumpf, C.R., Shimizu, K., Hsieh, A.C., Xue, S., Ishiijima, J.,  
2054        Shiroishi, T., and Barna, M. (2011). Ribosome-mediated specificity in Hox mRNA  
2055        translation and vertebrate tissue patterning. *Cell* 145, 383–397.  
2056        10.1016/j.cell.2011.03.028.

2057        147. Deliu, L.P., Turingan, M., Jadir, D., Lee, B., Ghosh, A., and Grewal, S.S. (2022).  
2058        Serotonergic neuron ribosomal proteins regulate the neuroendocrine control of  
2059        *Drosophila* development. *PLoS Genet.* 18, e1010371. 10.1371/journal.pgen.1010371.

## Translation and developmental robustness

2060 148. Adams, K.W., and Cooper, G.M. (2007). Rapid turnover of Mcl-1 couples translation to  
2061 cell survival and apoptosis. *J. Biol. Chem.* 282, 6192–6200. 10.1074/jbc.M610643200.

2062 149. Truckenbrodt, S., Viplav, A., Jähne, S., Vogts, A., Denker, A., Wildhagen, H., Fornasiero,  
2063 E.F., and Rizzoli, S.O. (2018). Newly produced synaptic vesicle proteins are preferentially  
2064 used in synaptic transmission. *EMBO J.* 37, e98044. 10.15252/embj.201798044.

2065 150. D'Agostino, I.B., Deruère, J., and Kieber, J.J. (2000). Characterization of the response of  
2066 the *Arabidopsis* response regulator gene family to cytokinin. *Plant Physiol.* 124, 1706–  
2067 1717. 10.1104/pp.124.4.1706.

2068 151. Bishopp, A., Help, H., El-Showk, S., Weijers, D., Scheres, B., Friml, J., Benková, E.,  
2069 Mähönen, A.P., and Helariutta, Y. (2011). A mutually inhibitory interaction between auxin  
2070 and cytokinin specifies vascular pattern in roots. *Curr. Biol.* 21, 917–926.  
2071 10.1016/j.cub.2011.04.017.

2072 152. Sud, M., Fahy, E., Cotter, D., Azam, K., Vadivelu, I., Burant, C., Edison, A., Fiehn, O.,  
2073 Higashi, R., Nair, K.S., et al. (2016). Metabolomics Workbench: An international  
2074 repository for metabolomics data and metadata, metabolite standards, protocols, tutorials  
2075 and training, and analysis tools. *Nucleic Acids Res.* 44, D463–D470.  
2076 10.1093/nar/gkv1042.

2077 153. Mähönen, A.P., Bonke, M., Kauppinen, L., Riikinen, M., Benfey, P.N., and Helariutta, Y.  
2078 (2000). A novel two-component hybrid molecule regulates vascular morphogenesis of the  
2079 *Arabidopsis* root. *Genes Dev.* 14, 2938–2943. 10.1101/gad.189200.

2080 154. Sotta, N., Shantikumar, L., Sakamoto, T., Matsunaga, S., and Fujiwara, T. (2016). TPR5  
2081 is involved in directional cell division and is essential for the maintenance of meristem cell  
2082 organization in *Arabidopsis thaliana*. *J. Exp. Bot.* 67, 2401–2411. 10.1093/jxb/erw043.

2083 155. Heisler, M.G., Ohno, C., Das, P., Sieber, P., Reddy, G. V., Long, J.A., and Meyerowitz,  
2084 E.M. (2005). Patterns of auxin transport and gene expression during primordium  
2085 development revealed by live imaging of the *Arabidopsis* inflorescence meristem. *Curr.*  
2086 *Biol.* 15, 1899–1911. 10.1016/j.cub.2005.09.052.

2087 156. Müller, B., and Sheen, J. (2008). Cytokinin and auxin interaction in root stem-cell  
2088 specification during early embryogenesis. *Nature* 453, 1094–1097. 10.1038/nature06943.

2089 157. Brackmann, K., Qi, J., Gebert, M., Jouannet, V., Schlamp, T., Grünwald, K., Wallner,  
2090 E.S., Novikova, D.D., Levitsky, V.G., Agustí, J., et al. (2018). Spatial specificity of auxin  
2091 responses coordinates wood formation. *Nat. Commun.* 9, 875. 10.1038/s41467-018-  
2092 03256-2.

2093 158. Argyros, R.D., Mathews, D.E., Chiang, Y.H., Palmer, C.M., Thibault, D.M., Etheridge, N.,  
2094 Argyros, D.A., Mason, M.G., Kieber, J.J., and Schallera, G.E. (2008). Type B response  
2095 regulators of *Arabidopsis* play key roles in cytokinin signaling and plant development.  
2096 *Plant Cell* 20, 2102–2116. 10.1105/tpc.108.059584.

2097 159. Rademacher, E.H., Möller, B., Lokerse, A.S., Llavata-Peris, C.I., Van Den Berg, W., and  
2098 Weijers, D. (2011). A cellular expression map of the *Arabidopsis AUXIN RESPONSE*  
2099 *FACTOR* gene family. *Plant J.* 68, 597–606. 10.1111/j.1365-313X.2011.04710.x.

2100 160. Saerens, D., Pellis, M., Loris, R., Pardon, E., Dumoulin, M., Matagne, A., Wyns, L.,  
2101 Muyldermans, S., and Conrath, K. (2005). Identification of a universal VHH framework to  
2102 graft non-canonical antigen-binding loops of camel single-domain antibodies. *J. Mol. Biol.*  
2103 352, 597–607. 10.1016/j.jmb.2005.07.038.

2104 161. Fujii, Y., and Kodama, Y. (2015). *In planta* comparative analysis of improved green  
2105 fluorescent proteins with reference to fluorescence intensity and bimolecular fluorescence  
2106 complementation ability. *Plant Biotechnol.* 32, 81–87.  
2107 10.5511/plantbiotechnology.15.0120a.

2108 162. Alamos, S., Reimer, A., Niyogi, K.K., and Garcia, H.G. (2021). Quantitative imaging of  
2109 RNA polymerase II activity in plants reveals the single-cell basis of tissue-wide  
2110 transcriptional dynamics. *Nat. Plants* 7, 1037–1049. 10.1038/s41477-021-00976-0.

## Translation and developmental robustness

2111 163. Alexa, A., Rahnenführer, J., and Lengauer, T. (2006). Improved scoring of functional  
2112 groups from gene expression data by decorrelating GO graph structure. *Bioinformatics*  
2113 22, 1600–1607. 10.1093/bioinformatics/btl140.

2114 164. Mustroph, A., Juntawong, P., and Bailey-Serres, J. (2009). Isolation of Plant Polysomal  
2115 mRNA by Differential Centrifugation and Ribosome Immunopurification Methods. In  
2116 *Methods in molecular biology* (vol. 553) (Humana Press, a part of Springer  
2117 Science+Business Media, LLC), pp. 109–126. 10.1007/978-1-60327-563-7\_6.

2118 165. Gao, X., Wan, J., Liu, B., Ma, M., Shen, B., and Qian, S.B. (2015). Quantitative profiling  
2119 of initiating ribosomes *in vivo*. *Nat. Methods* 12, 147–153. 10.1038/nmeth.3208.

2120 166. Busche, M., Regina Scarpin, M., Hnasko, R., and Brunkard, J.O. (2021). TOR  
2121 coordinates nucleotide availability with ribosome biogenesis in plants. *Plant Cell* 33,  
2122 1615–1632. 10.1093/plcell/koab043.

2123 167. Schindelin, J., Rueden, C.T., Hiner, M.C., and Eliceiri, K.W. (2015). The ImageJ  
2124 ecosystem: An open platform for biomedical image analysis. *Mol. Reprod. Dev.* 82, 518–  
2125 529. 10.1002/mrd.22489.

2126 168. Schindelin, J., Arganda-Carreras, I., Frise, E., Kaynig, V., Longair, M., Pietzsch, T.,  
2127 Preibisch, S., Rueden, C., Saalfeld, S., Schmid, B., et al. (2012). Fiji: An open-source  
2128 platform for biological-image analysis. *Nat. Methods* 9, 676–682. 10.1038/nmeth.2019.

2129 169. de Reuille, P.B., Routier-Kierzkowska, A.L., Kierzkowski, D., Bassel, G.W., Schüpbach,  
2130 T., Tauriello, G., Bajpai, N., Strauss, S., Weber, A., Kiss, A., et al. (2015).  
2131 MorphoGraphX: A platform for quantifying morphogenesis in 4D. *eLife* 4, e05864.  
2132 10.7554/eLife.05864.

2133 170. Schäfer, M., Brütting, C., Baldwin, I.T., and Kallenbach, M. (2016). High-throughput  
2134 quantification of more than 100 primary- and secondary-metabolites, and phytohormones  
2135 by a single solid-phase extraction based sample preparation with analysis by UHPLC-  
2136 HESI-MS/MS. *Plant Methods* 12, 30. 10.1186/s13007-016-0130-x.

2137 171. Kojima, M., Kamada-Nobusada, T., Komatsu, H., Takei, K., Kuroha, T., Mizutani, M.,  
2138 Ashikari, M., Ueguchi-Tanaka, M., Matsuoka, M., Suzuki, K., et al. (2009). Highly  
2139 sensitive and high-throughput analysis of plant hormones using ms-probe modification  
2140 and liquid chromatographytandem mass spectrometry: An application for hormone  
2141 profiling in *oryza sativa*. *Plant Cell Physiol.* 50, 1201–1214. 10.1093/pcp/pcp057.

2142 172. Novák, O., Antoniadi, I., and Ljung, K. (2017). High-resolution cell-type specific analysis  
2143 of cytokinins in sorted root cell populations of *Arabidopsis thaliana*. *Methods Mol. Biol.*  
2144 1497, 231–248. 10.1007/978-1-4939-6469-7\_1.

2145 173. R Core Team (2021). R: A language and environment for statistical computing. R  
2146 Foundation for Statistical Computing, Vienna, Austria. URL <https://www.R-project.org/>.

2147 174. Wickham, H. (2009). *ggplot2: Elegant Graphics for Data Analysis* R. Gentleman, K.  
2148 Hornik, and G. Parmigiani, eds. (Springer) 10.1007/978-0-387-98141-3.

2149 175. Perez-Riverol, Y., Bai, J., Bandla, C., García-Seisdedos, D., Hewapathirana, S.,  
2150 Kamatchinathan, S., Kundu, D.J., Prakash, A., Frericks-Zipper, A., Eisenacher, M., et al.  
2151 (2022). The PRIDE database resources in 2022: A hub for mass spectrometry-based  
2152 proteomics evidences. *Nucleic Acids Res.* 50, D543–D552. 10.1093/nar/gkab1038.

2153

## Translation and developmental robustness

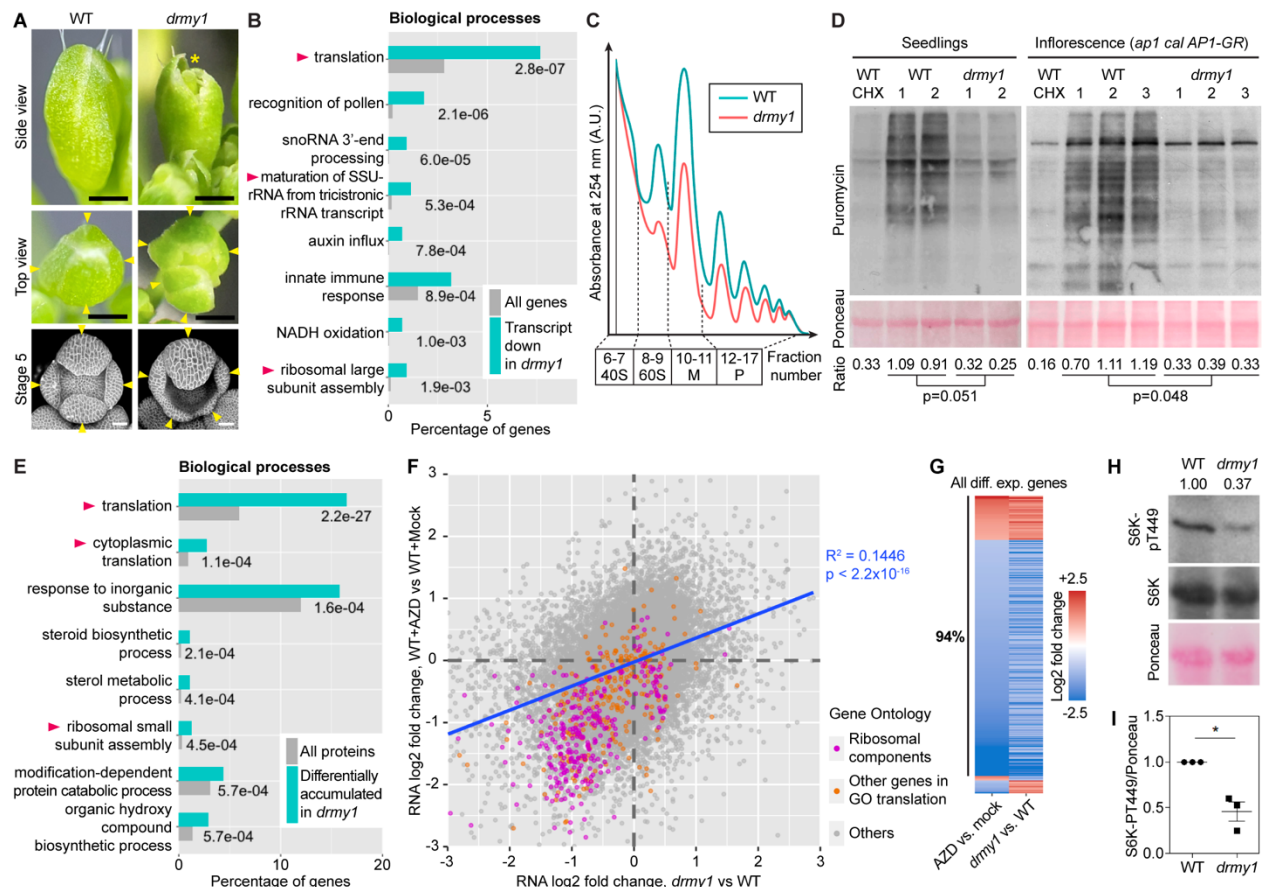


### Figure 1. *drmy1* has reduced ribosome abundance, translation rate, and TOR activity.

(A) Top row, stage 12 buds of WT (left) and *drmy1* (right) viewed from the side. Asterisk shows the gap between sepals with petals and carpels exposed. Middle row, stage 12 buds of WT (left) and *drmy1* (right) viewed from the top. Arrowheads point to sepals. Note that the *drmy1* bud has 5 sepals of unequal size and unevenly spaced, exposing the stamens and carpels. Bottom row, stage 5 buds of WT (left) and *drmy1* (right) containing 35S::*mCitrine-RCI2A* (plasma membrane marker). Arrowheads point to sepal primordia. Note that the *drmy1* bud has 5 sepal primordia of different sizes. Scale bars are 0.5 mm for stage 12 bud images and 25  $\mu$ m for stage 5 bud images.

(B) Gene ontology (GO) enrichment of downregulated genes in *drmy1* compared to WT, in the *ap1 cal AP1-GR* background. Shown are the top 8 GO terms and their enrichment p-values. A complete list can be found in Supplemental Dataset 1. Arrowheads highlight terms related to ribosome biogenesis or translation.

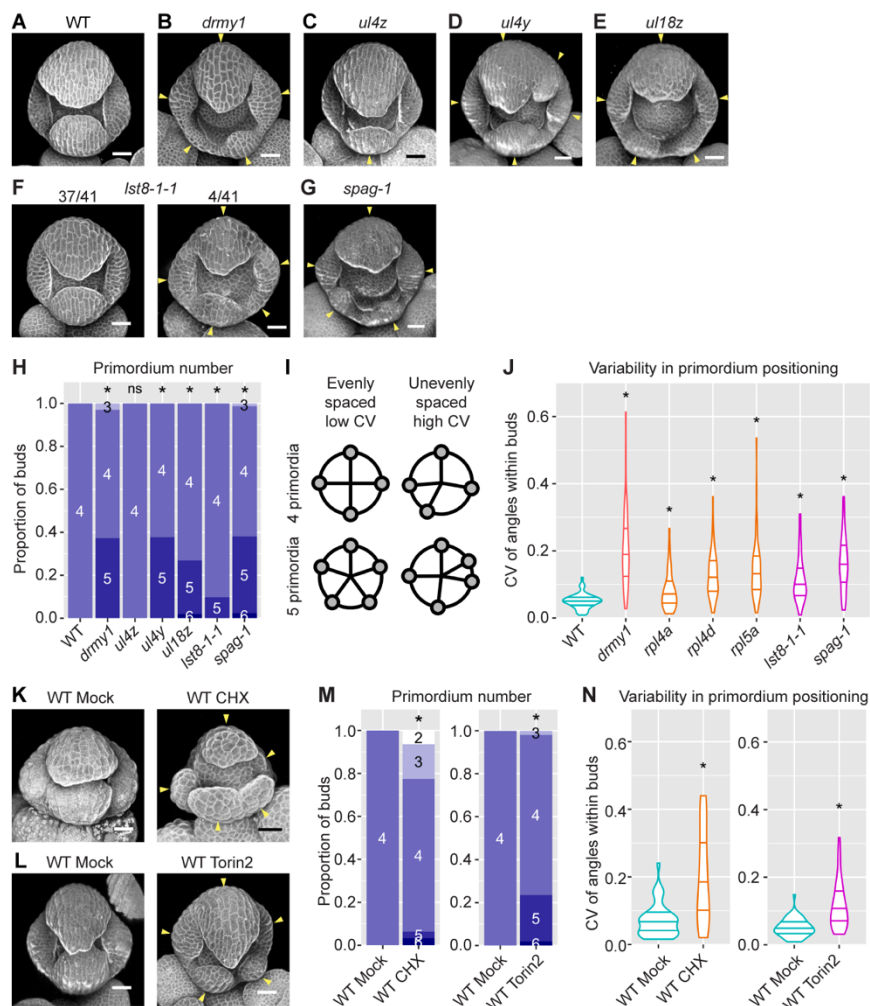
(C) Polysomal profiles of WT (blue) and *drmy1* (red) in the *ap1 cal AP1-GR* background, representative of 3 biological replicates each. Additional replicates are in Supplemental Dataset 2. M, monosomes. P, polysomes.

(D) Puromycin labeling of WT vs *drmy1*. Left, WT and *drmy1* seedlings. From left to right: WT pre-treated with CHX, two biological replicates of WT pre-treated with mock, and two biological replicates of *drmy1* pre-treated with mock. All groups were then treated with puromycin. For seedlings to match in size, WT seedlings were 8 days old and *drmy1* seedlings were 10 days old.

## Translation and developmental robustness

22 Right, WT and *drmy1* inflorescences of induced *ap1 cal AP1-GR* background. From left to right:  
23 WT co-treated with puromycin and CHX, three biological replicates of WT treated with puromycin,  
24 and three biological replicates of *drmy1* treated with puromycin. In both experiments, RuBisCO  
25 large subunit on Ponceau S-stained membrane is shown as a loading control (bottom). Ratio  
26 between puromycin and Ponceau S signals, normalized by the mean of WT, is shown on the  
27 bottom (p-values are from two-sided Student's t-test).  
28 **(E)** Gene ontology (GO) enrichment of differentially accumulated proteins in *drmy1* compared to  
29 WT, in the *ap1 cal AP1-GR* background. Shown are the top 8 GO terms and their enrichment p-  
30 values. A complete list can be found in Supplemental Dataset 1. Arrowheads highlight terms  
31 related to ribosome biogenesis or translation.  
32 **(F-G)** Coherent alteration of gene expression by *drmy1* and AZD-8055 TOR inhibitor treatment.  
33 **(F)** Scatterplot of RNA log2 fold change in *drmy1* vs WT (x-axis), and WT+AZD vs WT+Mock (y-  
34 axis), in 7-day-old seedlings. Genes are color-coded based on the following categories: genes in  
35 "Structural constituents of the ribosome" (GO:0003735) and its offspring terms (magenta); all  
36 other genes in "Translation" (GO:0006412) and its offspring terms (orange); all other genes (gray).  
37 Blue line shows a linear regression of all points ( $R^2 = 0.1446$ ,  $p < 2.2 \times 10^{-16}$ ). **(G)** Of the 466 genes  
38 that are differentially expressed under both conditions, 439 (94%) are coherently altered by AZD-  
39 8055 treatment and the *drmy1* mutation.  
40 **(H-I)** Phosphorylation of the direct TOR substrate, S6K-pT449, in WT and *drmy1*. **(H)** A  
41 representative blot. Top, S6K-pT449. Middle, total S6K protein. Bottom, Ponceau S staining. Ratio  
42 between S6K-pT449 signal and Ponceau S signal is shown above the blots. **(I)** Ratio between  
43 S6K-pT449 and Ponceau S signals normalized by WT, quantified across in three experiments,  
44 shows that TOR activity decreased by half in *drmy1*. (mean  $\pm$  SD; \*,  $p < 0.05$ ).  
45

## Translation and developmental robustness



46

### 47 **Figure 2. Defects in TOR activity, ribosome, and translation disrupt robust sepal initiation.**

48 **(A-G)** Representative images of stage 5 buds in WT (A), *drmy1* (B), *ul4z* (C), *ul4y* (D), *ul18z* (E),  
49 *lst8-1-1* (F), and *spaghetti-1* (G). Tissue morphology is visualized by either propidium iodide (a  
50 cell wall-staining dye) or a plasma membrane marker. Arrowheads indicate sepal primordia that  
51 are variable in number, position, and size. Note that *ul4z* flowers always develop four sepal  
52 primordia, although of different sizes; *lst8-1-1* occasionally (4/41, 9.8%) develops buds with more  
53 than four sepal primordia.

54 **(H)** Quantification of sepal primordium number, comparing *drmy1* (n = 67 buds), *ul4z* (n = 52  
55 buds), *ul4y* (n = 53 buds), *ul18z* (n = 52 buds), *lst8-1-1* (n = 41 buds), and *spaghetti-1* (n = 84  
56 buds) with WT (n = 51 buds). Asterisks indicate statistically significant (p < 0.05) differences from  
57 WT in Fisher's contingency table tests.

58 **(I)** Illustration of robust versus variable positioning of sepal primordia. Primordia are considered  
59 robustly positioned if they are evenly distributed around the edge of the bud. Within each bud,  
60 angles between adjacent primordia with respect to the center of the bud are measured, and  
61 coefficient of variation (CV) is calculated. A bud with robustly positioned primordia would have  
62 similar angular values and a low CV value. A bud with variably positioned primordia would have  
63 very different angular values and a high CV value.

## Translation and developmental robustness

64 **(J)** Quantification of variability in primordium positioning (CV) in the same buds as in (H), following  
65 illustration in (I). Asterisks indicate statistically significant ( $p < 0.05$ ) differences from WT in  
66 Wilcoxon's rank sum tests.

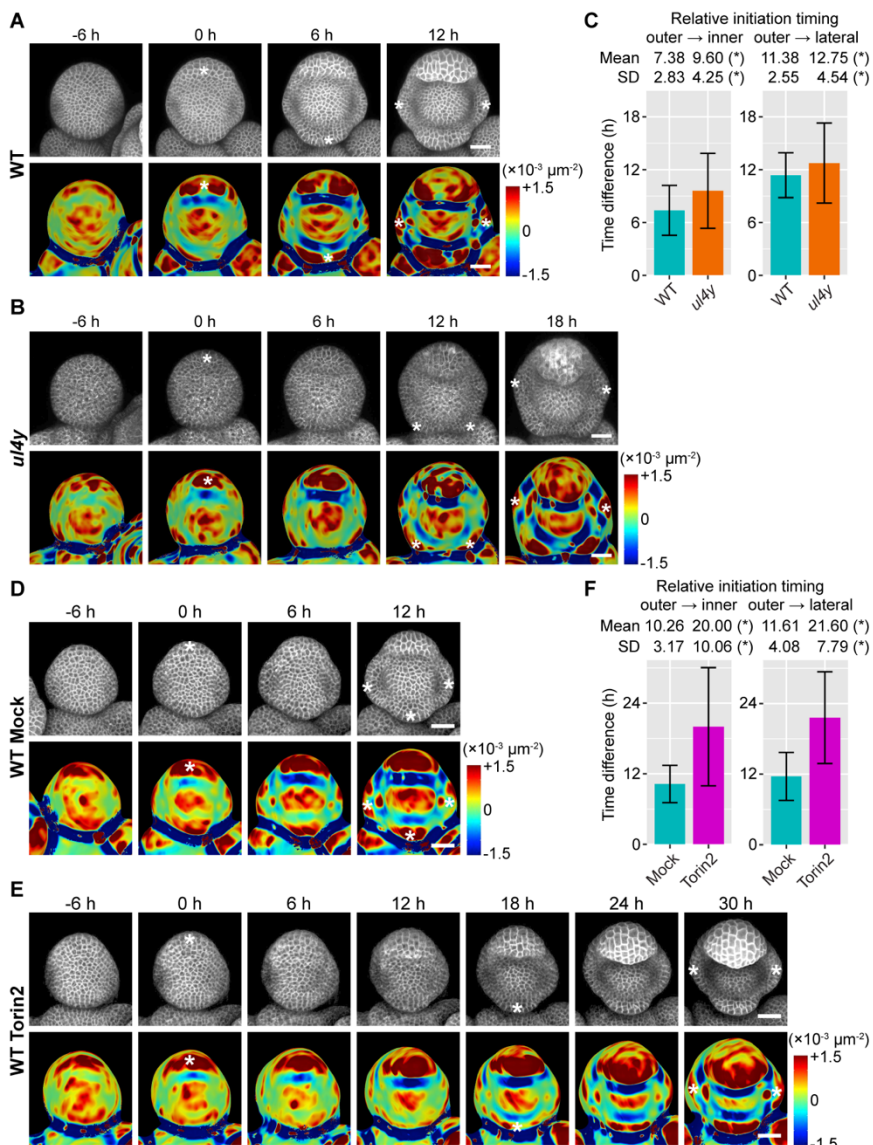
67 **(K)** Representative images of buds from *in vitro*-cultured WT inflorescences treated with mock or  
68 2  $\mu$ M CHX for 9-10 days. Arrowheads indicate sepal primordia that are variable in number,  
69 position, and size.

70 **(L)** Representative images of buds from WT plants treated with mock or 2 nmol Torin2 for 15 days.  
71 Arrowheads indicate sepal primordia that are variable in number, position, and size.

72 **(M-N)** Quantification of sepal primordium number (M) and positional variability (N) similar to (H,J),  
73 comparing CHX-treated ( $n = 31$  buds), CHX-mock ( $n = 42$  buds), Torin2-treated ( $n = 51$  buds)  
74 and Torin2-mock buds ( $n = 56$  buds). Scale bars in all micrographs, 25  $\mu$ m.

75

## Translation and developmental robustness



76

### 77 **Figure 3. TOR and ribosomal defects cause variability in the timing of sepal initiation.**

78 **(A-C)** 6h-interval live imaging of the sepal initiation process in WT (A) and *ul4y* (B), which is  
79 quantified in (C). n = 48 buds for WT; n = 40 buds for *ul4y*.  
80 **(D-F)** 6h-interval live imaging of the sepal initiation process in buds from WT plants treated with  
81 mock or 2 nmol Torin2 twice a day for 15 days, which is quantified in (F). n = 31 buds for mock; n  
82 = 15 buds for Torin2.

83 In **(A,B,D,E)**, top rows show the 35S::*mCitrine-RCI2A* membrane marker, and bottom rows show  
84 Gaussian curvature heatmaps of the same image stacks. Asterisks indicate sepal initiation events,  
85 defined as a dark red band (primordium with positive curvature) separated from the floral  
86 meristem by a dark blue band (boundary with negative curvature) in the heatmap. Scale bars, 25  
87  $\mu\text{m}$ .

88 In **(C,F)**, the amount of time between outer and inner sepal initiation (left) and between outer and  
89 lateral sepal initiation (right) were calculated for each bud. Bar plot shows mean  $\pm$  SD which is

## Translation and developmental robustness

90 also shown on top of each plot. Asterisks indicate statistically significant differences ( $p < 0.05$ ) in  
91 Wilcoxon's rank sum test (for mean) or Levene's test (for SD).  
92

## Translation and developmental robustness

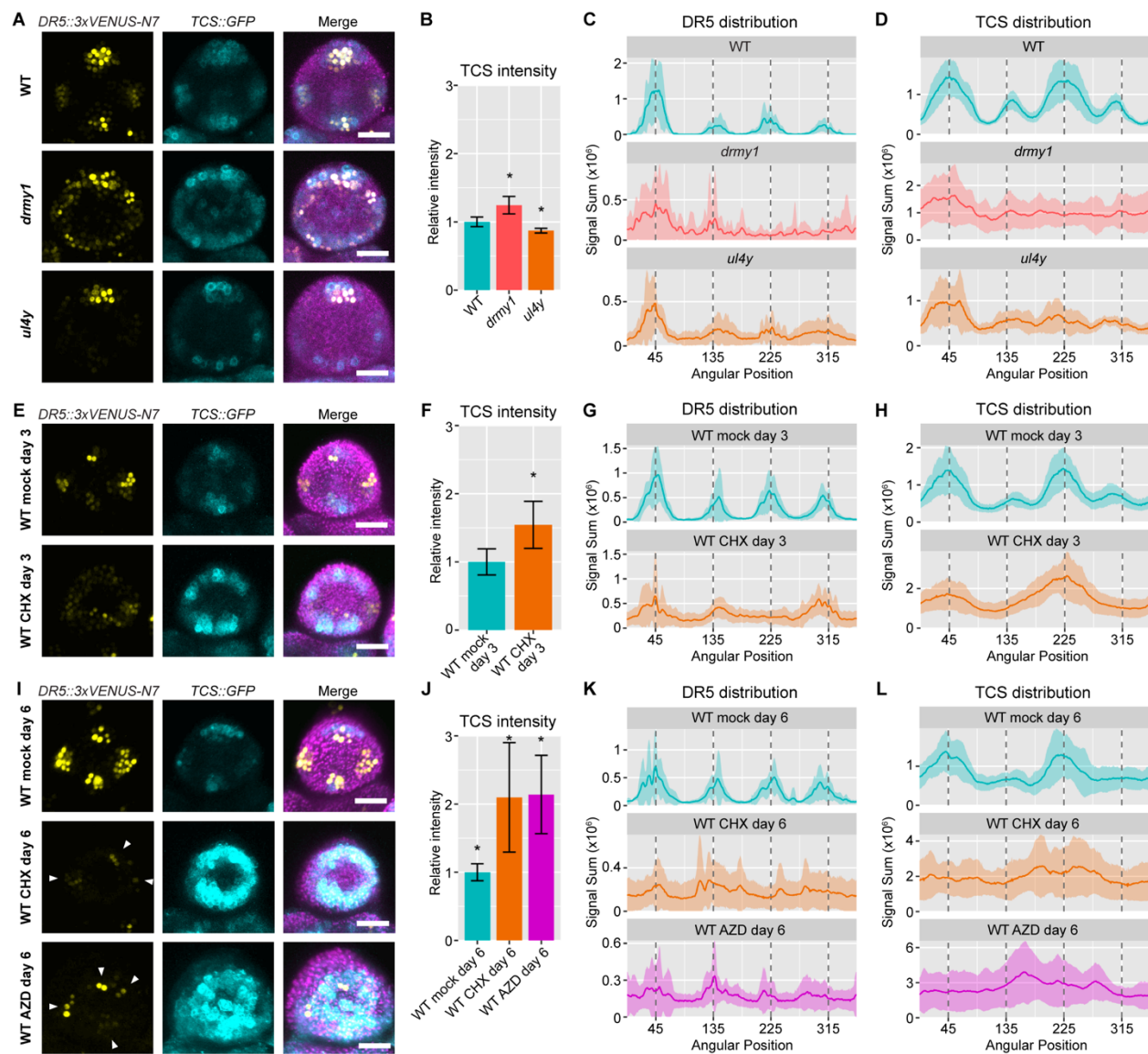


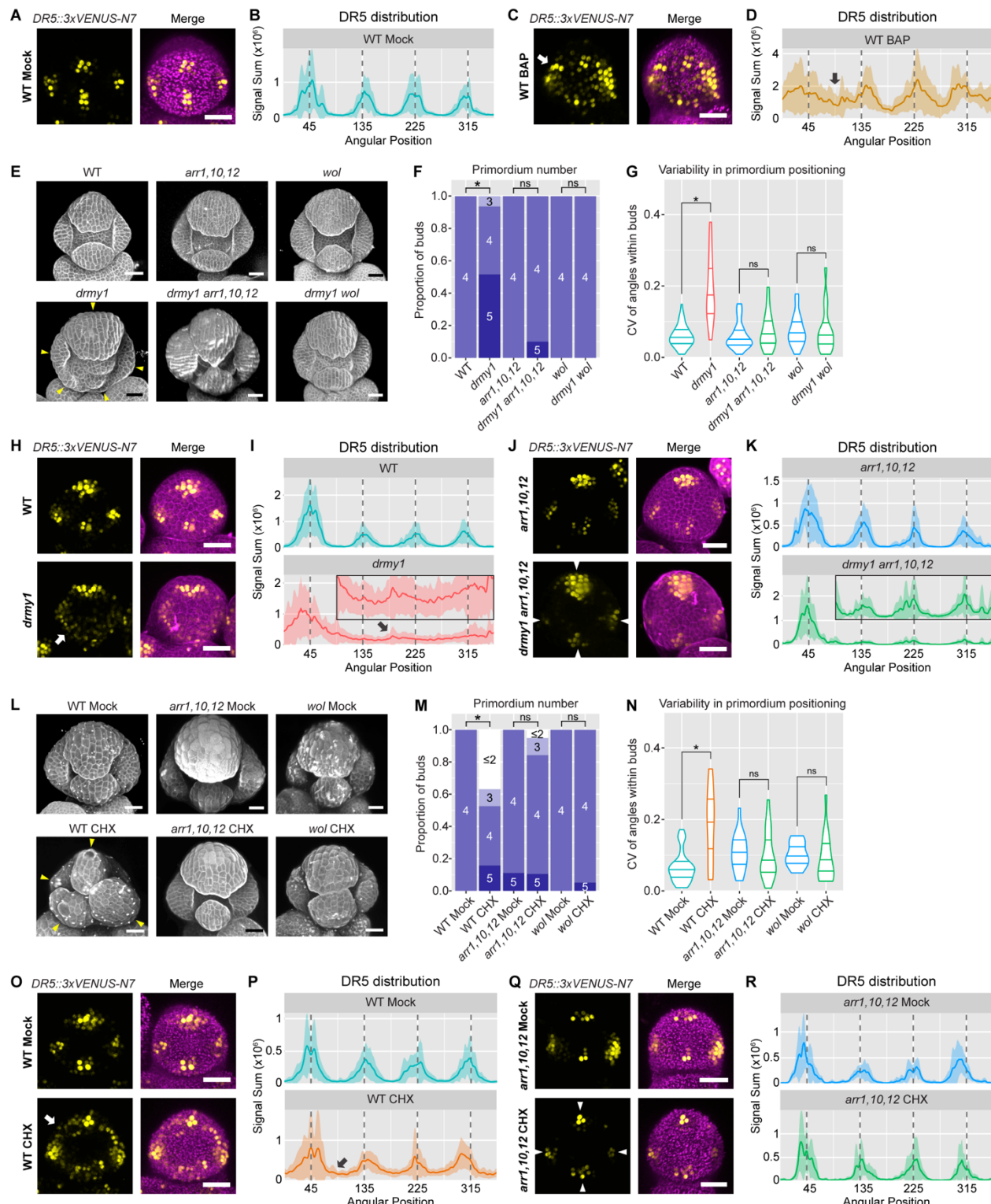
**Figure 4. Inhibition of TOR activity and translation cause variability in auxin and cytokinin signaling.**

**(A-D)** The ribosomal mutant *ul4y* loses robustness in auxin and cytokinin signaling. (A) Representative images of late stage 2 buds of WT, *drmy1*, and *ul4y*, showing the auxin signaling reporter *DR5::3xVENUS-N7* in yellow, the cytokinin signaling reporter *TCS::GFP* in cyan, and both merged with Chlorophyll (in WT) or *UBQ10::mCherry-RCI2A* (in *drmy1* and *ul4y*) in magenta. (B) Quantification of TCS intensity (integrated density divided by area) from maximum intensity projection images, normalized to mean of WT. Shown are mean  $\pm$  SD. Asterisks show statistically significant differences from WT in two-tailed Student's t-tests (*drmy1*,  $p = 2.1 \times 10^{-6}$ ; *ul4y*,  $p = 3.4 \times 10^{-5}$ ). (C) Circular histogram of DR5 signal distribution. Each bud was divided into 360 sectors of 1° each. Within each sector, DR5 signal measured in pixel intensity units (0-255 range) was summed. This sum was plotted along the x-axis starting from the sector at 1:30 position (between the incipient outer sepal and incipient right sepal) going counterclockwise. I.e., in WT, the outer

## Translation and developmental robustness

107 sepal is near 45°, the inner sepal near 225°, and the lateral sepals near 45° and 135° (vertical  
108 dotted lines). The mean was plotted as a solid line, and mean  $\pm$  SD was plotted as a shaded area.  
109 (D) Circular histogram of TCS signal distribution. Sample size for (A-D): WT, n = 12 buds; *drmy1*,  
110 n = 15 buds; *ul4y*, n = 10 buds.  
111 (E-H) 3 days of translation inhibition causes increased and diffuse cytokinin signaling, and diffuse  
112 auxin signaling. (E) Representative images of late stage 2 WT buds treated *in vitro* with mock or  
113 2  $\mu$ M CHX for 3 days. Shown are *DR5::3xVENUS-N7* in yellow, *TCS::GFP* in cyan, and both  
114 merged with Chlorophyll in magenta. (F) Quantification of TCS intensity from maximum intensity  
115 projection images, normalized to mean of WT mock day 3. Shown are mean  $\pm$  SD. Asterisk shows  
116 statistically significant difference in a two-tailed Student's t-test ( $p = 2.0 \times 10^{-4}$ ). (G) Circular  
117 histogram of *DR5* signal distribution. (H) Circular histogram of TCS signal distribution. Sample  
118 size for (E-H): WT mock day 3, n = 10 buds; WT CHX day 3, n = 12 buds.  
119 (I-L) 6 days of TOR or translation inhibition causes increased and diffuse cytokinin signaling, and  
120 randomly positioned auxin signaling maxima. (I) Representative images of late stage 2 WT buds  
121 treated *in vitro* with mock, 2  $\mu$ M CHX, or 2  $\mu$ M AZD for 6 days. Shown are *DR5::3xVENUS-N7* in  
122 yellow, *TCS::GFP* in cyan, and both merged with Chlorophyll in magenta. Arrowheads point to  
123 randomly positioned auxin maxima. (J) Quantification of TCS intensity from maximum intensity  
124 projection images, normalized to mean of WT mock day 6. Shown are mean  $\pm$  SD. Asterisks show  
125 statistically significant differences from mock in two-tailed Student's t-tests (CHX,  $p = 1.0 \times 10^{-3}$ ;  
126 AZD,  $p = 1.2 \times 10^{-4}$ ). (K) Circular histogram of *DR5* signal distribution. (L) Circular histogram of  
127 TCS signal distribution. Sample size for (I-L): WT mock day 6, n = 12 buds; WT CHX day 6, n =  
128 11 buds; WT AZD day 6, n = 10 buds. Scale bars in all micrographs, 25  $\mu$ m.  
129

## Translation and developmental robustness



130

131 **Figure 5. Cytokinin signaling is required for increased variability in auxin signaling and**  
132 **sepal initiation under translation inhibition.**

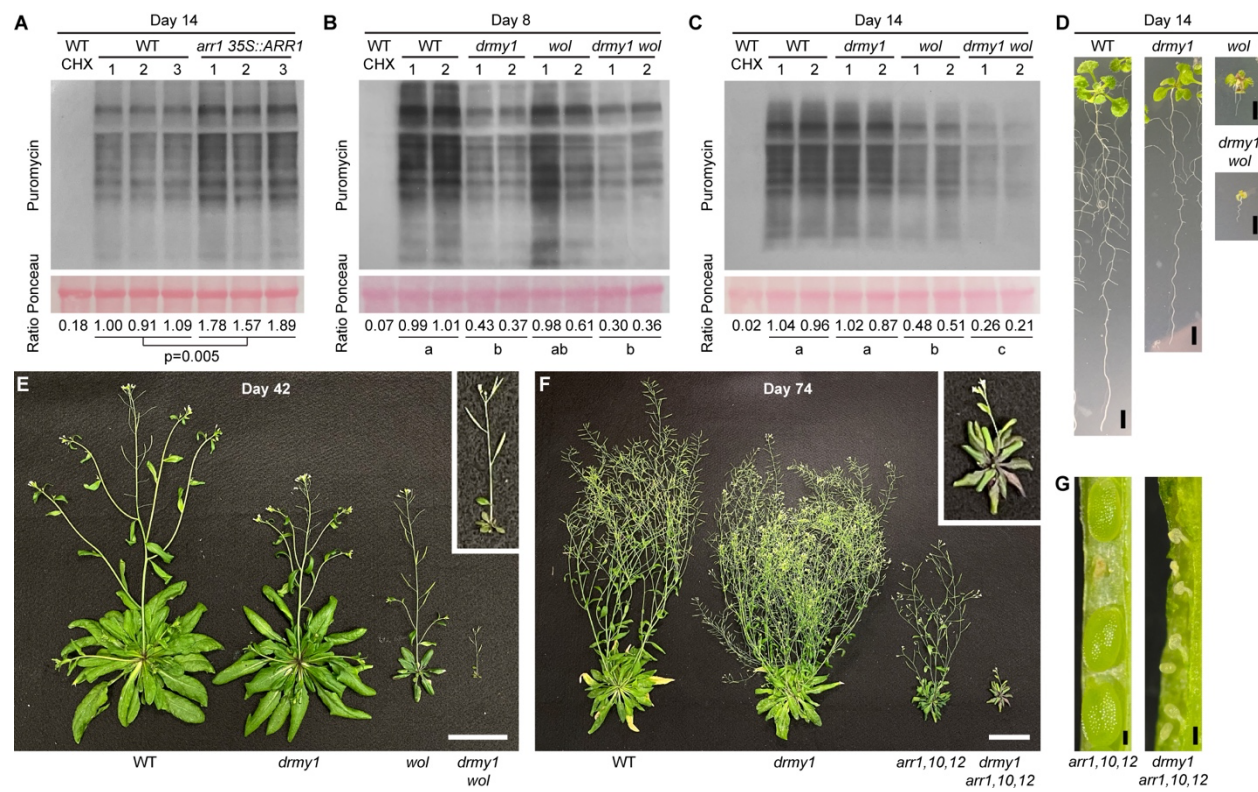
133 **(A-D)** Cytokinin treatment makes auxin signaling diffuse. Shown are late stage 2 WT buds under  
134 mock (A,B) or 5  $\mu$ M cytokinin (BAP) treatment (C,D) for 4 days. (A,C) Auxin signaling reporter

## Translation and developmental robustness

135 *DR5* in yellow, and *DR5* merged with Chlorophyll in magenta. (B,D) Circular histograms of the  
136 *DR5* signal, showing mean (solid line) and mean  $\pm$  SD (shaded area). Arrows point to *DR5* signal  
137 in variable positions. Sample size: WT Mock n = 10, WT BAP n = 10. Also see Zhu et al. (2020),  
138 in this reference see Extended Data Figure 7e.

139 **(E-G)** Cytokinin signaling is required for variable sepal initiation in *drmy1*. (E) Stage 5 buds. Sepal  
140 primordia in *drmy1* are variable (arrowheads), which does not occur in *drmy1 arr1,10,12* and  
141 *drmy1 wol* mutants. (F,G) Quantification of sepal primordium number (F) and positional variability  
142 (G), comparing WT (n = 58) with *drmy1* (n = 31), *arr1,10,12* (n = 24) with *drmy1 arr1,10,12* (n =  
143 20), and *wol* (n = 36) with *drmy1 wol* (n = 39). Asterisks indicate statistically significant (p < 0.05)  
144 differences in Fisher's contingency table tests (F) and Wilcoxon's rank sum tests (G) respectively.  
145 **(H-K)** Cytokinin signaling is required for variable patterning of auxin signaling in *drmy1*. Shown  
146 are late stage 2 buds of WT vs *drmy1* (H,I), and *arr1,10,12* vs *drmy1 arr1,10,12* (J,K). (H,J) Auxin  
147 signaling reporter *DR5* in yellow, and *DR5* merged with propidium iodide in magenta. Arrows point  
148 to diffuse *DR5* signal in variable positions of the *drmy1* bud. Arrowheads show four robust *DR5*  
149 maxima in the *drmy1 arr1,10,12* bud. (I,K) Circular histograms of the *DR5* signal, showing mean  
150 (solid line) and mean  $\pm$  SD (shaded area). For ease of visualization, circular histograms of *drmy1*  
151 and *drmy1 arr1,10,12* between 90 and 360 degrees are enlarged and shown as insets (y-axis  
152 range 0-0.4). Note the presence of *DR5* signal in inter-sepal regions in *drmy1* (black arrow) which  
153 is largely suppressed in *drmy1 arr1,10,12*. Sample size: WT n = 19, *drmy1* n = 16, *arr1,10,12* n =  
154 13, *drmy1 arr1,10,12* n = 9.  
155 **(L-N)** Cytokinin signaling is required for variable sepal initiation under translation inhibition. (L)  
156 Stage 6 buds of WT, *arr1,10,12*, and *wol*, treated with Mock or 2  $\mu$ M CHX for 10 days. WT initiates  
157 sepal primordia at variable positions when treated with CHX (arrowheads), which does not occur  
158 in *arr1,10,12* and *wol*. (M,N) Quantification of sepal primordium number (M) and positional  
159 variability (N), comparing mock and CHX within each genotype. Sample size: WT Mock n = 29,  
160 WT CHX n = 19, *arr1,10,12* Mock n = 18, *arr1,10,12* CHX n = 19, *wol* Mock n = 15, *wol* CHX n =  
161 19. Asterisks indicate statistically significant (p < 0.05) differences in Fisher's contingency table  
162 tests (M) and Wilcoxon's rank sum tests (N) respectively.  
163 **(O-R)** Cytokinin signaling is required for diffuse auxin signaling under translation inhibition. Shown  
164 are late stage 2 buds of WT (O,P) and *arr1,10,12* (Q,R), treated with Mock or 2  $\mu$ M CHX for 3  
165 days. (O,Q) Auxin signaling reporter *DR5* in yellow, and *DR5* merged with Chlorophyll in magenta.  
166 Arrows point to diffuse *DR5* signal in variable positions in CHX-treated WT. Arrowheads show  
167 four robust *DR5* maxima in CHX-treated *arr1,10,12*. (P,R) Circular histograms of the *DR5* signal,  
168 showing mean (solid line) and mean  $\pm$  SD (shaded area). Sample size: WT Mock n = 17, WT CHX  
169 n = 18, *arr1,10,12* Mock n = 7, *arr1,10,12* CHX n = 7. Scale bars in all micrographs, 25  $\mu$ m.  
170

## Translation and developmental robustness



171

172 **Figure 6. Upregulation of cytokinin signaling is required to maintain translation and fitness**  
173 **in drmy1.**

174 (A) Puromycin labeling of WT seedlings with 4 h CHX pre-treatment (control), and three biological  
175 replicates each of WT and *arr1 35S::ARR1* seedlings with 4 h mock pre-treatment. All seedlings  
176 are 14 days old. RuBisCO large subunit in Ponceau S-stained membrane is shown as a loading  
177 control. Signal ratio between puromycin and Ponceau S, normalized to mean of WT, is show on  
178 the bottom. P-value is from a two-sided Student's t-test. Also see Karunadasa et al. (2020).

179 (B,C) Puromycin labeling of WT seedlings with 4 h CHX pre-treatment (control), and two biological  
180 replicates of WT, *drmy1*, *wol*, and *drmy1 wol* seedlings with 4 h mock pre-treatment. Seedlings  
181 are 8 days old in (B) and 14 days old in (C). RuBisCO large subunit in Ponceau S-stained  
182 membrane is shown as a loading control. Letters show compact letter display of a Tukey's all-pair  
183 comparison in a one-way ANOVA model.

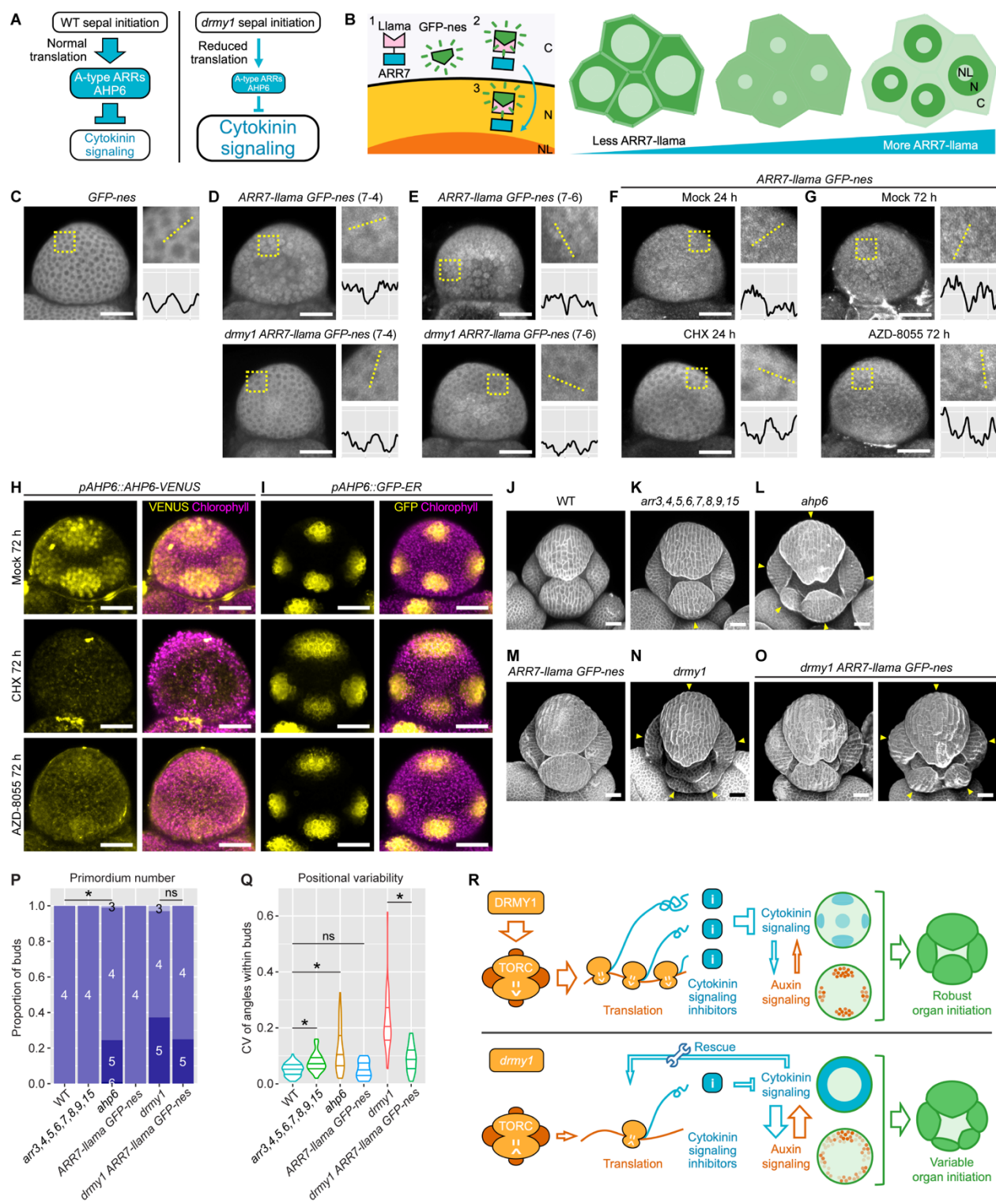
184 (D) Representative 14 days old seedling images of WT, *drmy1*, *wol*, and *drmy1 wol* used in (C).  
185 Notice that *drmy1 wol* is very small and pale. Scale bars, 5 mm.

186 (E) Representative aerial part images of 42 days old plants of WT, *drmy1*, *wol*, and *drmy1 wol*.  
187 Inset shows the zoomed-in *drmy1 wol* plant, which has a tiny rosette and a short inflorescence.  
188 Scale bars, 5 cm. See also Figure S6F.

189 (F) Representative aerial part images of 74 days old plants of WT, *drmy1*, *arr1,10,12*, and *drmy1*  
190 *arr1,10,12*. Inset shows the zoomed-in *drmy1 arr1,10,12* plant, which has pale leaves  
191 accumulating anthocyanin and a short inflorescence. Scale bars, 5 cm. See also Figure S6E.

192 (G) Dissected siliques of *arr1,10,12* (left) and *drmy1 arr1,10,12* (right) showing developing seeds.  
193 Notice that while *arr1,10,12* occasionally have aborted seeds, all seeds in the *drmy1 arr1,10,12*  
194 siliques were aborted. Scale bars, 0.2 mm.

## Translation and developmental robustness



## Translation and developmental robustness

200 level. In *drmy1*, reduced protein synthesis causes reduced levels of these cytokinin signaling  
201 inhibitor proteins, resulting in an upregulation of cytokinin signaling.

202 **(B)** Illustration of Llama Tag. Plants were co-transformed with *ARR7-llama* (*pARR7::ARR7-linker-*  
203 *llama-ARR7ter*) and *GFP-nes* (*pUBQ10::sfGFP-nes-UBQ3ter*). Without *ARR7-llama*, GFP  
204 localizes to the cytosol due to the nuclear export sequence (nes). *ARR7-llama* is produced in the  
205 cytoplasm, C, and translocates into the nucleus, N. The Llama Tag on *ARR7-llama* binds to GFP  
206 and drags GFP into the nucleus (note that from our observation it is excluded from the nucleolus,  
207 NL). Thus, at low *ARR7-llama* levels, GFP signal is mainly in the cytoplasm. At intermediate  
208 *ARR7-llama* levels, GFP is at comparable levels between the cytoplasm and the nucleus, and no  
209 clear pattern can be seen. At high *ARR7-llama* levels, GFP is mainly seen in the nucleus.

210 **(C)** A *GFP-nes* bud showing localization of the GFP signal to the cytoplasm.

211 **(D,E)** GFP images of buds from two independent transgenic lines of *ARR7-llama GFP-nes*, 7-4  
212 (D) and 7-6 (E), of WT (top) vs *drmy1* (bottom) genotypes. Images are representative of n = 17  
213 (line 7-4, WT), n = 40 (line 7-4, *drmy1*), n = 9 (line 7-6, WT), and n = 6 (line 7-6, *drmy1*) buds.  
214 Note that GFP is more cytoplasm-localized in *drmy1* than WT, indicating reduced *ARR7-llama*  
215 protein level.

216 **(F)** GFP images of WT *ARR7-llama GFP-nes* buds treated with mock (top) or 2  $\mu$ M CHX (bottom)  
217 for 24 hours. The mock image is representative of n = 20 buds from three independent lines. The  
218 CHX image is representative of n = 19 buds from these same lines.

219 **(G)** GFP images of WT *ARR7-llama GFP-nes* buds treated with mock (top) or 2  $\mu$ M AZD-8055  
220 (bottom) for 72 hours. The mock image is representative of n = 13 buds from two independent  
221 lines. The AZD-8055 image is representative of n = 11 buds from these same lines. For (C-G),  
222 each image was brightened to reveal subcellular localization patterns of GFP. A square region  
223 taken from the image containing 5-10 cells is enlarged and shown on the top right. Within the  
224 square, GFP intensity was quantified along the dotted line and plotted on the bottom right. X-axis,  
225 pixels (range 0-238). Y-axis, GFP intensity (smoothed by taking the average intensity of 11-  
226 pixel neighborhoods; range 90-210 in gray value).

227 **(H-I)** Response of the AHP6 protein reporter (H) and transcriptional reporter (I) to mock, CHX,  
228 and AZD-8055 treatments for 72 hours. For (H), images are representative of n = 29 (mock), n =  
229 29 (CHX), and n = 34 (AZD-8055) buds in three experiments. For (I), images are representative  
230 of n = 11 (mock), n = 9 (CHX), and n = 12 (AZD-8055) buds in two experiments.

231 **(J-Q)** Reduction of A-type ARR and AHP6 protein levels contribute to the variability in sepal  
232 initiation. (J-O) Stage 5-6 buds of indicated genotype stained with propidium iodide. Arrowheads  
233 indicate sepal primordia that are variable in number, position, and/or size. Note that the  
234 *arr3,4,5,6,7,8,9,15* bud has an inner sepal that is slightly smaller than its outer sepal and  
235 positioned slightly right-skewed (K). The *ahp6* bud develops five sepal primordia of variable sizes  
236 and unevenly positioned (L). The *ARR7-llama GFP-nes* constructs partially rescue the *drmy1*  
237 phenotype in some buds (O, left) but not others (O, right). (P) Quantification of sepal primordium  
238 number. Asterisk indicates statistically significance difference in a Fisher's exact test (WT vs *ahp6*,  
239 p =  $3.026 \times 10^{-7}$ ; *drmy1* vs *drmy1 ARR7-llama GFP-nes*, p = 0.4389). (Q) Quantification of  
240 variability in sepal primordium position. Asterisk indicates statistically significant difference in a  
241 Wilcoxon rank sum test (WT vs. *arr3,4,5,6,7,8,9,15*, p =  $2.948 \times 10^{-4}$ ; WT vs *ahp6*, p =  $2.137 \times 10^{-4}$ ).

## Translation and developmental robustness

242 <sup>11</sup>; WT vs *ARR7-llama GFPnes*, p = 1; *drmy1* vs *drmy1 ARR7-llama GFPnes*, p = 1.538×10<sup>-7</sup>).  
243 Data for *drmy1* were reused from Figure 2H, 2J. Data for *ARR7-llama GFP-nes* and *drmy1 ARR7-*  
244 *llama GFP-nes* were pooled from two independent lines (7-4 and 7-6). Sample size: WT, n = 78;  
245 *arr3,4,5,6,7,8,9,15*, n = 28; *ahp6*, n = 106; *ARR7-llama GFPnes*, n = 16; *drmy1*, n = 67; *drmy1*  
246 *ARR7-llama GFP-nes*, n = 20.

247 **(R)** Working model. In WT, DRMY1 maintains TOR activity and translation, which sustains the  
248 rapid production of cytokinin signaling inhibitors (ARR7 and AHP6) in response to cytokinin  
249 signaling. These inhibitors maintain cytokinin signaling at a normal level, allowing auxin and  
250 cytokinin signaling to interact and form robust spatial patterns. Robust patterning of auxin and  
251 cytokinin signaling gives rise to robustly initiated sepal primordia. In *drmy1*, due to decreased  
252 TOR signaling and translation rate, the meristem cannot rapidly produce cytokinin signaling  
253 inhibitor proteins in response to cytokinin signaling. As a result, cytokinin signaling is upregulated,  
254 which rescues the translation rate reduction in a homeostatic mechanism. This upregulation of  
255 cytokinin signaling disrupts the robust spatial pattern of both cytokinin and auxin signaling, which  
256 in turn causes variability in sepal initiation. Scale bars in all micrographs, 25  $\mu$ m.

257